Understanding visual snow syndrome
a clinical characterization and functional imaging approach

Puledda, Francesca

Awarding institution:
King's College London

Understanding Visual Snow Syndrome:

A Clinical Characterization and Functional Imaging Approach

Francesca Puledda

Institute of Psychiatry, Psychology and Neuroscience

King's College London

A Thesis Submitted for the Degree of Doctor of Philosophy (Clinical Neuroscience)

February, 2020

Supervisors:

Professor Peter J. Goadsby

Professor Steven C.R. Williams

Professor Dominic ffytche

Abstract

Visual snow is a neurological condition that was first described and defined clinically a little over five years ago. The main clinical feature is an unremitting, positive visual phenomenon present in the entire visual field and characterized by uncountable tiny flickering dots. The pathophysiology of this disorder is largely unknown, making treatment of affected patients extremely challenging.

The aim of this PhD was to understand more about the biology of visual snow, first through its clinical characterization and then with the use of neuroimaging.

The first objective has been addressed with a large web-based survey that involved visual snow subjects (*n* = 1104), who were defined according to the recently proposed diagnostic criteria. This study (chapter 2) allowed recognition of the common clinical presentation of the syndrome and of its principal comorbidities, as well as prediction of its severity.

The second aim was carried out with a multimodal structural and functional magnetic resonance imaging study, comparing twenty-four visual snow patients with an equal number of healthy volunteers (chapter 3).

Voxel based-morphometry (chapter 4) was used to study structural changes in the brain; arterial spin labelling (chapter 5) to analyse regional cerebral blood flow; functional connectivity (chapter 6) and task-based functional magnetic resonance imaging (chapter 0) to study localised brain responses at rest and in response to a 'visual snow-like' stimulus; finally magnetic resonance spectroscopy (chapter 0) was employed to study neurochemical properties of the brain.

The imaging data show that visual snow is characterized by subtle morphological, as well as widespread functional, changes that involve important brain networks regulating attention, salience, sensory processing and cognition.

Statement of scientific contribution

I here declare that the work presented in this thesis is my own.

Data collection and analysis of online surveys was undertaken by myself, with the exception of the latent class analysis, for which I was aided by Dr Sam Norton.

I personally recruited all patients and healthy controls for the MRI study. Scanning was carried out by radiographers at the King's College London MRI Major Research Facility, on a scanner based in the Wellcome NIHR King's Clinical Research Facility.

I carried out all data processing and imaging analyses reported here, under the supervision of my supervisors. ASL analysis was completed with the help of Dr Fernando Zelaya. Functional connectivity and VBM analyses were completed with the help of Dr Owen O'Daly. SUIT analysis was completed with the help of Dr Muriel Bruchhage. Task-based fMRI data was analysed with the help of Dr Dominic ffytche. MRS analysis was completed with the help of Dr David Lythgoe. The hypotheses and plan of investigation for this thesis were formulated primarily after discussions with my first supervisor, Professor Peter J. Goadsby.

Publications

Journal publications arising from the work presented in this thesis:

- **Puledda F**, Ffytche DH, Lythgoe DJ, O'Daly O, Schankin C, Williams SC, Goadsby PJ. Insular and occipital changes in visual snow syndrome: a BOLD fMRI and MRS study. *Annals of Clinical and Translational Neurology* 2020; in press.
- **Puledda F**, Schankin C, Goadsby PJ. Visual snow syndrome. A clinical and phenotypical description of 1,100 cases. *Neurology* 2020; doi: 10.1212/WNL.0000000000008909
- **Puledda F**, Ffytche DH, O'Daly O, Goadsby PJ. Imaging the Visual Network in the Migraine Spectrum. *Frontiers in neurology* 2019; 10(1325); doi: 10.3389/fneur.2019.01325
- **Puledda F**, Schankin C, Digre K, Goadsby PJ. Visual Snow Syndrome: what we know so far. *Current opinion in neurology* 2018; 31(1): 52-8; doi: 10.1097/WCO.0000000000000523.

Articles submitted for peer-review:

- **Puledda F**, Bruchhage M, O'Daly O, Ffytche D, Williams SC, Goadsby PJ. Occipital cortex and cerebellum grey matter changes in visual snow syndrome.
- **Puledda F**, Schankin C, ffytche D, O'Daly O, Eren O, Karsan N, Williams SC, Zelaya F, Goadsby PJ. Localised increase in regional cerebral perfusion in patients with visual snow. A pseudo-continuous arterial spin labelling study.

Abstracts presented at international conferences:

- Functional and metabolic changes in visual snow syndrome: a combined BOLD fMRI and MR-spectroscopy study. Oral presentation at the *International Headache Conference,* 2019.
- Alterations in regional cerebral blood (rCBF) in visual snow assessed using arterial spin-labelled (ASL) functional magnetic resonance imaging (fMRI). Late-breaking electronic poster at the *Migraine Trust International symposium,* 2018
- Clinical characterization of visual snow. Electronic poster at the *International Headache Conference,* 2017.

Acknowledgments

This thesis goes first and foremost to my Mom, the strongest person I know, for never doubting that I could achieve anything I put myself into. This would not have been possible without you.

I would like to thank my three supervisors: Dominic, for his great knowledge and brilliant remarks, his humour and insight on any topic; Steve, for his unique ideas, his capacity of making complex things look intuitive and for never sparing a word of support; Prof Goadsby, for being the best mentor I could ever have, for making me thrive and always desire to better myself.

To Professor Di Piero, for guiding me along for so many years in my research and clinical interests.

To all the patients who took part in the study, for making this research possible.

To the King's CNS team, who have helped me in so many ways throughout this project. To Owen, for always pushing me to go beyond the easy answer, to Fernando for all his patience and kindness, to Muriel for her enthusiasm.

To all the headache team members, present and past: we really are an amazing group! Thanks in particular to Roby for being such a great companion even from afar, to Alison for her continuous help, to Nazia for the laugh that always gets you smiling, to Fiona for her optimism and cheerfulness, to Diana for our endless hours of brainstorming, to David for his constant encouragement.

To my wonderful aunts, real and 'acquired', for always believing in me, no matter what.

To Valentina, Mikiko, Silvia and Emilia: I wish studying were always as fun as when we were in Med school! We have grown so much together, even when scattered all over the world.

To Fabrizia and Sara, we planned this journey together and supported one another through everything, learning and improving from each other. You are simply irreplaceable.

To my incredible, wonderful friends: Michele, Lorenzo, Ombretta, Alessandro, Giulia, Claudia, Matteo, Daniele, Massimo, a.k.a Le Fragole Blu. Because real families are the ones we choose, and you will always be my home.

To my partner Filippo, for never failing to show me what real love, support and understanding are. You are, quite simply, the most wonderful human being. I am so happy to have been in this PhD adventure together, sharing all the difficulties, the pain and the success, but I also can't wait to start several new chapters with you!

And finally, to my Dad.

For teaching me to be always curious, to look for the true meaning of things, to never give up, to be serious most times and silly when needed. For being the reason of a never-ending relationship with science.

I hope you would be proud.

Contents

List of Figures

List of Tables

Abbreviations

[^{18}F]-FDG PET	Positron emission tomography (PET) with 2-deoxy-2-[fluorine-18] fluoro-D-glucose
ACC	Anterior cingulate cortex
ADNI	Alzheimer's Disease Neuroimaging Initiative
AFNI	Analysis of Functional NeuroImages
AG	Angular gyrus
ANCOVA	Analysis of covariance
ANOVA	Analysis of variance
ASAP	Automated Software for ASL Processing
ASL	Arterial spin labelling
BA	Brodmann area
BOLD	Blood-oxygen-level dependent
Cb	Cerebellum
CBF	Cerebral blood flow
CBS	Charles-Bonnet syndrome
CEN	Central executive network
CHESS	Chemically selective suppression
CNS	Central nervous system
CON	Cingulo-opercular network
CRF	Clinical research facility
CSF	Cerebrospinal fluid
DAN	Dorsal attention network
DARTEL	Diffeomorphic anatomical registration through exponentiated lie algebra
DMN	Default-mode network
EPI	Echo-planar imaging
FC	Functional connectivity
FG	Fusiform gyrus

FDR	False discovery rate
fMRI	Functional magnetic resonance imaging
FOV	Field of View
FP	Fronto-parietal network
FEF	Frontal eye fields
FSL	FMRIB Software Library
FWE	Family-wise error rate
GABA	Gamma aminobutyric acid
GLM	General linear model
Gln	Glutamine
Glu	Glutamate
GM	Grey matter
HC	Healthy controls
HPPD	Hallucinogen persisting perception disorder
ICV	Intracranial volume
IFG	Inferior frontal gyrus
IN	Insula
IoPPN	Institute of Psychiatry, Psychology and Neuroscience
IPL	Inferior parietal lobule
LCA	Latent class analysis
LG	Lingual gyrus
LGN	Lateral geniculate nucleus
Lum	Luminance
MATLAB	Matrix laboratory
mm	Millimetre
mM	Millimolar
MNI coordinates	Montreal Neurological Institute coordinates
MNI	Montreal Neurological Institute
MRI	Magnetic resonance imaging

MRS	Magnetic resonance spectroscopy
ms	Milliseconds
NAA	N-acetylaspartate
pCASL	Pseudo-continuous arterial spin labelling
PCC	Posterior cingulate cortex
PCu	Precuneus
PoG	Postcentral gyrus
PPI	Psychophysiological interaction
PrG	Precentral gyrus
PRESS	Point resolved spectroscopy
Pv	Pulvinar
ROI	Region-of-interest
SD	Standard deviation
SMA	Supplementary motor area
SMG	Supramarginal gyrus
SN	Salience network
SNR	Signal-to-noise ratio
SPL	Superior parietal lobule
SPM	Statistical Parametric Mapping
SPSS	Statistical Package for the Social Sciences
STG	Superior temporal gyrus
TCV	Total cerebellar volume
TE	Echo time
TI	Time to inversion
TIV	Total intracranial volume
TPJ	Temporo-parietal junction
TR	Repetition time
V1	Primary visual area V1
V5	Motion area V5

VBM	Voxel-based morphometry
vPMC	Ventral premotor cortex
VS	Visual snow
VSS	Visual snow syndrome
WM	White matter

1 Introduction

1.1 A definition of visual snow

Visual snow (VS) is a neurological condition that was first described and defined clinically a little over five years ago. The main clinical feature of the disorder, described consistently by patients, is an unremitting, positive visual phenomenon present in the entire visual field and characterized by uncountable tiny flickering dots interposed between the person's vision and the background (Figure 1.1) (Schankin et al., 2014a). This 'static' is typically black and white but can also be coloured, flashing or transparent. In addition to the static, or snow, patients with visual snow can experience additional visual symptoms of either direct neurological origin, such as palinopsia (Figure 1.2), photophobia and nyctalopia (i.e. impaired night vision), or that arise from the optic apparatus. This is the case with entoptic phenomena, that may manifest in the visual snow syndrome as blue field entoptic phenomenon, floaters, self-light of the eye and/or spontaneous photopsia. Different combinations of these additional symptoms, together with the static itself, constitute the 'visual snow syndrome' (VSS) which is outlined by a set of specific criteria (Table 1) (Puledda et al., 2018). In the past years, recognition of the disorder has grown considerably, to the point where VS is now included in the appendix of the International Classification of Headache Disorders as a complication of migraine (Headache Classification Committee of the International Headache Society (IHS), 2018).

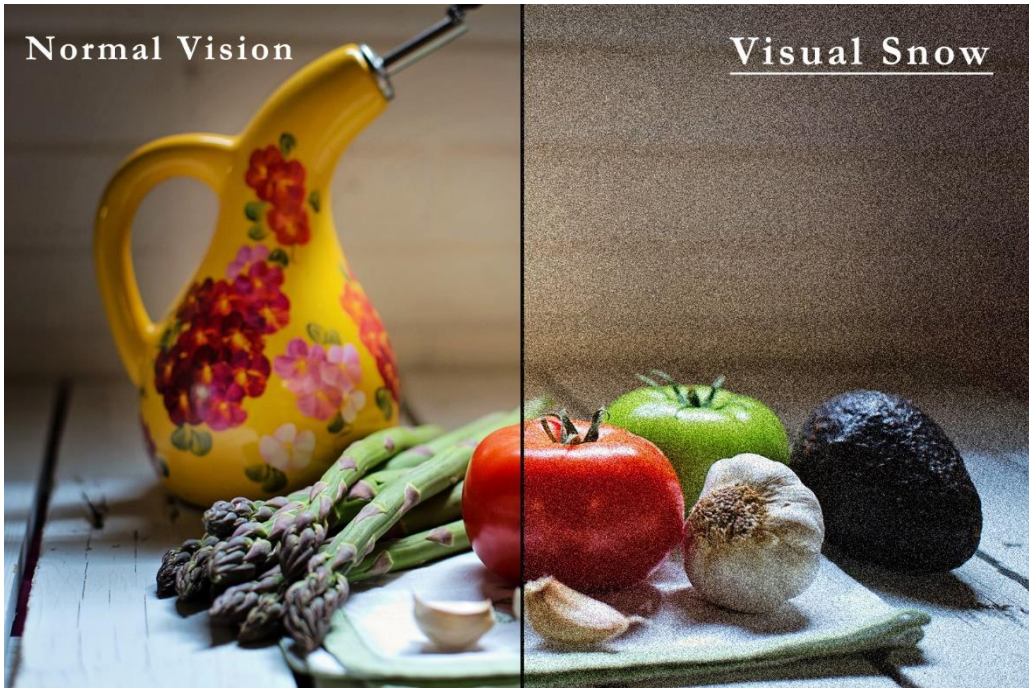

Figure 1.1 An illustration of visual snow.

Reproduced with permission (Puledda et al., 2020b).

Figure 1.2 An example of afterimages, in the form of palinopsia.

A	**Visual snow: dynamic, continuous, tiny dots in the entire visual field lasting longer than 3 months.** *The dots are usually black/grey on white background and grey/white on black background; they can also be transparent, white flashing or coloured.*
B	**Presence of at least two additional visual symptoms of the four following categories:** (i) Palinopsia. At least one of the following: afterimages or trailing of moving objects. *After images should be different from retinal afterimages, which occur only when staring at a high contrast image and are in complementary colour.* (ii) Enhanced entoptic phenomena. At least one of the following: excessive floaters in both eyes, excessive blue field entoptic phenomenon, self-light of the eye, or spontaneous photopsia. *Entoptic phenomena arise from the structure of the visual system itself. The blue field entoptic phenomenon is described as uncountable little grey/white/black dots or rings shooting over visual field in both eyes when looking at homogeneous bright surfaces, such as the blue sky; self-light of the eye is described as coloured waves or clouds when closing the eyes in the dark; spontaneous photopsia is characterized by bright flashes of light.* (iii) Photophobia. (iv) Nyctalopia.
C	**Symptoms are not consistent with typical migraine visual aura.** *As defined by the International Headache Society in the International Classification of Headache Disorders (Headache Classification Committee of the International Headache Society (IHS), 2018).*
D	**Symptoms are not better explained by another disorder.** *Normal ophthalmology tests (best corrected visual acuity, dilated fundus exam, visual field and electroretinogram); not caused by previous intake of psychotropic drugs.*

Table 1 Criteria for the definition of the visual snow syndrome.

1.2 Early literature reports of the condition

In the scientific literature, what can now in hindsight be considered as early clinical reports of visual snow, appear typically as case reports in the context of larger series of patients with persistent visual disturbances. These cases were often attributed to migraine aura and drug use, therefore providing a possible explanation as to why visual snow was only described recently.

The first clear case report of visual snow was made by Liu and colleagues (1995). In this paper, ten migraine patients presenting with 'positive persistent visual phenomena' were grouped into three categories, which were then defined by the authors on the basis of the relationship between the headache condition and the visual symptoms. Three of the patients were categorized in a group for which the visual problems were not necessarily linked with migraine, but possibly represented a 'migraine equivalent'. By looking back at the clinical descriptions of these patients' symptoms - '…for the next 6 months he had persistent television-set "snow" and grainy vision throughout all fields…'; '…she saw constant white and black dots, "snow," and "TV static" over her entire visual field…'; '…He complained of 8 months of "snow" and "flickering" similar to what was "between TV channels" …' - one can see that they were suffering from visual snow. The authors further noted that, even if those three patients all had a positive history for both VS and migraine, there was in fact no temporal or causal association between the two conditions.

Ten years later, Jager and colleagues were the first to use the term 'visual snow phenomenon' in the medical literature. They did so in describing what they thought of as a possible phenotypic variant of aura, in a study using magnetic resonance perfusion and diffusion imaging on four patients with long lasting visual disturbances (Jager et al., 2005). Two of these patients were defined as having visual snow, and one reported her disturbance as '…thousands of small yellow, white or silvery dots over the whole of both visual fields…'. In this study, the authors found no diffusion or perfusion differences in the visual cortices of these patients, with respect to other cortical regions.

In 2008 Wang and colleagues used the Visual Aura Rating Scale (VARS) to assess patients with persistent visual disturbance (Wang et al., 2008), and described two subjects with continuous TV static and noise in their vision or, to use the patient's words, 'tiny black and white dots scattered throughout the entire visual field'.

The first characterization of visual snow as a distinct phenomenon finally came in 2013, in the form of a report by Simpson and colleagues (2013). The authors described the case of a pediatric patient affected by migrainous headaches since the age of seven, who presented at age twelve with the sudden onset of a persistent visual disturbance described as 'white bright jagged spots and black and white flashes with sparkles and dots'. The patient also reported other key additional symptoms of visual snow, such as palinopsia and photophobia, and reproduced her symptoms in an illustration, which now represents the first recorded image of visual snow (Figure 1.3).

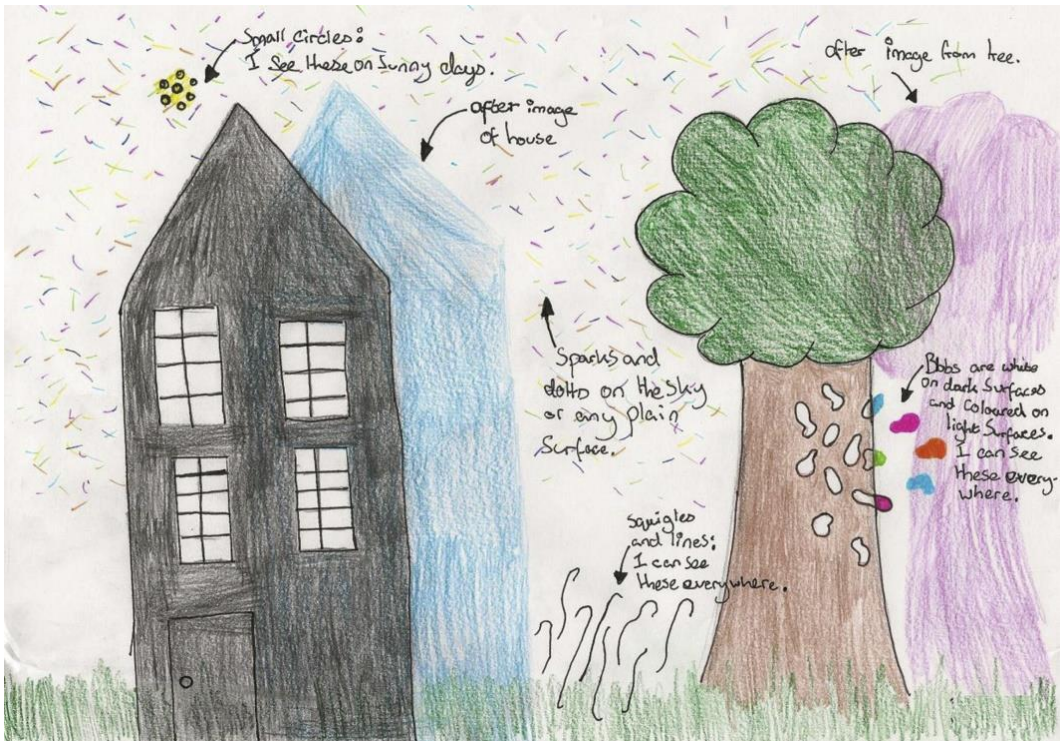

Figure 1.3 An original drawing of visual snow made by a 12-year-old patient.

Reproduced with permission (Simpson et al., 2013).

1.3 Systematic characterization of the syndrome

These case reports or series, even if isolated and collected over decades, all describe patients complaining of a reasonably homogeneous set of symptoms, thus suggesting a unique common syndrome. The recognition of this phenomenon led to the first systematic characterization of visual snow, which appeared in the study that provided the defining clinical criteria for VSS (Schankin et al., 2014a).

This study used a three-step design: first, a preliminary set of criteria were proposed based on the reports of twenty-two patients seen in a clinical setting, as well as an internet survey completed by patients with self-assessed visual snow. These criteria were then prospectively tested in seventy-eight patients who all had visual snow, defined as 'dynamic, continuous, tiny dots in the entire visual field lasting longer than 3 months'. Seventy-two (92%) of these patients had at least three additional visual symptoms, thus supporting the hypothesis of a clinical syndrome, which was finally defined and outlined through novel criteria (see Table 1).

With regards to these additional visual symptoms, palinopsia in VS was found to manifest either as afterimages - defined as the persistence of an image after the removal of the original stimulus (Critchley, 1951; Ffytche et al., 2010) - which was present in up to 80% of individuals in the study, or as visual trailing, present in up to 60% of subjects. Of note, afterimages in visual snow are to be distinguished from retinal afterimages, a phenomenon that can commonly be experienced by healthy individuals (Kinsbourne et al., 1963).

An exaggerated entoptic phenomenon was reported in 81% of individuals in the study. Entoptic phenomena can be perceived quite commonly in the general

population; however, the difference with visual snow patients is that they perceive them on a daily basis and in a bothersome, debilitating manner.

Nearly two-thirds of individuals with visual snow reported photophobia, which is also very common in migraine and in other ocular pathologies. The key characteristic of photophobia is the avoidance of light, that can be reported as either too bright (photic hypersensitivity) or painful (photic allodynia) (Maniyar et al., 2014).

Finally, about two-thirds of individuals with VS reported nyctalopia, defined as a difficulty seeing at night or in the dark.

Interestingly, most patients in this seminal study had comorbid migraine, and many (27%) even typical migraine aura. This, together with the defined clinical similarities of VS with prolonged visual aura (Schankin et al., 2017), could allow speculation on a possible overlap between the conditions. Nonetheless, the continuing and unremitting symptomatology of visual snow, as opposed to the ictal nature of both migraine and aura, as well as the absence of any aura manifestations during onset in the majority of the VS population (Schankin et al., 2014a), suggest that visual snow is a different entity from migraine with and without persistent aura.

This relationship was further analysed in a study on one-hundred and twenty VS patients (Schankin et al., 2014b). Here, patients with visual snow and concomitant migraine were found to have more additional symptoms - in particular photophobia, palinopsia, photopsia, nyctalopia and tinnitus - than patients with VS alone. The results therefore seemed to suggest that migraine, when present, can aggravate the clinical presentation of the visual snow syndrome.

The aforementioned study also importantly represented the first neuroimaging investigation of visual snow, involving seventeen VSS patients who underwent scanning with [^{18}F]-FDG PET (Schankin et al., 2014b). Results of the study showed that patients exhibited significantly increased brain metabolism in the area of the right lingual gyrus, as well as a trend for an area in the left cerebellum, when compared to healthy volunteers (Figure 1.4). The distribution of this hypermetabolism was very similar to an area previously shown to be involved in ictal migrainous photophobia (Denuelle et al., 2011), thus providing a further pathophysiological link between the conditions.

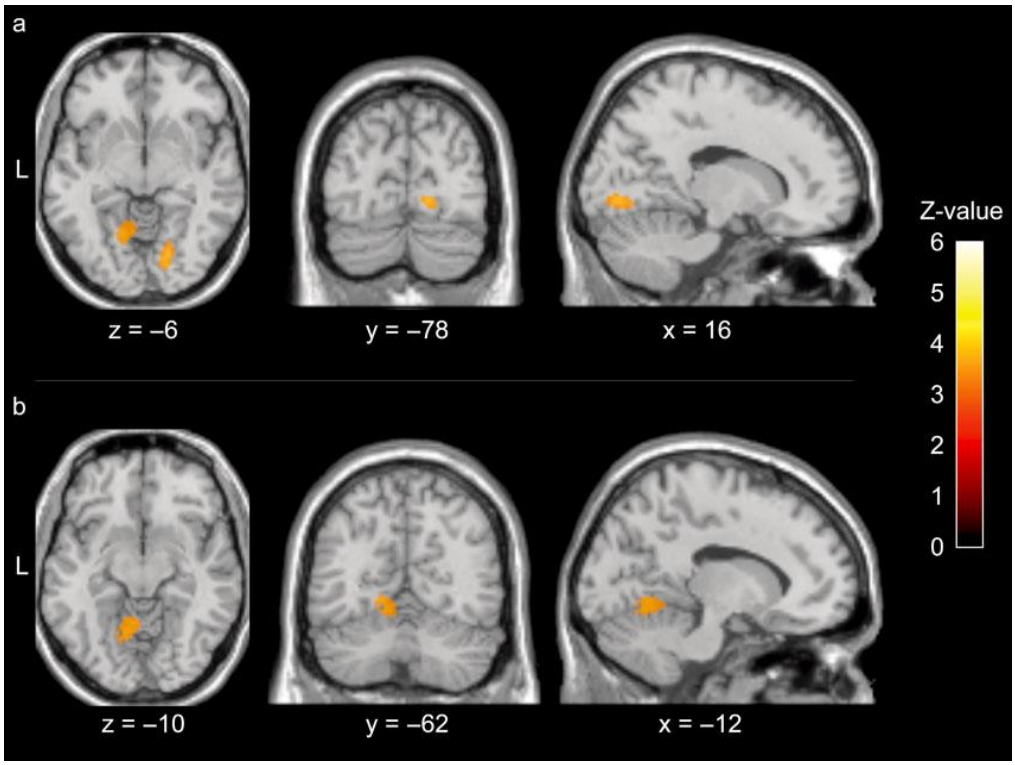

Figure 1.4 Areas of increased metabolism in the right lingual gyrus (a) and anterior lobe of the left cerebellum (b) in patients with visual snow, measured through [^{18}F]-FDG PET.

Reproduced with permission (Schankin et al., 2014b).

Even following the publication of the distinct criteria, the nosology of visual snow remains somewhat under debate. Some authors have argued that the condition may not represent a disease, but rather a heightened awareness of a physiological phenomenon (Kondziella et al., 2020). However, following the Oxford English Dictionary, we know that a disorder is defined as: 'A disturbance of the bodily (or mental) functions; an ailment, disease.' Given the neurophysiological and neuroimaging findings that have been linked to the condition, which are described in this chapter and in the following sections, there are indeed multiple indications of a brain dysfunction in VS. Further, when considering the definition of visual snow, one must take into account the high levels of disability declared by most patients, particularly those with the complete syndrome, which are very clear to any physician with clinical experience in this population. Another evidence of the level of suffering experienced by patients is seen in the high degrees of anxiety and/or depression that is found as a consequence of the condition, and which has been documented in several previous case studies (Kondziella et al., 2020; Lauschke et al., 2016; Schankin et al., 2014a).

1.4 Neurobiology of visual snow: pathophysiological hypotheses

The neurophysiological mechanisms causing visual snow syndrome are currently unknown, having been infrequently studied. Nonetheless, the large homogeneity of its clinical description makes it likely, at least in the majority of cases, to hypothesize the existence of a common pathological biology in the disorder.

Some possible theories on visual snow pathogenesis will be described, proceeding anatomically from the periphery onto higher-order areas of visual processing, and across the different features that characterize the condition.

These hypotheses take into account the literature that has been published to date; they have also largely been described in previous publications (Puledda et al., 2019; Puledda et al., 2018).

The most obvious biological explanation for VS, would be to regard it as directly or indirectly caused by a disorder of the eye or visual pathways. In fact, several types of ophthalmic conditions can present with clinical features of 'static' similar to visual snow. Even in our clinical research group, a subject with VS who was also affected by X-linked Retinitis Pigmentosa has been seen in the past.

Further, it would be possible to explain the similarity of visual snow to tinnitus - a highly common comorbidity (Schankin et al., 2014a) and in a way the auditory counterpart of visual snow - with a form of de-afferentation, in which even a temporary alteration in retinal firing could cause a dissociation between peripheral sensory input and central visual perception. A similar mechanism is indeed present

in the classic hallucinatory condition of Charles-Bonnet syndrome (CBS), where progressive loss of visual function causes hypo-connectivity from the visual periphery to the brain, giving rise to hallucinations (Ffytche, 2008).

It is also tempting to explain the associated entoptic phenomena of the VS syndrome as something arising plainly from the eye. These symptoms are in fact often caused by ophthalmic conditions (Brown et al., 2015; Khaleeli et al., 2018) or can present in healthy individuals as a consequence of strands of vitreous or white blood cells, stimulating retinal neurons (Sinclair et al., 1989; Tyler, 1978).

The main counter-argument to interpreting VS as a purely ocular phenomenon however, lies in the main criterion for VS, which requires the absence of ophthalmic disorders (Table 1), and also in the normality of basic eye electrophysiology, such as ERG or VEPs, reported in previous VS cohorts (Lauschke et al., 2016; Schankin et al., 2014a). Furthermore, it is unlikely for a whole-field visual disturbance to be caused by a localized disorder of the anterior retino-geniculate visual pathway or of the optic radiations, since these are organized in a monocular or homonymous fashion.

These considerations do not exclude that some cases of visual snow might be triggered by eye conditions. In this respect it is interesting to recall that in certain examples, CBS hallucinations are characterized by simple flashes, dots of light, or even palinopsia, an important feature of the VS syndrome (Santhouse et al., 2000).

A second theory on VS pathophysiology could involve a direct thalamic dysfunction. In a process known as thalamo-cortical dysrhythmia, there is a dissociation between the sensory inputs from the thalamus and its projections to the cortex. This

mechanism was first described by Llinas in the context of tinnitus (Llinas et al., 1999), and is characterized by an increase in unusual, large-scale and coherent thalamo-cortical low-frequency oscillations. These delta and theta oscillations are likely caused by a switch from tonic to high-frequency thalamic bursting - due to protracted cell hyperpolarization - and ultimately determine a disintegration of sensory perception at the cortical level.

It is certainly possible to hypothesize a role for thalamo-cortical dysrhythmia in visual snow. Potentially, an underlying homeostatic imbalance of the visual pathways, either from altered retinal activity or genetic predisposition, could cause a disinhibition of projections from the posterior visual thalamus to the primary and secondary visual cortices, as well as the parietal cortex, which could in turn affect normal visual perception and at the same time explain both palinopsia and the continuous perception of movement (Lauschke et al., 2016).

The fact that this same mechanism is thought to be involved in both tinnitus (De Ridder et al., 2015) and migraine pathophysiology (Coppola et al., 2007) is indeed interesting. In this context, it is important to note that more than 60% of the seventy-eight patients from the 2014 study reported having tinnitus (Schankin et al., 2014a), which is therefore significantly more prevalent in visual snow than in the general population (Shargorodsky et al., 2010; Wu et al., 2015). This suggests that the visual snow syndrome could represent a more complex dysfunction of sensory processing, not necessarily limited to the visual system.

In a more simplistic view, the thalamus could be responsible for VS symptoms through a localized increase in activity of the LGN or the pulvinar. The pulvinar is part

of the ‘thalamic matrix’ and projects diffusely to the cortex, playing a significant role in cognition and attentive stimulus processing (Lakatos et al., 2016). Recent studies have confirmed that the pulvinar can facilitate attention-related communication across widespread neuronal networks, including higher-order sensory cortices (Jaramillo et al., 2019). The pulvinar also has a role in photophobia (Maleki et al., 2012), a key symptom of VS, and could ultimately represent an important structure in visual snow biology.

A third possibility is to imagine VS as a purely cortical phenomenon. In visual hallucinatory syndromes, the percept of hallucinations has been shown to correspond to a dysfunction in the cortical area where that particular perception is represented (Ffytche et al., 1998). If the ‘cortical dysfunction theory’ were true, we should therefore expect altered brain structure, compensatory neuroplasticity or functional activity to be constrained to visual association/motion areas. It is known that topological visual disorders caused by hyper-function in V1/V2 areas can present with hallucinations similar to visual snow (Ffytche et al., 2010). Further, a recent case of sporadic Creutzfeldt-Jakob disease presenting with features of visual snow has been reported in the literature (BS Chen et al., 2019). These cases are, however, exceptional, and they would certainly not explain most cases of VS, in which gross central nervous system abnormalities are not found.

A more complex explanation of the role of the cortex could involve a widespread dysfunction of higher-order visual processing areas, particularly of the extrastriate cortex. Certainly the previous [^{18}F]-FDG PET study, showing increased metabolic

activity in the lingual gyrus, points to this (Schankin et al., 2014b). There have also been important neurophysiological (Eren et al., 2018; Luna et al., 2018; Yildiz et al., 2019) and behavioural (McKendrick et al., 2017) studies demonstrating an altered processing and dishabituation in the visual network of the VS brain. Further, certain elements of the VSS phenotype, particularly palinopsia, hint to a direct dysfunction of the parietal lobe (Ffytche et al., 2010), even though the palinopsia typically seen in parietal lobe lesions is retinotopically fixed.

The dorsal visual network, involved in the processing of visual motion, is also particularly likely to play a role in a condition characterized by the perception of constantly moving objects. The motion network is part of what was originally described as the dorsal 'action' stream (Goodale et al., 1992) and has now been renamed as the 'how-pathway'; it spreads from V1 dorsally to the parietal lobe, involving visual motion area V5 located in the temporo-parietal-occipital junction, which specifically responds to motion stimuli (Zeki et al., 1991).

VS syndrome could therefore potentially involve an abnormal processing of visual information and altered neuronal excitability in the supplementary visual cortices, downstream of the primary visual cortex.

The question of visual cortical hyperexcitability in the pathophysiology of visual snow has been addressed by Chen and colleagues (2011), who studied six patients with persistent visual disturbance using visual-evoked magnetic field recording. Two patients had reported what seemed to be visual snow for many years, and were found to have a persistent cortical hyperexcitability, that was inversely correlated with disease duration. In a case report, Unal-Chevik and Yildiz (2015) similarly found

a potentiation of repetitive visual evoked potentials in a patient with VS and migraine; this alteration normalized after treatment with lamotrigine in parallel to a clinical improvement. Whether the lack of habituation in these studies was due to comorbid migraine (Schoenen et al., 1995) or is in fact a feature of visual snow, remains an open question.

Finally, an altered connection between the visual system and other brain networks involved in salience, cognition and attention, is possible in a disorder like VS. Vision is a dynamic, active process in which top-down influences are seen at all stages of the visual hierarchy - with the exception of the retina - and which control various functional properties of vision, particularly attention (Gilbert et al., 2013). We can hypothesize that visual snow may be characterized by a general altered excitability and connectivity of the visual network with either the salience and/or default mode networks, which typically exert top-down influence on the visual cortex, or the dorsal and ventral attention networks, which have been abundantly implicated in theories of visual hallucinations (Collerton et al., 2005; Shine et al., 2014; Shine et al., 2011).

A final, overarching framework for visual snow that was developed at the start of this PhD encompasses the three aforementioned hypotheses. If a combination of peripheral, subcortical and cortical dysfunctions were all at play, either in different subjects or in different moments of the natural disease history, this would explain not only the main symptom of the snow common to all patients, but also the variety of symptoms characterizing the VS syndrome. Similarly to a model that has been used to explain tinnitus, and that is potentially linked to chronic pain as well (Sedley et al.,

2016), we could imagine that subcortical spontaneous activity normally ignored and considered as erroneous by the brain in normal conditions, might for various reasons increase in salience and be considered as the default visual perception, particularly if the hierarchical sensory processing networks in the brain do not correct this faulty perception. This model would certainly explain the continuous background perception of the simple static or snow, and also the more complex phenomena typical of the syndrome: palinopsia, entoptic phenomena, photophobia and even nyctalopia, which could in fact simply represent an increased perception of the 'noise' when no other stimulus is present. Figure 1.5 summarizes the salient aspects of this theory, showing the most important brain structures and connections likely to be involved in visual snow pathophysiology.

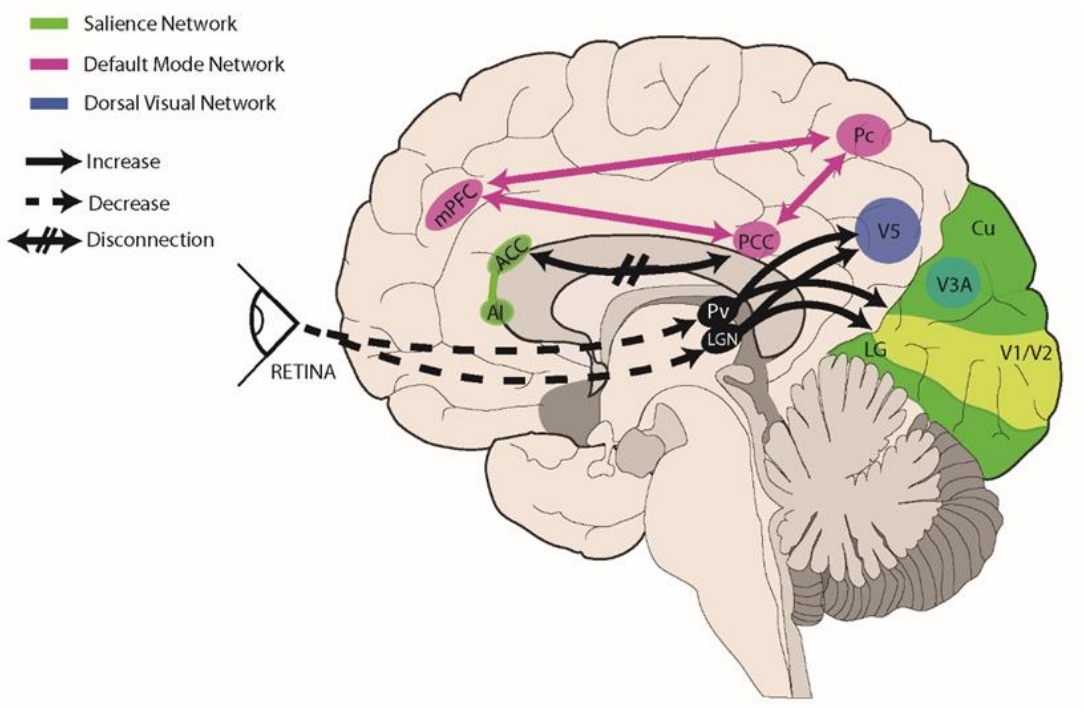

Figure 1.5 A proposed model for visual snow pathophysiology.

A form of genetic predisposition or a transient alteration in peripheral visual stimulation could induce dysrhythmic connections between thalamic structures and cortical visual areas. The lateral geniculate nucleus (LGN) and pulvinar (Pv) in particular are directly connected to motion area V5 and the lingual gyrus (LG). Relevant to VS biology is the motion processing network, which is composed of areas within the primary visual cortex (V1/V2), area V3A within the cuneus (Cu), area V5 located ventrolaterally among the lateral occipital sulcus and inferior temporal sulcus, and Brodmann area 7 in the precuneus. Structures pertaining to the default mode network (PCC = posterior cingulate cortex; Pc = Precuneus; mPFC = middle prefrontal cortex) and/or the salience network (AI = anterior insula; ACC = anterior cingulate cortex) are involved in salience and interoception. Disruption of these networks, possibly through altered connectivity between cortical areas, could also play a role in VS pathophysiology.

1.5 Main objectives

The primary objective of this PhD project was to understand more about the pathophysiology of visual snow.

In a first part of the study, the aim was to describe the clinical characteristics of a large population of VS patients, both with and without the complete syndrome, through the use of a large web-based questionnaire. The questionnaire was used to test the current clinical criteria, to confirm the typical presentation of the main symptom of visual snow - i.e. the static -, to define the differences between visual snow and the presentation as a 'complete' syndrome, to determine broad differences related to geography, and finally, to dissect possible subgroups and biological subtypes within the condition.

Additional questions were those regarding the interaction between visual snow and its main comorbidities migraine and tinnitus, as well as to compare VS with hallucinogen persisting perception disorder (HPPD), given that hallucinogenics can produce a similar static-like disturbance (Abraham, 1983). The starting position was that by observing the clinical distinctions of VS with these comorbidities and overlapping disorders, some information may be gained on its underlying biology.

In the second part of the PhD, a neuroimaging study using different magnetic resonance imaging (MRI) approaches was undertaken in patients with VSS, comparing them with healthy volunteers. The ultimate aim was to investigate morphological and functional changes of the visual snow brain.

An overview of these MRI methods, and the specific reasons for applying them in visual snow, is described in the next chapters.

1.6 Focus on MRI techniques

Magnetic resonance imaging is a non-invasive approach that allows direct investigation of brain biology. Different MRI methods serve a variety of scientific purposes, with structural approaches defining brain morphology and functional MRI (fMRI) techniques providing information on neuronal activity.

1.6.1 Voxel based morphometry

Voxel-based morphometry (VBM) is an objective and automated method that is commonly used to analyse changes in brain structure. By comparing local grey and white matter concentration differences between groups of subjects, it can provide important insights into the morphological characteristics of key structures across different brain conditions (Ashburner et al., 2000; Wright et al., 1995).

VBM typically involves a voxel-wise comparison of the concentrations of grey matter (GM) and white matter (WM) starting from a high-resolution T1-weighted image. This is achieved through segmentation of tissue components on the basis of probability maps, either preceded or followed by spatial normalization of the images from all subjects in the study into a common stereotactic space through affine transformation. The aim of this registration step is to correct for global brain shape differences while allowing for individual differences in structure. Normalization is generally associated with modulation, whereby the voxel values are multiplied by the deformation parameters (Jacobian determinants) from the spatial normalisation step, and which allows for the comparison of relative volumes rather than

concentrations. Finally, images are smoothed with a Gaussian kernel for appropriate statistical comparisons between groups.

An automated method that is currently well-accepted for VBM analyses is Diffeomorphic Anatomical Registration Through Exponentiated Lie Algebra (DARTEL) (Ashburner, 2007). It achieves more accurate registration of brain images than standard VBM methods, by modelling the spatial deformations through a single velocity field that is constant over unit time.

VBM has been widely used in neuroscience in various patient populations, such as schizophrenia (Honea et al., 2005), Alzheimer's (Matsuda, 2016), epilepsy (Bernasconi et al., 2004; Keller et al., 2002) and cluster headache (May et al., 1999), allowing exploration of important changes in brain structures involved in the pathophysiology of these neurological conditions.

1.6.2 Arterial spin labelling

Arterial spin labelling (ASL) is a quantitative, non-invasive functional MRI technique that allows the quantification of perfusion as an indirect but sensitive marker of neuronal activity. Perfusion refers to the delivery of blood to a tissue or organ; brain perfusion is also termed cerebral blood flow (CBF) and is expressed in units of mL/g/min, reflecting the volume of flow per unit brain mass per unit time. Absolute quantification of CBF requires a tracer that can diffuse from the vasculature into tissue, and for this purpose ASL uses magnetically labelled arterial blood water (Wolf et al., 2007).

ASL has gained considerable interest in clinical (Detre et al., 2009; Pollock et al., 2009) and non-clinical (Howard et al., 2012; Modinos et al., 2018; Wolke et al., 2019) neuroscience investigations due to its robust nature, high reproducibility and ability to provide absolute, non-invasive measures of whole-brain tissue perfusion that are reliably associated with neuronal activity, thanks to the phenomenon of neuro-vascular coupling (Howard et al., 2011; Williams et al., 1992).

The ASL method relies on the process of converting arterial blood flowing in the neck into an endogenous MR tracer, through magnetic inversion (labelling) of the hydrogen nuclei in the blood water molecules (Chappell et al., 2017), which is achieved through radiofrequency pulses. This labelled blood, after a delay period, is carried to the brain where it accumulates within the microvasculature of the tissue. By comparing the labelled image obtained after the delay and a control image taken before blood labelling (control acquisition), it is possible to obtain measures of brain perfusion.

The two major approaches for arterial spin labelling are continuous and pulsed ASL (Wong, 2014), which differ in both the spatial extent and the duration of the labelling. In continuous ASL, arterial blood water is labelled continuously over a relatively long period as it passes through a labelling plane, that is typically applied at the base of the brain (Detre et al., 1992). Conversely, in pulsed ASL, a short radiofrequency pulse is used to invert instantaneously the magnetization of blood and tissue, and can be applied either below the brain or to the entire brain (Edelman et al., 1994).

Continuous ASL has the advantage of a higher signal-to-noise ratio (SNR) compared to pulsed ASL (Dai et al., 2008). Pseudo-continuous ASL (pCASL) in particular, is a

relatively new technique that until recently remained challenging to implement in clinical scanners. This ASL variant has the advantage of using short (500 µs) pulses of radiofrequency and gradient fields which are more compatible with clinical body coil transmission hardware, and has hence become the method of choice for *in vivo* cerebral perfusion investigations (Alsop et al., 2015).

pCASL has been used in neuroscience research to study, among other conditions, surgical and chronic pain (Hodkinson et al., 2013; Keszthelyi et al., 2018), psychosis (Modinos et al., 2018), headache (Karsan et al., 2018), and neural correlates of behavioural traits or states (Beschoner et al., 2008; Hermes et al., 2009).

1.6.3 Functional MRI

Functional MRI (fMRI) is a widely popular imaging technique that uses blood-oxygen-level dependent (BOLD) contrast to highlight dynamic changes in neuronal activity in the brain. In its most common form, fMRI is used to produce spatial maps of functional activation in areas showing changes when subjects are asked to perform a task (task-based fMRI), which is usually of sensory, cognitive, motor or physiological type (Bandettini et al., 1992; Heeger et al., 2002; Worsley et al., 1995).

The BOLD signal in fMRI results from the differing magnetic properties of deoxygenated and oxygenated haemoglobin, and is considered an indirect measure of neuronal activity (KJ Friston et al., 1995; Kwong et al., 1992; S Ogawa et al., 1990; S. Ogawa et al., 1992). This is based on the observation that deoxyhaemoglobin contains paramagnetic iron - while oxyhaemoglobin contains diamagnetic oxygen-bound iron - and as such is capable of causing local increases in the magnetic field inside the scanner. When an area of the brain is undergoing functional stimulation,

there is a change in the cerebral blood flow and the rate of metabolic consumption of oxygen, with more oxygen being supplied to the brain than is consumed (Buxton et al., 1998). This causes the fraction of deoxyhemoglobin in activated brain regions to be lower, which in turn causes local increases in T2* MR signal. These localised variations in T2* signal are easily detected by high speed gradient-echo imaging techniques with long echo times (TE), such as echo-planar imaging (EPI). Within the EPI techniques, multi-echo planar imaging represents an emerging approach that allows to distinguish BOLD from artefact signal with higher fidelity and interpretability than single-echo fMRI (Prantik Kundu et al., 2017).

A different application of the BOLD signal, and in particular of its spontaneous coherent fluctuations, permits investigation of the functional connectivity (FC) between different brain areas that are linked in their activity and that communicate by processing shared information (Biswal et al., 1995). FC specifically relies on the statistical correlation between the time courses of signal intensities in spatially remote regions, which has been shown to manifest the functional relationship of spontaneous neuronal activity across such areas (M. D. Fox et al., 2007; Sporns et al., 2004). Functional connectivity is typically used to investigate the brain when it is at rest and not exposed to an external stimulus, however, it can also be used to study the changes of the baseline neuronal activity in response to a stimulus. These types of experiments have revealed the existence of large-scale intrinsic networks that alternate their function across rest and activation and that are capable of regulating different brain states (Raichle et al., 2001).

1.6.4 Magnetic resonance spectroscopy

MR spectroscopy (MRS) is a rapidly developing field of neuroimaging that allows investigation of metabolism *in vivo* by directly exploiting the magnetic properties of certain nuclei (Gujar et al., 2005). MRS differs from conventional neuroimaging as it provides, rather than anatomy, biological and chemical information regarding cellularity, energy and neuron viability (Bertholdo et al., 2013). It does so by providing accurate quantification of the main brain metabolites, in particular of N-acetylaspartate, creatine, choline, myo-inositol, glutamate, GABA and lactate.

MRS is performed in a similar fashion to conventional MRI, with the difference that its chemical specificity to a particular nucleus depends not only on the local magnetic field strength, but also on its local chemical environment, a phenomenon referred to as chemical shift (Novotny et al., 2003). Many nuclei can be used to obtain MR spectra, however, because of its inherent physical properties and high natural abundance, the hydrogen (^{1}H) nucleus is the most widely used in human MRS studies. Spectroscopy is an insensitive tool, as it can only detect compounds that have a concentration of at least 0.5–1.0 mM. Therefore, to improve the signal-to-noise ratio, MRS studies are usually limited to a single voxel where one large region of the brain is analysed at a time.

MRS has been performed in patients with a large range of neurological and psychiatric disorders, as it allows understanding of their pathophysiological mechanisms directly, as well as examination of the relationship between cognitive processes and neurometabolite values (Ross et al., 2004).

1.7 Planned neuroimaging investigations

In the neuroimaging project of this PhD, brain anatomy, function and metabolism of the visual snow syndrome were investigated.

1.7.1 Structural neuroimaging

Structural imaging was used to detect focal differences in brain morphology in VS. As shown in Table 1, gross neuroanatomical abnormalities need to be excluded for the diagnosis of visual snow, as this is not a 'secondary' neurological condition. Nonetheless, it is unclear whether subtle morphological differences, that are not typically detected by standard clinical neuroimaging, could be driving part of the syndrome's symptomatology, or perhaps even be caused by it.

In this context, a whole-brain voxel-based morphometry approach allowed investigation of the neuroanatomical differences between patients with visual snow syndrome compared to healthy volunteers, while the high-resolution atlas template SUIT method (Diedrichsen, 2006; Diedrichsen et al., 2009) allowed investigation of cerebellar anatomy directly. The leading hypothesis was that structural differences in VSS, if present, would involve the visual network, in particular the primary and secondary visual cortices (areas V1/V2), as well as the visual motion processing area V5. A further hypothesis was that the lingual and cerebellar areas showing metabolic alterations with [^{18}F]-FDG PET (Figure 1.4) could potentially present morphological grey and white matter differences in VSS subjects.

1.7.2 Functional neuroimaging

Brain function in visual snow was examined through multiple techniques: arterial spin labelling, functional connectivity and task-based fMRI.

With pCASL, differences in blood flow in whole-brain CBF maps were measured, both at rest (watching a dark screen) and during exposure to a visual stimulus mimicking visual snow itself. This particular stimulus was chosen in order to investigate differences in the patient population between an external and an internally perceived snow, and also to evaluate the effects of visual snow on healthy individuals. The hypothesis was that areas in the visual network, particularly visual motion areas, would be characterised by changes in cerebral blood flow in visual snow subjects, indirectly reflecting changes in neuronal activity. A further hypothesis was that these areas would not show particular changes in different states of brain activity, since visual snow is a continuous phenomenon that does not appear to be influenced by external conditions (in fact, all patients in the imaging population reported visual snow to be visible in the dark).

The FC experiment was conducted to investigate the connectivity of major cerebral networks in visual snow. By studying the BOLD fluctuations of the VS brain at rest, it was hypothesized that any dysfunction in the attention, default and/or salience networks would be elucidated. Further, to study how an external input could modify and influence the baseline brain activity, the 'visual snow-like' stimulus was shown continuously in a second connectivity experiment. The hypothesis was that, similar

to the pCASL experiment, changes at baseline would match similar changes in the active state, thus representing a possible hallmark of the condition.

Functional connectivity experiments allow the study of large-scale networks; however, they do not elucidate fast-changing brain responses to an external input. In the hypothesis that the visual snow brain would also be characterized by changes in the immediate physiological response to an exogenous sensory input, as measured through BOLD responses, a task-based fMRI block-design experiment was conducted, in which the same 'visual snow-like' stimulus, used as an active visual task, was rapidly alternated with a dark screen.

Finally, proton magnetic resonance spectroscopy (^{1}H MRS) was used to measure brain metabolite concentrations directly. As the only neuroimaging study previously performed in visual snow showed altered metabolism in the right lingual gyrus (Figure 1.4), this area was chosen as the voxel of interest for the spectroscopy analysis, in the hypothesis that MRS would allow confirmation and reproduction of the metabolic alterations found with [^{18}F]-FDG positron emission tomography.

2 Questionnaire study

This chapter contains the methods and results of the questionnaire study. The study was approved by the KCL Research Ethics Panel. I was responsible for all recruitment for the study. All analyses were undertaken by myself, with the exception of the latent class analysis. The data presented here have been published in article form in a peer-reviewed journal (Puledda et al., 2020b).

2.1 Methods

2.1.1 Participant selection and survey

For this part of the study, an online survey was prepared in collaboration with a visual snow patient group, Eye On Vision. This survey was then directly advertised on the group website (http://www.eyeonvision.org/). Most of the patients involved in the study approached the King's College London headache team through a dedicated research email, which they could find on the website. A smaller group of patients had contacted the group individually asking to be involved in research, and were redirected to the website. The survey is illustrated in Table 2; it presents a series of open and dichotomous questions aimed to characterize the symptoms of visual snow. These were entirely based on the published criteria for visual snow syndrome (Schankin et al., 2014a). Migraine and tinnitus presence were also investigated through the questionnaire, as well as age of symptom onset and previous exposure to illicit drugs (as the VSS criteria outline the need to exclude illicit/psychotropic substances).

Name Address Date of Birth (Day/Month/Year) Telephone number
1) Please make a brief statement that you are willing to be contacted for research. This is a European data protection issue. example: "Yes, please keep my contact details and you may contact me for research purposes."
2) Brief description of all symptoms you relate to visual snow syndrome.
3) Date or age when your symptoms started.
4) Visual snow: what type - black and white (i.e. only black dots on white background, white dots on black background) - clear (i.e. colour of the background) - flashing (i.e. always white, brighter than background) - coloured - all of these
5) Other symptoms (please only answer yes or no) - After images - Trailing of images in the vision - Blue field entoptic phenomenon (i.e. white squiggly lines moving pulsating on the blue sky) - Floaters in vision - Coloured clouds or waves with eyes closed - Flashes of light - Impaired night vision - Sensitive to light - Tinnitus
6) Have you ever been diagnosed with migraine or have you had a headache of moderate or severe intensity in the past? (Please answer yes or no)
7) Have you ever taken any illicit drugs in the past?

Table 2 Online visual snow survey.

2.1.2 Patient characterization

Following the criteria for VS (Table 1), patients who self-reported visual symptoms corresponding to criterion A (as evaluated by responses to questions 2, 3 and 4 of the survey) and who also fit criterion B (as evaluated by responses to question 5), were defined as having visual snow syndrome (VSS). Criterion C and D were evaluated on a case-to-case basis, based on answers to questions 2, 6 and 7 and eventual follow up questions by email when in doubt. Patients who did not report more than two additional visual symptoms of the four main categories - therefore lacking criterion B - but who fit all the other criteria, were considered to have visual snow without the syndrome (VS).

To avoid confounding with hallucinogen persisting perception disorder, patients who answered 'yes' to question 7 in the survey were further followed up with in-depth questions aimed at assessing when their symptoms appeared with respect to the intake of recreational drugs. All subjects who reported the onset of visual snow symptoms in the 12 months following any exposure to recreational drugs were excluded from the first two groups, regardless of the remaining symptoms, and were added to a third group called 'possible HPPD' (HPPD). It must be noted that a definitive diagnosis of HPPD was not possible based on this questionnaire, and that this criterion was rather used as a means to exclude HPPD. All subjects in this third group who fit criterion A for typical visual snow were included in the analysis.

2.1.3 Statistical analysis

Data was tabulated in Excel 2016 for Windows. Descriptive statistics, analysis of variance or χ^2 analysis for comparisons, respectively, of continuous and categorical variables, and cluster analysis were performed with SPSS Statistics Version 24.0 for Windows (IBM, Armonk, NY: IBM Corp.). Regression analysis, multiple imputations and latent class analysis were performed in Stata (StataCorp. 2017. Stata Statistical Software: Release 15. College Station, TX: StataCorp LLC). $P < 0.05$ was considered significant.

Patients were separated into three different groups according to their diagnosis: patients with VSS were coded as group 1, patients with VS as group 2 and patients with possible HPPD as group 3.

An ordinal variable was created to measure disease severity based on the number of visual symptoms experienced. For the largest cohort (i.e. group 1), this outcome variable was regressed on selected variables using ordinal logistic regression. The variables included as covariates in this model were selected in a previous step, based on a correlation with the number of symptoms experienced defined by significant correlations at the 5% level using Spearman's correlation.

Finally, in order to investigate possible biological subtypes of the condition, a latent class analysis (LCA) was performed. This is a form of statistical modelling used to identify groups or subtypes of cases, termed classes, in categorical data. LCA was done first on group 1 only, then on group 1 and 2 combined.

2.2 Results

2.2.1 Demographic characteristics and group comparisons

For the questionnaire study, a total of *n* = 1400 subjects contacted the study group through the designated email. Of these, *n* = 210 either gave incomplete data in the initial survey or never replied after having been redirected to the patient website; these subjects were excluded from further data collection. Two subjects had an insufficient English language level, six subjects had a serious underlying ophthalmic condition and eight subjects did not fulfil criterion A, meaning the static they reported was either of episodic nature or was present in only one part of the visual field. All of these subjects were excluded from the analysis.

Demographic characteristics of the remaining subjects (*n* = 1174) are presented in Table 3, which also shows details of symptom onset and associated comorbidities. The majority of the cohort (*n* = 1061, 90%) had complete visual snow syndrome. Forty-three subjects in the cohort were considered to have visual snow alone, as they provided a very clear description of the dynamic continuous pan-field tiny dots described in criterion A. These subjects however, did not present at least two visual symptoms from the additional categories, and were therefore grouped in the category 'VS'. Of these, seven subjects had no additional symptoms, twenty had only one and sixteen had between two and four symptoms of the same category, e.g. palinopsia for stationary objects and trailing, or several entoptic phenomena. Seventy subjects were grouped as possible HPPD following the criteria described in the methods (section 2.1.2). With the exception of exposure to recreational drugs on

the 12 months prior to the onset of symptoms, they all respected the remaining criteria for visual snow syndrome diagnosis, which is the reason they were kept in this analysis.

In Table 3, the three cohorts (VS, VSS and possible HPPD) are compared among themselves and with the cohort from the 2014 study (Schankin et al., 2014a), when the required data were available.

The four groups did not differ with regards to age. Male and female ratios were similar for visual snow subjects (VSS and VS), however, in the HPPD population most patients (71%; $p < 0.001$) were male. The large majority of subjects came from Europe ($n = 497$, 48% for VSS; $n = 15$, 35% for VS; $n = 41$, 61% for HPPD) and North America ($n = 429$, 41% for VSS; $n = 23$, 54% for VS; $n = 21$, 31% for HPPD).

Subjects with possible HPPD had a significantly later onset of symptoms compared to visual snow patients, both with and without the syndrome ($p < 0.001$). As a consequence, the average years with disease was lower in the HPPD group ($p < 0.001$). A small number ($n = 99$) of subjects in the VSS group reported a clear 'stepwise' worsening of symptoms at some point of the condition, however, this feature was not routinely screened for so it is not possible to infer its actual prevalence. Forty percent of VSS patients, for which data on onset age was available, reported the presence of symptoms since childhood, meaning for as long as they could recall. This was higher than the proportion found in the 2014 study. About one quarter of the visual snow subjects (VSS and VS) reported a sudden onset of their symptoms, however, the real frequency of this form of onset might be different, as

subjects were not interrogated about it directly. Of these spontaneous reports of sudden onset, some were related to specific conditions indicated in the table, of which a migraine attack was the most frequent. In the majority of cases however, the subjects could not recall any specific associated event. A sudden onset of symptoms was significantly more frequent in the HPPD group (81%; $p < 0.001$). By definition, all of these patients had the start of symptoms within a year after using recreational drugs. Four of these subjects could also recall other specific events (i.e. a migraine attack, a new medication and a mild head trauma) in strict temporal relation to the beginning of their symptoms.

The presence of tinnitus in the VSS population was the highest, but overall similar to that of the HPPD and 2014 cohorts. The frequency of this symptom was, however, significantly lower in the VS group in respect to the others. This was also the case for migraine, which was significantly less frequent in the VS population and more frequent in the VSS population. The presence of migraine aura was not routinely investigated, as this diagnosis was considered unreliable for a dichotomous questionnaire. It was spontaneously reported in 37% ($p = 0.05$) of subjects in the VSS group, and in all these cases the diagnosis was confirmed with thorough follow up questions.

	VSS	VS	HPPD	Schankin et al.
Number of patients (% of thesis cohort)	1061 (90%)	43 (4%)	70 (6%)	78
Age (mean ± SD)	30 ± 10	29 ± 12	28 ± 7	30 ± 10
Female : Male (*p* within group)	521:539 (*p*=0.6)	18:25 (*p*=0.3)	20:50 ***	37:41
Region of origin				/
Europe	497 (48%)	15 (35%)	41 (61%)	
North America	429 (41%)	23 (54%)	21 (31%)	
Central/South America	23 (2%)	0	1 (2%)	
Central Asia/Middle East	28 (3%)	1 (2.3%)	0	
Southeast Asia	17 (2%)	1 (2.3%)	0	
Oceania	49 (5%)	3 (7%)	4 (6%)	
Africa	3 (.3%)	0	0	
Age at symptom onset (mean ± SD)	13 ± 13	9 ± 10	21 ± 7 ***	21 ± 9
data available	823	28	60	
since childhood	326 (40%)	13 (46%)	1 (.01) ***	19 (24%)
Years of disease (mean ± SD)	17 ± 14	20 ± 17	7 ± 8 ***	/
Stepwise worsening	99 (9%)	0	4 (6%)	10 (13%)
Sudden onset of symptoms	176 of 691 (26%)	4 of 16 (25%)	38 of 47 (81%) ***	
with migraine attack	42 of 176	/	1 of 47	
with medication	20 of 176	/	2 of 47	
with trauma	10 of 176	/	1 of 47	
with infection	10 176	/	/	
with recreational drugs	/	/	38 of 47	
no apparent cause	94 of 176	4 of 16	/	
Comorbidities				
Tinnitus	793 (75%)	18 (42%) ***	48 (69%)	48 (62%)
Migraine	557 of 775 (72%)	7 of 18 (39%) ***	26 of 46 (57%)	46 (59%)
Migraine aura	127 of 345 (37%) *	1 of 6 (17%)	1 of 10 (10%)	21 (27%)

Table 3 Demographic and clinical characteristics of questionnaire study cohort.

** p<0.05, ** p<0.01, *** p<0.001 measured accordingly by ANOVA or χ^2 tests. Column on the right shows comparison with 2014 study cohort (Schankin et al., 2014a).*
/ means data is not available.

2.2.2 Clinical features of visual snow symptoms

To assess the clinical aspects of visual snow, information on the type of static that patients experienced was collected, as well as the associated visual symptoms that are part of the visual snow syndrome. Table 4 shows the frequencies of these characteristics, comparing them across the three groups and with the 2014 study cohort.

Each of the four static types was reported more frequently in the VSS group. This is probably accounted for by the fact that this group had a significantly higher proportion of subjects reporting all four types of static. The most common type of static differed between the VSS and VS groups compared to the HPPD group. When only one type of static was present, this was most commonly black and white in the VSS and VS groups, and transparent in the HPPD group. When two types of static were present, the most frequent combination was black and white and transparent for the VSS and VS groups, and coloured and flashing for the HPPD group. When three types of static were present, the combination of black and white, flashing and transparent was the most common in the VSS and VS groups, whereas coloured flashing and transparent was the most common in the HPPD group. The 2014 cohort showed different results from all groups in the study, with no patients reporting more than a combination of two types of static. This could be due to the fact that the current questionnaire was more flexible on static types, accounting for all types as defined by criterion A.

With regards to the associated visual symptoms, VSS and HPPD groups did not significantly differ in the mean number of associated visual symptoms reported by each patient. The three most common symptoms in the VSS group were, in order: floaters, afterimages and photophobia. In the VS cohort the most frequent symptoms were all of the entoptic phenomena group: floaters, self-light of the eye and flashes. In the HPPD group the four most commonly reported symptoms were: afterimages, photophobia, floaters and nyctalopia. Taking each symptom separately, the VSS and HPPD groups did not differ among themselves or with the 2014 cohort with regards to the frequencies of each symptom.

	VSS (*n*=1061)	VS (*n*=43)	HPPD (*n*=70)	Schankin et al. (*n*=78)
Types of static				
Black and white	609 (58%) [0.54-0.60]*	17 (40%) [0.26- 0.54]	30 (44%) [0.32-0.55]	34 (44%) [0.33-0.55]
Coloured	467 (44%) [0.41-0.47]*	11 (26%) [0.15- 0.40]	26 (38%) [0.27-0.49]	15 (19%) [0.12-0.29]
Flashing	495 (47%) [0.44-0.50]*	11 (26%) [0.15- 0.40]	27 (40%) [0.28-0.50]	19 (24%) [0.16-0.35]
Transparent	555 (53%) [0.49-0.55]*	15 (35%) [0.22-0.50]	41 (60%) [0.47-0.69]	16 (21%) [0.13-0.31]
Total number of static types				
One	560 (53%) [0.5-0.56]*	36 (84%) [0.76-0.95]	44 (64%) [0.51-0.73]	71 (91%) [0.82-0.96]
Two	172 (16%) [0.14-0.19]	5 (12%) [0.05-0.25]	9 (13%) [0.07-0.23]	7 (9%) [0.04-0.17]
Three	70 (7%) [0.05-0.08]	0	3 (4%) [0.01-0.12]	0
Four	253 (24%) [0.21-0.27]*	2 (5%) [0.01 -0.16]	13 (19%) [0.11-0.29]	0
Associated visual symptoms				
Afterimages	861 (81%) [0.79-0.83]	1 (2%) [0.00-0.12]***	58 (83%) [0.72-0.90]	67 (86%) [0.77-0.92]
Trailing	626 (59%) [0.56-0.62]	0 ***	45 (64%) [0.53-0.75]	47 (60%) [0.50-0.70]
Blue field entoptic phenomenon	704 (67%) [0.63-0.69]	7 (16%) [0.08-0.30]***	47 (67%) [0.56-0.77]	62 (79%) [0.70-0.87]
Floaters	906 (86%) [0.83-0.87]	19 (44%) [0.30-0.59]***	54 (77%) [0.66-0.85]	63 (81%) [0.71-0.90]
Self-light of the eye	749 (71%) [0.68-0.73]	11 (26%) [0.15- 0.40]***	49 (70%) [0.59-0.80]	41 (53%) [0.42-0.63]
Flashes	668 (63%) [0.60-0.66]	9 (21%) [0.11-0.35]***	42 (60%) [0.48-0.70]	49 (63%) [0.52-0.73]
Nyctalopia	821 (78%) [0.75-0.80]	6 (14%) [0.07-0.27]***	54 (77%) [0.66-0.85]	53 (68%) [0.56-0.76]
Photophobia	856 (81%) [0.78-0.83]	3 (7%) [0.02-0.19]***	56 (80%) [0.69-0.88]	58 (74%) [0.64-0.83]
Total number of associated visual symptoms				
Mean ± SD	5.8 ± 1.7	1.3 ± .95 ***	5.9 ± 1.9	
Median, IQR	6.0, 7-5	1, 2-1	6.0,8-4.5	

Table 4 Characteristics and frequencies of visual snow symptoms.

n values (percentages within groups) [95% confidence intervals of proportions]
** p<0.05, ** p<0.01, *** p<0.001 measured accordingly by ANOVA or χ^2 tests. Column on the right shows comparison with 2014 study cohort (Schankin et al., 2014a).*

2.2.3 Predicting the severity of visual snow

In order to predict severity of visual snow, an ordinal logistic regression, with the number of visual symptoms experienced as dependent variable, was performed.

Using multiply imputed analysis, first a complete case analysis was completed, where any case with a missing value on either the outcome or the covariates was omitted from the analysis. Then, the same analysis was done using 10 imputed datasets, where a chained equations approach was used and the imputations stratified by gender. The parameter estimates were similar across both models. This is unsurprising since there was no missing data for the symptoms, and the level of missing data was low for most covariates (<2%), except for disease duration and presence of migraine. These two variables were added later to the data collection procedure and thus likely to be missing at random. One subject for whom gender was not specified was excluded from the analysis.

The results from this regression are shown in Table 5. The analysis indicated that females were approximately one-third more likely to experience a higher number of symptoms than males. Those reporting migraine were more than two and a half times more likely to experience a higher number of symptoms, and those with tinnitus around twice as likely to experience a higher number of symptoms. A test for an interaction between migraine and tinnitus was not significant, indicating that these two concomitant conditions exert independent and additive effects on the number of visual snow symptoms experienced. Neither age, disease duration nor type of onset were related to the number of symptoms experienced.

		Complete cases (*n* = 694)		Multiple imputations (*n*=1060)	
		OR	C.I.	OR	C.I.
Age		0.99	[0.97-1.01]	0.98	[0.97-1.00]
Female		1.34*	[1.02-1.75]	1.32*	[1.05-1.64]
Disease duration		1.00	[0.98-1.02]	1.00	[0.98-1.02]
Migraine		2.68***	[1.98-3.64]	2.67***	[1.96-3.64]
Tinnitus		2.10***	[1.55-2.85]	1.98***	[1.54-2.55]
Onset	From childhood	1.00	.	1.00	.
	Later (not sudden)	1.10	[0.70-1.74]	1.03	[0.68-1.56]
	Later (sudden)	1.02	[0.58-1.80]	1.03	[0.60-1.77]

Table 5 Ordinal logistic regression of frequency of additional visual symptoms.

** p<0.05, ** p<0.01, *** p<0.001.*

The results of the latent class analysis are shown in: Appendix A - Latent class analysis. This was performed first on VSS subjects only (Appendix A - Latent class analysis-1), with the exclusion of the one subject for whom gender was not defined (*n* = 1060). Model fit criteria suggested that a two class solution provided the most parsimonious explanation of the data, where classes 1 and 2 accounted for x and y of the sample, respectively. The classes that were obtained separated the patients into groups based on additional visual symptom frequency. Logistic regression indicated that the same variables as the ordinal logistic regression for symptom frequency were related to latent class membership (Appendix A - Latent class analysis-2). The same analysis was then performed on VSS and VS subjects (*n* = 1104; Appendix A - Latent class analysis-3), excluding only the ones with HPPD. The analysis showed that a third latent class was obtained with this further step, however, the model still showed a group separation solely based on additional visual symptom frequency.

2.3 Discussion

In the questionnaire study, a large cohort of patients with visual snow has been described and analysed.

2.3.1 Visual snow phenotype

In this cohort, subjects with VSS were usually young and most commonly presented with black and white or transparent static, as well as a high number of additional visual symptoms. It is highly likely that the method of recruitment used here was biased to the selection of a younger population; this is somewhat confirmed by a very recent population-based study that identified the average age of patients with visual snow syndrome in the UK to be around fifty years of age (Kondziella et al., 2020). Given that the results from the current study are in line with the previous one by Schankin and colleagues, it is possible that younger patients with visual snow, who present higher levels of disability than those seen in the general population, are more likely to seek a diagnosis and reassurance on their symptoms, as well as to proactively volunteer for participation in this type of research.

Even if there was no specific gender prevalence, being of female gender was significantly associated with reporting increased severity of the condition. The visual static occurred in different combinations of colour. Of the common visual disturbances, floaters, afterimages and photophobia were almost invariably present, possibly constituting a hallmark of the syndrome. The disorder usually started in early life, and in many cases patients could never recall seeing differently. In a significant number of subjects, on the other hand, visual snow started abruptly and

spontaneously. This sudden onset was not necessarily related to a higher number of symptoms.

2.3.2 Homogeneity and spectrum of visual snow

Another important finding made clear from the study is that once specific criteria are defined and followed, visual snow is a recognizable disorder, with a very homogenous clinical presentation. The description of the primary symptom (i.e. the static) was highly reproducible across the study cohort, with only a few subjects actually presenting a visual disturbance not attributable to visual snow. The overall clinical presentation was quite similar across the subjects and with the second largest cohort in the literature. Some small variations are probably attributable to different sample sizes or different methodology.

The criteria for the syndrome also eliminated false positive subjects. In fact, only a small minority of self-reporting patients consecutively recruited in the study did not fit the full syndrome definition. In these subjects, early recognition of visual snow even in the absence of additional visual disturbances is nonetheless important. These symptoms in fact characterize a higher severity and define the VS syndrome, but are not a *sine qua non* for visual snow itself.

These results indeed highlight that different patients with visual snow manifest with different degrees of severity, configuring this condition as a 'spectrum-type' disorder. A severe end of the spectrum seems to be represented by those patients who have static with all the visual disturbances and are highly affected by them, and a mild one by those who only have static and are not bothered by it, even considering it normal for most of their lives. This theory is reinforced by the fact that visual snow syndrome

and visual snow did not differ in their key clinical features, such as average age, gender distribution, mode and age of onset. They did however differ when it came to comorbidities, which were more likely to be found within the syndrome in patients with a higher number of associated symptoms (i.e. a more severe condition) and were less frequent in subjects with visual snow but no syndrome with respect to VSS patients. This is also emphasized by the latent class analysis (Appendix A - Latent class analysis) showing that visual snow does not present with specific biological subtypes and is classified predominantly on its severity (measured with the burden of additional symptoms).

2.3.3 Visual snow comorbidities

Visual snow has two main comorbidities, migraine and tinnitus (chapters 1.3 and 0) (Bessero et al., 2014; Fraser et al., 2018; Lauschke et al., 2016; Rastogi et al., 2016; Schankin et al., 2014a; Simpson et al., 2013; Unal-Cevik et al., 2015). The presence of these comorbidities in a larger sample of VS subjects was here confirmed, with a further demonstration that both conditions are associated with a worse presentation of visual snow, defined by having more additional visual symptoms. Interestingly, these comorbidities independently predicted the affinity to a severity class in the latent class model, as well as the number of additional symptoms in the ordinal logistic regression.

Tinnitus is a common disorder in the general population, with a prevalence ranging between 5% and 25% (Kim et al., 2015; Shargorodsky et al., 2010; van den Berge et al., 2017; Wu et al., 2015). In this cohort, three quarters of VSS patients also had

tinnitus, suggesting a more than chance association between the two conditions. On a theoretical basis, visual snow and tinnitus may represent two different manifestations of a similar disorder, which is the perception of a sensory stimulus that is not present or is sub-threshold.

Given that tinnitus is not only more frequently present, but also predicts the severity of visual snow, it is possible that both disorders share a common pathophysiological mechanism, which, if sufficiently active, can manifest clinically with both conditions. These hypothesized mechanisms could involve the already described thalamo-cortical dysrhythmia, or an altered cortical excitability, allowing again to hypothesize visual snow as a complex abnormality of sensory perception, potentially involving multiple senses at once, as outlined in chapter 0.

A similar dishabituation mechanism common to migraine (Coppola et al., 2007b) and visual snow would explain the worsening of the VS condition when migraine is present, as well as the strong comorbidity between the two disorders. The presence of associated visual symptoms, enhanced entoptic phenomena in particular, also potentially points to a disorder of habituation and sensory processing, which allows the perception of stimuli that are normally ignored by the brain. A migrainous pathophysiology alone however is not sufficient to explain the visual snow biology, as detailed in chapter 1.3. This is also confirmed by the fact that most preventive migraine medications used empirically show very little effect in visual snow (Puledda et al., 2017a).

Another important issue with visual snow, which was tackled in this questionnaire study, is the assumption that its symptoms could be due to consequences of hallucinogen intake, i.e. to hallucinogen persisting perception disorder. HPPD is a condition codified in the Diagnostic and Statistical Manual of Mental Disorders (DSM-V) (American Psychiatric Association, 2013) characterized by the re-experiencing of perceptual symptoms ('flashbacks' - typically of visual type), which follow the cessation of the use of a hallucinogenic, and that were experienced during the intoxication (Halpern and Pope, 2003). Visual snow and HPPD indeed share some clinical aspects, mostly characterized by the possibility of the latter to manifest with visual static, palinopsia, flashes and other types of visual dysperceptions (Abraham, 1983; Halpern and Pope, 2003; Martinotti et al., 2018). Recent literature seems to suggest that HPPD can be distinguished into two main entities. In type 2 HPPD the visual symptoms are constant or near-constant (Halpern et al., 2018), and this is consistent with the group of subjects from this cohort.

In this study, to avoid any possible confounding overlap between HPPD and visual snow, strict criteria to identify VSS and VS were applied. Twelve months from the intake of any recreational drugs was considered as an appropriate time to exhaust possible effects of psychotropic substances on the visual system, given that most cases of hallucinogenic 'flashbacks' usually appear a few weeks or months after the first intake of psychedelics (Abraham et al., 2002). Any subjects exposed within this time frame were excluded from the visual snow groups. This has allowed to confirm that visual snow pathophysiology does not have a connection with the use of recreational substances. Further, it allowed analysis of a group of patients presenting with the VSS phenotype, but for which HPPD could not be excluded. These subjects

were mostly male - although this might be due to substance use being generally more common in men than women (Smith, 2013) - and exhibited a later onset of visual snow symptoms, in most cases with an abrupt start. They, however, fulfilled all remaining criteria for the VS syndrome and did not differ from the main VSS group with regards to clinical visual snow characteristics. This suggests an interesting overlap between VSS and drug intake, and most importantly that HPPD can manifest in the VSS clinical spectrum. It is possible that these conditions represent different aspects of the same disorder, or perhaps two distinct conditions with shared pathophysiological mechanism; or further, that hallucinogens can trigger visual snow syndrome in susceptible subjects.

2.3.4 Limitations

An important limitation of this survey, aside from the described selection bias, was related to fact that it did not specifically capture psychiatric comorbidities and psychological consequences of visual snow. As specified in the introduction (1.2), these conditions have been reported in previous publications, and explain at least part of the disability and suffering experienced by patients. While a focus on these conditions has been part of the clinical approach to VSS patients in this research group, a conscious decision was made at the start of the study to deliberately exclude questions focusing on anxiety and depression from the questionnaire. This was done following extensive dialogue with the patient self-help groups, for whom it was essential to destigmatize visual snow from the prejudice of considering it as a simple functional disorder, or even attributable to malingering.

3 Magnetic resonance imaging study: general methods

In this chapter I will present an overview of the general methods for the MRI project. This study was approved by the London - City & East Research Ethics Committee (Reference number: 16/LO/0964).

As the MRI study involved exclusively patients with the complete visual snow syndrome, the terms visual snow and visual snow syndrome, as well as their respective abbreviations (VS and VSS), will be used interchangeably within the relevant chapters.

Part of the data presented here are currently in press in a peer-reviewed journal (Puledda et al., 2020a) or have been submitted for peer-review (see Publications).

3.1 Subject population and recruitment

Twenty-four patients with a diagnosis of visual snow syndrome following the current criteria (Table 1) and an equal number of age and gender matched healthy volunteers were selected for the study. This number of subjects per group was chosen on the basis of previous literature (Murphy et al., 2011; Thirion et al., 2007).

Patients were recruited by email, re-approaching subjects who had previously contacted the study team at King's College London asking to participate in research studies. Healthy volunteers were recruited through internal advertisement at King's College London.

Recruitment was limited to individuals of 20–60 years of age with no contraindications to MRI, no serious medical conditions, consumption of no more

than five cups of coffee per day and who were naïve to any type of recreational drugs, including cannabis. This was, again as in the questionnaire study (chapter 2), in order to exclude any possible misdiagnosis or overlap with HPPD, and to allow homogeneity between the two subject cohorts. Any participant taking recurrent medications with an action on the central nervous system was excluded from the study. Patients with a history of psychosis, depression or psychological diseases that were thought to affect the patient's neural pathways or requiring ongoing psychoactive drugs were excluded from the study. Volunteers were selected based on matching age (± 5 years) and gender of the patient population. All controls with a history of migraine or recurrent headaches were excluded. All participants gave their informed consent.

There were no significant differences with regards to age (mean ± standard deviation for VS patients 28 ± 6 and controls 28 ± 5; $p = 0.8$), gender (female: male ratio for VS patients 12:12 and controls 14:10; $p = 0.6$) or handedness (right: left ratio for VS patients 21:3 and controls 23:1; $p = 0.3$) among the patient and control groups. Demographic characteristics and clinical features of the visual snow patient group are summarized in Table 6, along with presence of migraine and tinnitus comorbidities and list of concomitant medication at the time of the study.

G, Age	Onset of VS	Static type	Additional symptoms								TIN	MIG	Meds
			A	T	B	F	S	FL	N	P			
F,33	#	BW,C, F,T	+	+	+	+	+	+	+	+	+	+	Multivitamins
M,28	10	C	+				+				+		
M,29	26	BW	+		+	+	+	+		+	+	+	L-thyroxine, paracetamol PRN
M,25	19	BW,F,T	+	+	+	+	+	+	+	+	+	+	
F,20	#	BW,T	+		+	+	+	+		+	+	+	Fexofenadine
M,31	9	BW,F	+		+	+		+	+		+		Pimecrolimus topical, betamethasone topical
F,34	#	BW,C, F	+		+		+	+	+			+	
F,23	#	BW,C	+	+		+	+	+	+			+	OCP
F,21	#	BW,F,T	+	+	+	+	+	+	+	+	+	+	Paracetamol PRN
M,27	21	BW	+	+	+	+	+	+		+			
F,26	26	BW	+	+	+	+	+	+	+	+	+		Multivitamins, ibuprofen PRN
F,43	43	BW,F,T	+		+	+	+		+		+		
F,34	12	BW		+	+	+	+		+	+	+	+	
F,22	#	T	+		+	+	+	+			+	+	Multivitamins, Paracetamol, Nexplanon
F,34	31	BW,T	+	+	+	+	+	+	+	+	+	+	
M,22	15	F,T			+	+	+		+				
F,25	#	T	+	+	+	+	+			+	+		Salbutamol inhaler, multivitamins
F,26	25	BW,C, F,T	+	+	+		+	+	+	+	+	+	Paracetamol PRN
M,22	17	F	+		+	+			+	+	+	+	Magnesium
M,31	24	BW	+	+	+	+	+	+		+		+	Paracetamol PRN
M,35	33	BW	+	+	+	+	+		+	+	+	+	L-thyroxine, CQ10
M,19	#	BW				+				+	+		
M,29	#	F,T		+	+	+	+				+		
M,30	#	BW,F	+	+	+	+	+	+	+		+	+	Fluticasone nasal spray

Table 6 Demographic and clinical characteristics of VS patients in the MRI study.

 # = Symptoms present for as long as patient could recall;
+ = present;
Age and onset of VS are presented in years
G = Gender
Meds = Concomitant medication
BW = black and white static; C = coloured static; F = flashing static; T = transparent static;
A = Afterimages; T = Trailing; B = blue-field entoptic phenomena; F = floaters; S = self-light of the eye; FL = flashes; N=nyctalopia; P = Photophobia;
TIN = Tinnitus
MIG = Migraine
OCP = oral contraceptive pill
PRN = pro re nata (i.e. when necessary)

3.2 Study protocol

The study involved a telephone interview, in which eligibility of the participant was assessed, followed by two visits to the Clinical Research Facility for patients and a single visit for healthy controls (HCs). During the first visit patients had a full medical history taken, as well as a general examination and neurological examination, blood pressure and heart rate monitoring. If patients were deemed eligible they were invited for a second visit in which the scanning took place, that lasted approximately 70 minutes. Healthy controls were invited for the scanning visit directly, if they were considered eligible during the telephone interview.

All participants were scanned at the same time of day, between 9 and 12 am, as it is known that circadian rhythms can influence regional cerebral blood flow and consequently the interpretation of neuroimaging data (Hodkinson et al., 2014). Subjects were instructed to consume a light breakfast and to avoid caffeine on the morning of the visit. Participants were asked to refrain from the use of any type of medication for 24 hours prior to scanning. If this was not avoidable, the scanning visit was postponed. Female patients were asked to keep a menstruation diary for the time of the study, in order to avoid scanning on days of active menstruation. For any patient with a concomitant migraine diagnosis, scanning was avoided in the ictal period (i.e. 48 hours before or after an attack).

3.3 Imaging procedure

All scans were conducted on a 3T General Electric MR750 MRI scanner at the NIHR-Wellcome Trust King's Clinical Research Facility, King's College Hospital, London, using a 12-channel head coil. The scanning protocol was the same for both groups and was conducted over a single session.

First, high resolution 3D T1-weighted IR-SPGR images were acquired with the following parameters: TR = 7.312 ms; TE = 3.016 ms; TI = 400 ms; FOV = 270 mm; matrix = 256x256; slice thickness = 1.2 mm; 196 slice partitions, ASSET factor = 1.75, in-plane resolution = 1 mm (Jack et al., 2010).

Two separate pCASL scans and two separate functional connectivity fMRI scans were acquired for each individual, respectively, at rest while looking at a blank, dark screen (baseline) and during a visual task simulating visual snow (described in section 3.4). These scans were done in random order at each visit.

Proton spectra for MRS were acquired using a point resolved spectroscopy (PRESS) protocol with chemically selective suppression (CHESS) water suppression (Haase et al., 1985), while patients were at rest. A 1.5x3x1.5 cm^3 voxel was placed over the right lingual gyrus. Anatomically, this was defined by identifying the area between the calcarine and collateral fissure, as anterior as possible in order to avoid areas of exclusive retinotopic representation. Voxel location was adjusted for each participant to maximize grey matter content. Figure 3.1 shows an example location of the voxel.

Finally, task-based BOLD activity was quantified with a single fMRI experiment, characterized by a block-design paradigm of visual stimulation and rest blocks of 40

seconds each. Participants were presented with either a dark screen or the same simulation of visual snow as above (described in section 3.4), and were asked to keep their eyes open for the duration of the entire fMRI experiment. The onset of visual stimulation was triggered by the start of the scan acquisition.

Unless otherwise specified, all MRI data was processed and analysed using the Statistical Parametric Mapping software suite, version 12 (SPM 12; www.fil.ion.ucl.ac.uk/spm/) on a MatLab platform (MATLAB R2017a; (https://uk.mathworks.com/). For all voxel-wise analyses, significance was defined with an initial cluster-forming voxel threshold of $p < 0.001$ and subsequent family-wise error (FWE) correction, on the basis of cluster extent, at $p < 0.05$, using the Gaussian random field theory. Images are displayed with left corresponding to the left side of the brain and vice versa, with the only exception of Figure 3.1. Cluster size is referred to as k.

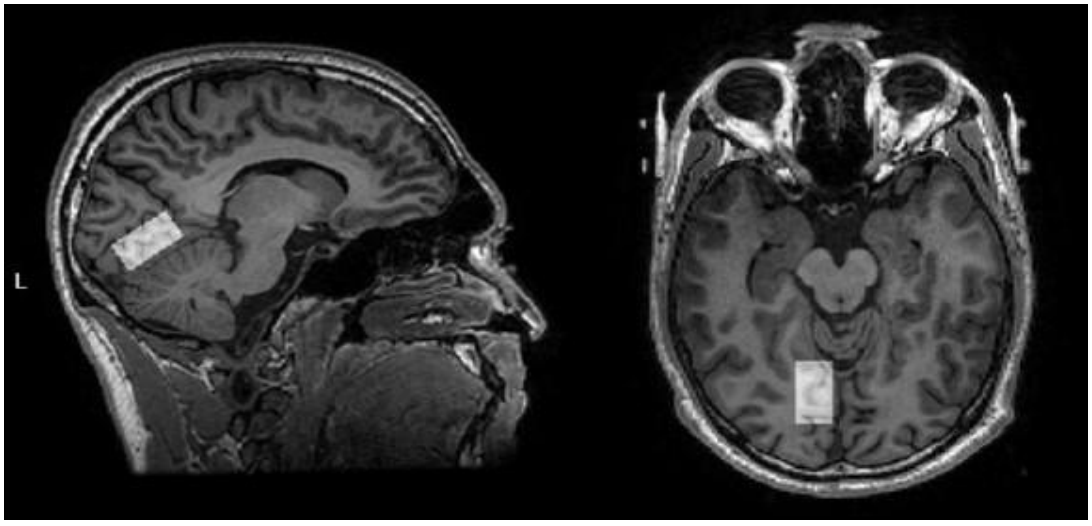

Figure 3.1 Example of MRS voxel placement in the right lingual gyrus.

3.4 Visual snow simulation

For the visual stimulus sequence of one pCASL acquisition, one functional connectivity acquisition and for the BOLD visual task, a simulation video mimicking the static of visual snow was developed and shown to all subjects in the scanner. The visual stimulus was projected onto a screen, viewed by the participants through a mirror of 18 cm width positioned at 8 cm from the eyes, with the maximal extent of visual field stimulated ±48 degrees along the horizontal meridian assuming central fixation.

The visual task was developed by creating 20 bitmaps that were displayed in a continuous loop with 20 ms between frames. Each bitmap was created as random 'snow squares' on a black background. Snow squares were blocks of 2 x 2 pixels (pixel size 1.0 mm x 1.0 mm). Five values of greyness were used to create these squares. They were: 40, 80, 120, 160 and 200, where 0 = black, 255 = white. Luminance values from the Microsoft Windows software (Cd/m2 values would not be accurate for small individual dots) for these were, respectively: 38 Lum, 75 Lum, 113 Lum, 151 Lum, 181 Lum. For each greyness value, two snow squares were created. These snow squares were randomly distributed within the black background in the ratio of 10:200 snow squares to background squares. See Figure 3.2 for a screenshot of this simulation.

At the end of each scanning session, VS patients were asked to rate the similarity of the simulation to their own visual snow experience by rating the following parameters: density, speed, colour and size. A summary of the patients' evaluations can be found in Appendix B - Evaluation of visual snow MRI simulation.

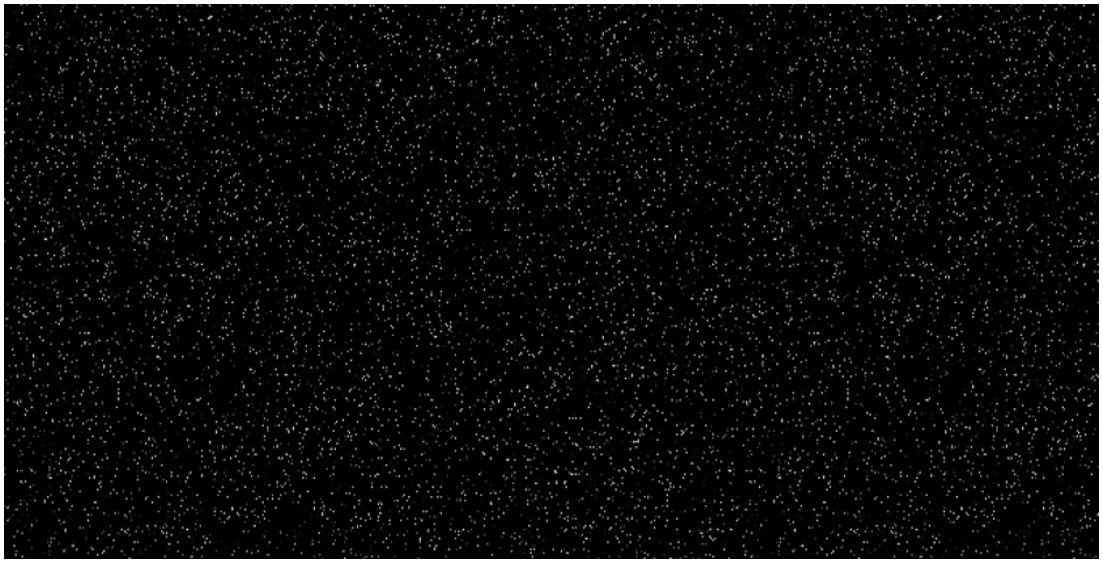

Figure 3.2 Screenshot of visual snow simulation video.

3.5 Statistical analysis

All descriptive statistics, between-group differences and correlation analyses for the imaging study were performed with SPSS Statistics Version 24.0 for Windows (IBM, Armonk, NY: IBM Corp.; http://www.spss.com). Shapiro-Wilk Test was used to assess normal distribution of variables. Student's *t*-test or Mann-Whitney *U* test for non-parametric variables were used to compare mean values between groups. Pearson correlation coefficients or Spearman's Rho were used to analyse correlations between variables. A moderated regression analysis was used to determine if relationships between variables depended on group membership. $P < 0.05$ was considered significant.

4 Structural imaging in visual snow

This chapter will outline the methods, results and discussion for the structural imaging part of the MRI project.

4.1 Methods for voxel based morphometry

High resolution 3D T1-weighted IR-SPGR images were acquired as part of the neuroimaging experiment, with the parameters described in section 3.3.

Prior to analysis, raw T1 images were visually inspected for artefacts and structural abnormalities that could interfere with the analysis. None of the acquired images were discarded.

VBM to localize regional differences in grey and white matter volume was conducted by applying diffeomorphic anatomic registration exponentiated lie algebra (DARTEL) algorithm following the default parameters (Ashburner, 2007). The first step of the procedure segments each subject's image into grey matter, white matter and cerebrospinal fluid (CSF). The second step creates a DARTEL population template derived from nonlinear deformation fields for the segmentation procedure and registers all individual deformations to the DARTEL template. In the next registration step, a non-linear warping of the segmented images allowed to register the DARTEL template in Montreal Neurological Institute (MNI) space. Furthermore, the voxel values in the tissue maps are modulated by the Jacobian determinant calculated during spatial normalization. Total intracranial volume (TIV) was calculated for each subject within Matlab from the sum of the GM, WM and CSF tissue components.

Finally, all modulated and normalized grey and white matter segments were smoothed with full width at half-maximum isotropic Gaussian kernel of 8-mm.

Within the morphological analysis, cerebellar anatomy using a high-resolution atlas template (SUIT) was also investigated. To analyse regional cerebellar volumes the SUIT toolbox (http://www.icn.ucl.ac.uk/motorcontrol/imaging/suit.htm/) within SPM12 was used. This toolbox provides a high-resolution atlas template of the human cerebellum and brainstem that preserves the anatomical detail of cerebellar structures, as well as dedicated procedures to isolate automatically cerebellar structures from the cerebral cortex and to normalise accurately cerebellar structures to this template. Prior to normalisation, the individually created isolation maps were loaded into FSLView (www.fmrib.ox.ac.uk/fsl/) where they were visually inspected against the cropped image and hand corrected if necessary. Using the inverse of the resulting normalisation transform, a parcellation of the cerebellum was obtained, based on the probabilistic magnetic resonance atlas of the human cerebellum (Diedrichsen et al., 2009) provided within the SUIT toolbox. Volumes of interest were then overlaid onto each individual participant's structural scan and inspected to ensure accurate registration.

VBM analyses included whole-brain and parcellated cerebellar GM and WM analyses, as well as region-of-interest (ROI) grey matter analyses.

For the whole-brain voxel-wise analysis, GM and WM volumes between subgroups of VSS patients and controls were reviewed with 2-sample *t*-tests. Total intracranial volume, subject age, gender, handedness and number of disease years were added

as covariates in the model. We ran a second model with migraine history as a covariate, since this condition was not present in the control group (3.1). An absolute threshold mask of 0.1 was used on both the GM and WM to avoid possible edge effects around the border between the two.

For the cerebellar analysis, morphological group differences in parcellated cerebellar grey and white matter volumes were assessed using the general linear model. TIV of each participant was entered into the design matrix as a nuisance covariate.

ROI analyses were carried out in the following visual areas: bilateral primary visual cortex (V1/V2), visual motion processing areas V5 and the pulvinar. To create ROIs for these anatomical areas, the 'wfu_pickupatlas Anatomical Library' (https://www.nitrc.org/projects/wfu_pickatlas) as implemented in the SPM toolbox was used, with the exception of the V5 ROI which was created from the 'Juelich Histological Atlas' within FSLeyes. The resulting images were used as a binary mask in the map resulting from group comparisons. Two *a priori* ROIs were also used, based on coordinates from the previous PET study on visual snow (see chapter 1.3) (Schankin et al., 2014b). These were namely the right lingual gyrus (x = 16, y = -78, z = -5) and left cerebellum (x = -12, y = -62, z = -9); the coordinates were used for small volume correction (SVC) with a sphere of radius 10mm. Having analysed multiple ROIs, adjusted *p* values corrected for FDR (following the Benjamini-Hochberg's procedure) are reported as well, in order to account for multiple comparisons correction.

4.2 Results: morphological changes in the VS brain

4.2.1 Whole-brain VBM-DARTEL analysis

The average total intracranial volume was measured for both groups, and no differences were found between visual snow patients and controls (1465 ± 113 ml vs. 1450 ± 146 ml respectively; $p = 0.6$).

A whole-brain voxel-wise analysis comparing grey and white matter volumes between groups was performed. This analysis revealed a cluster of increased GM volume in patients with visual snow with respect to controls in the left primary visual cortex (x = -2, y = -98, z = 3; k = 594; $p = 0.007$ uncorrected, $p = 0.06$ FWE; Figure 4.1). In this whole-brain analysis, the cluster did not quite reach the significance threshold. However, when the cluster forming threshold was reduced to $p = 0.005$, this area was significant ($p = 0.02$ FWE corrected).

In order to verify if this difference in GM volume was in effect lateralized, for exploratory purposes the cluster-forming threshold was lowered to $p = 0.01$. With this lower statistical threshold, the significant cluster appeared to extend to the homologous region of the contralateral side as well.

No differences in white matter volumes were found between the two groups.

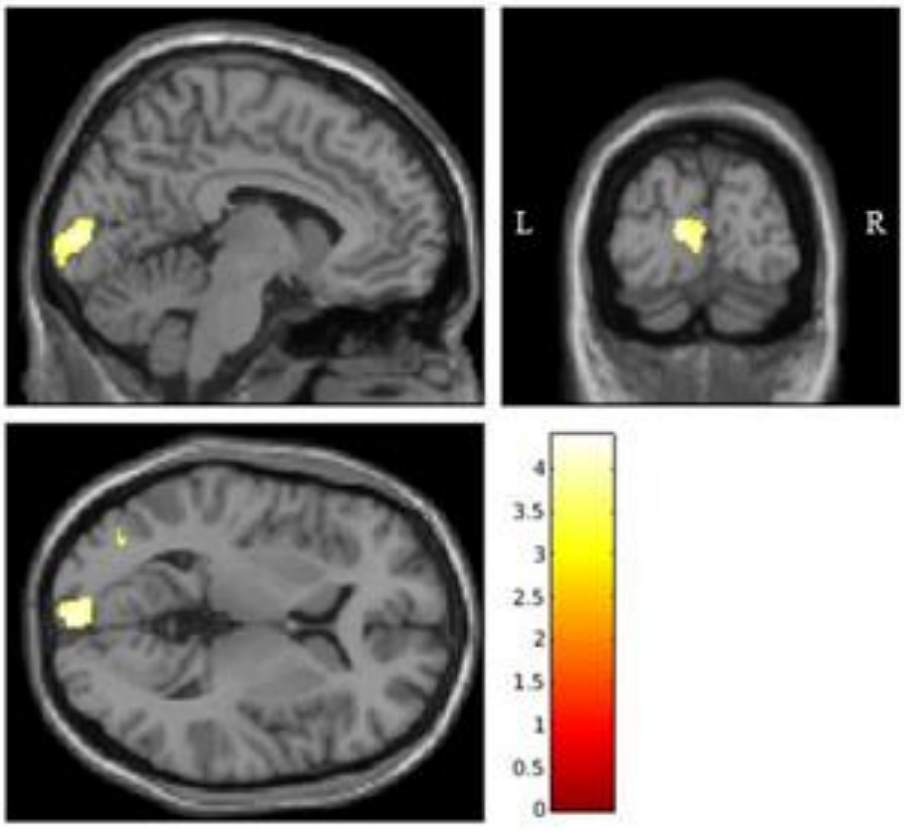

Figure 4.1 Left primary visual cortex increases in grey matter volume in VS patients with respect to controls.

4.2.2 ROI analysis of GM volumes

As explained in chapter 4.1, ROI analyses were carried out in the bilateral primary visual cortex (V1/V2), bilateral area V5 and bilateral pulvinar.

Results for this constricted analysis showed a significant GM volume increase in the left V1/V2 area (main cluster: x = -3, y = -94, z = 0; k = 22; p = 0.04 FWE). This area was analogous to the whole-brain analysis (section 4.2.1), confirming its significance. There was also a significant cluster of GM volume increase in the left V5 area (x = -38, y = -75, z = 4; k = 32; p = 0.04 FWE; Figure 4.2) in VS. When covarying for migraine

presence, both of these areas survived significance. However, following FDR correction for multiple comparisons, these regions did not survive significance.

There were no other significant grey matter volume differences for the remaining regions of interest.

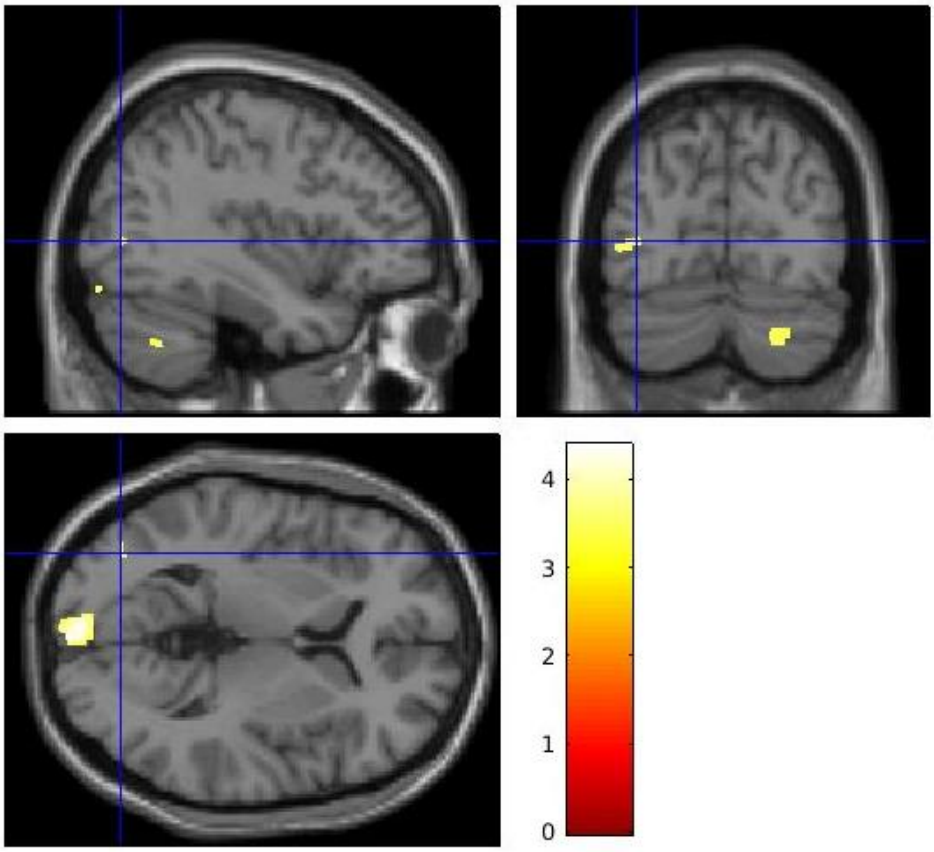

Figure 4.2 ROI analysis showing significant GM volume increase in left V5 in visual snow patients with respect to controls.

4.2.3 Cerebellar analysis with SUIT

Cerebellar images for one control subject had to be discarded due to poor image quality.

While the whole-brain VBM analysis did not reveal any specific morphological differences in the cerebellum of VS patients, when analysing the parcellated volumes created with SUIT, there was an area of significant increase of grey matter volume in crus I/lobule VI of the left cerebellar hemisphere (x = -12, y = -62, z = -23; k = 25; *p* = 0.02 FWE; Figure 4.3).

There were no significant WM volume differences or GM volume decreases in the cerebellum in patients with VS with respect to healthy controls.

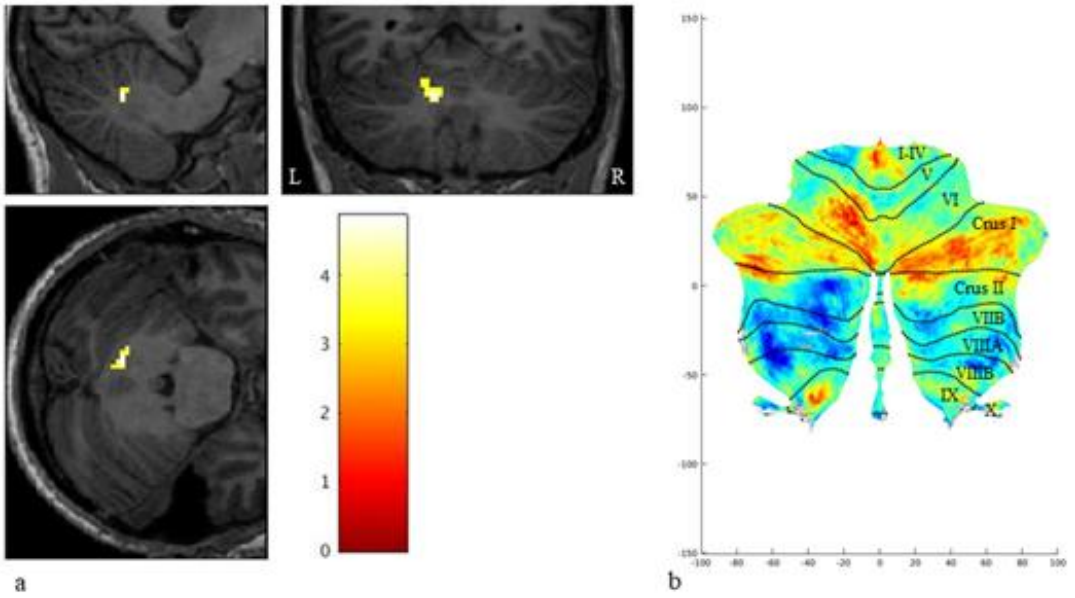

Figure 4.3 Cerebellar morphological analysis using SUIT

a) Area of cerebellar grey matter volume increase in VS patients. GM volume differences between groups are outlined over parcellated cerebellar T1 images.
b) Cerebellar flatmap of plotted t-values from VS patients compared to controls with labels for anatomical regions.

4.2.4 Summary of volumetric changes in VS

In summary, the areas of significant grey matter volume increase in patients with VS compared to healthy controls involved the left primary visual cortex, the left visual motion area V5 and the left cerebellar cortex in lobule VI/crus I (Figure 4.4).

Details for these significant clusters, which derived either from the ROI analysis or the SUIT analysis, can be found in Table 7.

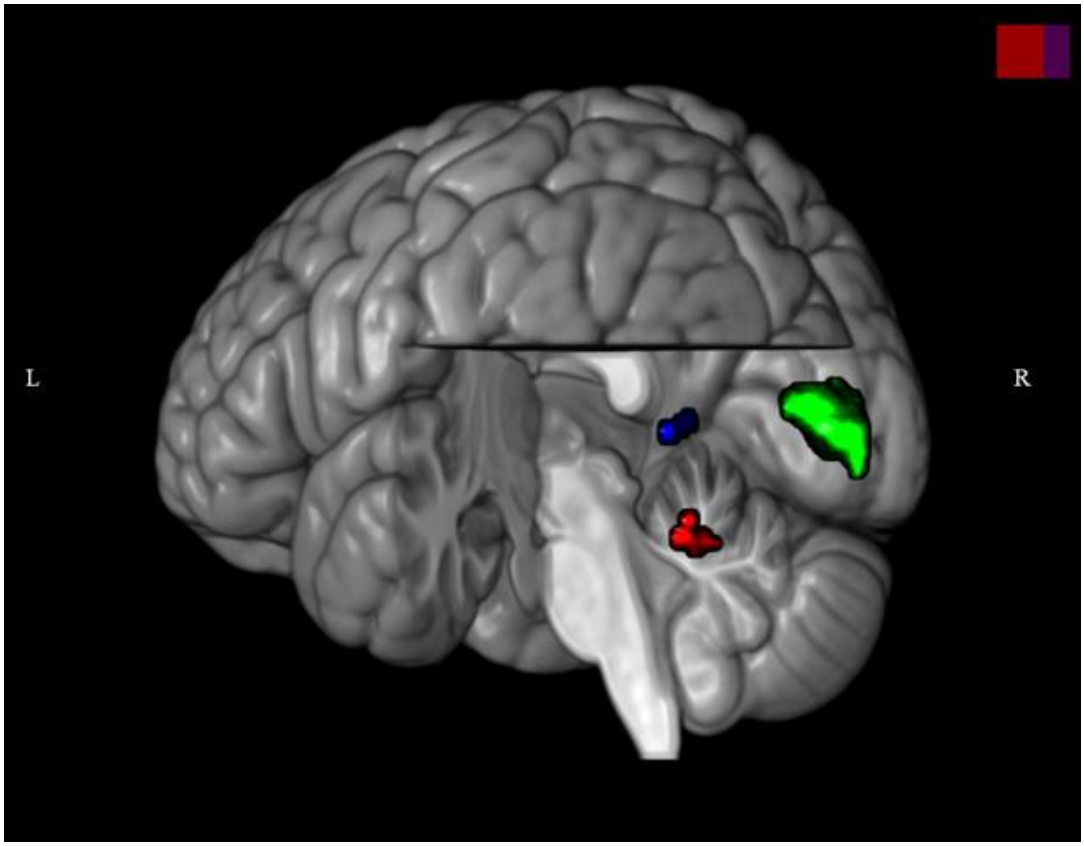

Figure 4.4 Render illustration of the three brain regions of increased grey matter volume in patients with visual snow syndrome, compared to healthy controls. Left V1 cluster is illustrated in green; left V5 cluster in blue; left cerebellum cluster in red.

Region	*p* (FWE)	*p* (FDR)	T-value	k	MNI coordinates		
					x	y	z
Left V1	0.04	0.01	4.06	22	-3	-94	0
	0.03	0.01	3.95	33	-6	-90	4
	0.04	0.01	3.94	12	-9	-87	0
	0.04	0.01	3.56	16	-2	-99	-4
Right V1	/						
Left V5	0.04	0.01	3.52	32	-38	-75	4
Right V5	/						
Left pulvinar	/						
Right pulvinar	/						
Right lingual gyrus	/						
Left cerebellum	/						
Cerebellum Crus I/lobule VI	0.02		4.86	25	-12	-62	-23

Table 7 Areas of grey matter volume increase in patients with visual snow compared to controls, showing the eight examined ROIs, with initial p values (FWE) and adjusted p values for FDR correction. In the final row, results from the SUIT cerebellar analysis are shown. / stands for absence of suprathreshold clusters.

4.2.5 Correlations with clinical features

The contrast tissue volume estimate values from the left V1, left V5 and cerebellar *a priori* defined ROIs were extracted for all participants. This was done in order to avoid circularity (Kriegeskorte et al., 2009). These values were then correlated with the following variables: age, gender, handedness (in both groups), sum of associated visual symptoms, migraine, tinnitus presence and disease years (in patients only). No significant correlation was found.

4.3 Discussion of VBM findings

4.3.1 Overview of grey matter changes in visual snow

In this chapter, three different voxel-based morphometry approaches (whole-brain, seed-based and parcellated cerebellar images) were used to determine structural brain changes pertaining to visual snow. The main finding was that patients with VS exhibit morphological changes in the grey matter volume of the left visual cortex (areas V1 and V5) and cerebellum, when compared with matched healthy controls (Figure 4.4 and Table 7). It must be noted that the left visual cortical areas did not survive significance following FDR multiple comparisons corrections across ROIs. However, considering the exploratory nature of this first VBM analysis in VSS, that the abnormality in left V1 matched the whole-brain analysis, and the fact that the changes all point in the same direction of a lateralized cortical GM volume increase, it is possibly still worth discussing the significance of these results.

The morphological differences involving the primary visual cortex and the visual motion network are in line with the perception of a moving, pan-field visual illusion in VS. The *a priori* interest in these areas was fully justified in the context of a condition that is characterized by the perception of a moving visual illusion. The fact, however, that these areas also emerged from the whole-brain analyses and not just in the seed-based analysis, confirms their importance in VS. The further involvement of important cerebellar areas, suggests that aside from a sensory dysfunction of visual perception - which would have limited significant findings to primary visual areas - VS could also represent a broader network-type disorder, in which more

complex alterations of cognitive processing and integration of internal and external stimuli are at play. Given that the anatomical changes were not associated with clinical parameters, such as the total number of disease years and the number of associated visual symptoms, they may indeed represent an inherent trait of visual snow, rather than a consequence of the condition.

4.3.2 Primary visual cortex involvement

Considering that visual snow is a disorder linked to brain function, the absence of major changes in brain morphology was expected. Conversely, an altered structure of primary and secondary cortical visual areas is in keeping with the clinical experience of simple visual illusions typical of visual snow (Ffytche et al., 2010). Furthermore, GM increases in the primary visual cortex very clearly followed the calcarine fissure (Figure 4.1), showing a correspondence to the retinotopic mapping of the entire hemi-field.

The fact that the morphological V1 change was only found in the left side is more difficult to interpret. It is possible that this finding was due to a statistical issue, rather than to a truly lateralized morphological difference, given that a grey matter volume increase was also present in the same region on the right side when lowering the significance threshold.

4.3.3 Changes within the visual motion network

The visual motion network spreads from V1 dorsally to the parietal lobe, encompassing visual motion area V5 (Zeki et al., 1991) (chapter 0). As a result of

containing neurons characterized by large receptive fields and high sensitivity to speed gradients, this area is involved primarily in the integration of inputs from the primary visual cortex, decoding information and patterns of direction, speed and motion (Born et al., 2005). The motion network is also composed of sub-compartments within V1/V2, of area V3/V3A in the cuneus and finally of Brodmann area 7 in the precuneus (Braddick et al., 2001; Watson et al., 1993). It is also part of the dorsal stream, now renamed the 'how-pathway' (Goodale et al., 1992) (chapter 0), which integrates information on spatial localisation of incoming visual information for the purpose of skilled motor planning.

Therefore, an increased volume in area V5 confirms visual snow as, among other things, a disorder of complex visual processing.

4.3.4 Cerebellar alterations

In addition to the involvement of neocortical visual networks, the VBM analysis also showed differences in the lateral cerebellum in VSS patients when compared with controls. As discussed in chapter 1.3, the left lobule VI showed increased metabolism in a previous [^{18}F]-FDG PET study (Figure 1.4) in an area that is contiguous with the one found in the present study. This constitutes a possible link between a previously documented functional alteration of this condition and the underlying structural abnormality found here.

The cerebellar lobule VI is an area that plays a significant role in in spatial processing functions and particularly in the 'preparation' of somatosensory integration (Stoodley et al., 2010). Here, somatosensory information is actively integrated in a first step before the execution of an action. Furthermore, this structure has been

implicated in spatial processing, oro-facial movements (Dresel et al., 2005), and is reciprocally connected with the somatosensory neocortex (Middleton et al., 1998). Most importantly, the cerebellar lobule VI/Crus I forms part of the so-called 'cognitive cerebellum' (Stoodley et al., 2009), which, thanks to widespread cerebello-cortical connections, has a role in complex functions such as language, executive action and visual working memory (King et al., 2019). In particular, these cerebellar sub-regions have been associated with the fronto-parietal, attention and default mode networks (DMN) in resting state analyses (Guell et al., 2018). These networks are control systems that work in synergy when the brain is respectively involved in a task or at rest (Raichle et al., 2001; Shulman et al., 1997) and will be discussed in more detail in chapters 5 and 6.

4.3.5 A complex dysfunction of visual processing and brain networks

The finding that important pathways involved in integration and processing of visual stimuli, as well as action and attention networks, were simultaneously affected in visual snow syndrome is relevant. In a condition where internal visual information is constantly being perceived, a state of increased cortical activation, justified by a form of processing overload, is certainly plausible and in line with the hyperexcitation hypothesis (chapter 0). An increase in functional activation in certain cortical areas could in turn justify a localised increase in grey matter volume, such as the one found here.

5 Functional imaging in visual snow: arterial spin labelling

This chapter will outline the methods, results and discussion for the ASL functional imaging part of the MRI project.

5.1 Pseudo-continuous ASL methods

Whole brain CBF maps were generated by means of two 3D pseudo-continuous Arterial Spin Labelling MRI sequences, at rest and during a visual stimulation, as described in section 3.3.

Labelling of arterial blood was achieved with a 1825 ms train of Hanning shaped RF pulses of 500 µs duration in the presence of a net magnetic field gradient along the flow direction (the z-axis of the magnet). After a post-labelling delay of 2025 ms, a whole brain volume was read using a 3D inter-leaved 'stack-of-spirals' Fast Spin Echo readout, consisting of 8 interleaved spiral arms in the in-plane direction, with 512 points per spiral interleave. The images had 60 axial slice locations (3mm thickness) and an in-plane FOV of 240 × 240 mm after transformation to a rectangular matrix (TE/TR = 11.088/5180 ms, flip angle (FA) = 111°). A proton density image volume with the same parameters was acquired within the same sequence in order to use as a reference to compute the CBF maps in conventional physiological units (ml blood per 100 g tissue per minute).

The sequence used four background suppression pulses to minimise static tissue signal at the time of image acquisition. Four control-label pairs were acquired. CBF

maps were computed from the mean perfusion weighted difference image derived from the four control-label pairs, by scaling the difference image against a proton density image acquired at the end of the sequence, using identical readout parameters. This computation was done according to the formula suggested in the recent ASL consensus (Alsop et al., 2015). The entire acquisition time of each 3D-pCASL sequence was 6 minutes and 20 seconds.

Preprocessing of pCASL images (spatial normalisation) was performed using Automated Software for ASL Processing (ASAP (Mato Abad et al., 2016)) toolbox, which employs SPM 12. Computation of CBF maps was performed by the scanner computer using the following formula:

$$CBF = 600 \frac{e^{w/T_{1a}}}{2\varepsilon T_{1a}(1 - e^{-\tau/T_{1a}})} \frac{P}{\frac{R}{\lambda}}$$

in which P is the signal in the perfusion-weighted image (control–label), R is the signal in the reference image, ε is the combined efficiency of labelling and background suppression (~65%), w is the postlabelling delay (2025 ms), τ is the label duration (1825 ms), T_{1a} is the T_1 of arterial water, and λ is the brain/blood partition coefficient in mL/g.

For spatial normalization of the CBF maps to the space of the Montreal Neurological Institute within the ASAP framework, a multistep approach was used: CBF maps were co-registered to the high-resolution T1-weighted structural ADNI images, after coarse alignment of the origin of both images. Unified segmentation of the T1-weighted image normalised this image to the MNI space and was used to produce a 'brain-only' binary mask which was multiplied by the co-registered rCBF map to

produce an image free of extra-cerebral artefacts. The spatial transformation matrix was applied to the clean CBF images and then smoothed using an 8 x 8 x 8mm Gaussian kernel as described (Mato Abad et al., 2016).

The pCASL data were analysed using a voxel-wise general linear model. A whole brain flexible-factorial design using two-way ANOVA allowed analysis of changes in CBF related to group and stimulus effect. Mean global CBF was included as a covariate in the design matrix using ANCOVA, to account for inter-individual differences in global perfusion.

All brain locations are reported as x, y, and z coordinates in MNI space. A neuroanatomy atlas (Mai et al., 2008), as well as the Harvard-Oxford cortical and subcortical structural atlases from the FSL software (FSL 5; https://fsl.fmrib.ox.ac.uk/fsl/fslwiki), were used to identify the correct anatomical locations of clusters of statistically significant changes within MNI space.

To measure global CBF signal, the ASAP toolbox was used to extract average CBF values from a grey matter mask of each subject. Probabilistic grey matter images in MNI space, derived from the FSL voxel-based morphometry toolbox, were thresholded to produce a mask which included all voxels with a >20% likelihood of being grey matter. The mean global CBF value, defined as the mean of all grey matter voxels within the mask, was computed for each individual pCASL CBF map in each subject. Mean global CBF for patients and controls in both conditions were compared with standard *t*-test. Global CBF differences were tested in an ANCOVA model, while controlling for the underlying experimental condition (i.e. baseline vs snow-like stimulus).

5.2 Main pCASL results

The first approach in the pCASL analysis was to study changes in mean global CBF in the grey matter. As would be expected, there were no difference in values between the two groups, whether global CBF was measured at baseline (mean ± standard error 53.5 ± 10.6 in the VS group and 51.7 ± 12 in controls; $p = 0.6$), when looking at the snow-like stimulus (54.9 ± 10.5 in the VS group and 53.3 ± 12.8 in controls; $p = 0.6$) or when both conditions were averaged out (54.2 ± 10.5 in the VS group and 52.5 ± 12.3 in controls; $p = 0.5$). An ANCOVA analysis confirmed no significant differences in median global CBF values between groups, when accounting for stimulus type.

The following step was to perform whole brain voxel-wise analyses of CBF maps. These are detailed in the following sections, in a specific order: first the two groups (VS patients vs. healthy controls) were compared. This was done considering both conditions together, and then separately at rest and during the visual stimulus. The task effect of the snow-like stimulus vs. the baseline rest condition was then studied in both subject groups. Finally, the interaction effects between the two conditions (group and stimulus) were formally tested.

Given that changes in regional cerebral blood flow are indirectly associated with neuronal activity (as outlined in chapter 1.6.2), for simplicity the words ‘increases’ and ‘decreases’ - when referring to rCBF changes measured through pCASL - will be used interchangeably with ‘activations’ and ‘deactivations’, respectively.

5.2.1 Comparing VS patients to controls - group effects

Group effects with and without stimulus - by performing a whole-brain comparison for the main effect of group, both with and without the 'snow-like' stimulus condition, an extensive network of unilateral and bilateral brain regions showed an increase in regional CBF in patients with VS compared to healthy controls (Figure 5.1). Anatomic locations and descriptions of all the significant clusters are highlighted in Table 8. Areas are shown in coordinate MNI space with relative T scores and k values, as well as percentage of rCBF increase compared to the HC group.

Bilateral clusters of significant CBF change were found in the cuneus, precuneus, inferior parietal lobule (IPL), superior parietal lobule (SPL), supplementary motor area (SMA), frontal eye fields (FEF), premotor cortex, posterior cingulate cortex, middle frontal gyrus, angular gyrus (AG), post central gyrus, middle and superior occipital lobule. In the left hemisphere clusters were found in the primary auditory cortex, fusiform gyrus (FG), area VI of the cerebellum and supramarginal gyrus (SMG).

In order to exclude a migraine effect for the areas that emerged in the whole-brain analysis described here, a *post-hoc* analysis was performed in subjects without concomitant migraine (*n* = 9) compared to healthy volunteers (*n* = 24). Results from this analysis are outlined in: Appendix C - pCASL *post-hoc* analysis.

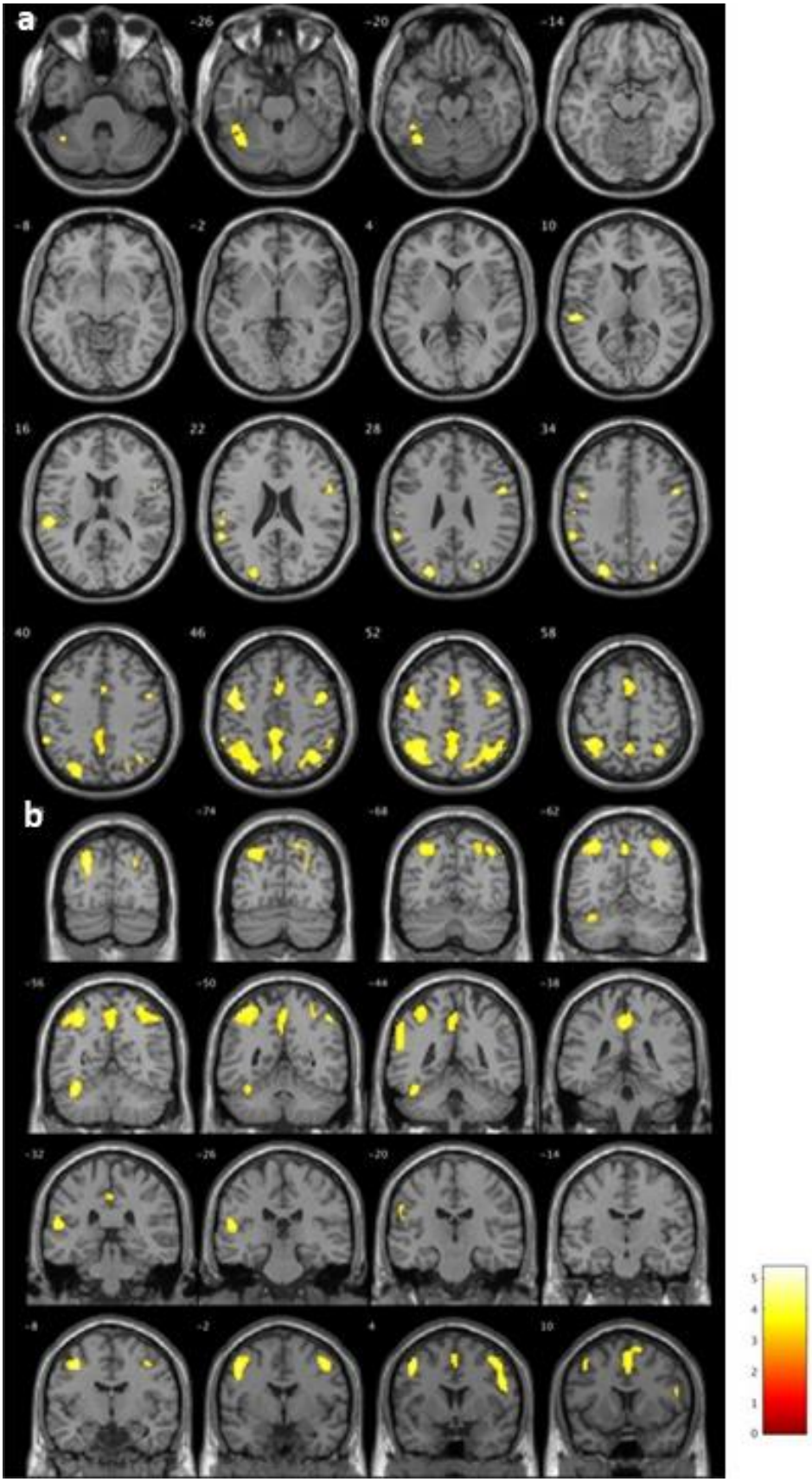

Figure 5.1 Clusters of significant rCBF increase in VS patients compared to HCs when accounting for main effect of group (with and without stimulus) in axial (A) and coronal (B) view.

Brain region Cluster description	Peak description	T	k	Peak coordinates			% rCBF increase patients
				x	y	z	
Cuneus and precuneus	Right cuneus, precuneus, IPL, SPL, angular gyrus, superior occipital lobule, post central gyrus, BA 7	5.37	742	52	-54	54	15%
Cuneus and precuneus	Left cuneus, precuneus, IPL, SPL, middle occipital lobule, angular gyrus, post central gyrus, BA 7	4.7	1380	-26	-82	32	14%
Superior temporal gyrus	Left superior temporal gyrus, primary auditory cortex, inferior parietal lobule, transverse temporal gyrus	4.62	219	-54	-30	14	8%
Precentral gyrus	Left premotor cortex, FEF, middle frontal gyrus, inferior frontal gyrus, Brodmann area 6	4.61	460	-46	0	46	12%
Precentral gyrus	Right premotor cortex, FEF, middle frontal gyrus, inferior frontal gyrus, Brodmann area 6	4.35	422	44	0	48	11%
Cerebellum and fusiform gyrus	Left cerebellum, FG, inferior temporal gyrus	4.22	310	-38	-56	-22	13%
Inferior parietal lobule	Left IPL, superior temporal gyrus, supramarginal gyrus, Brodmann area 40	4.13	209	-64	-40	42	11%
Posterior cingulate gyrus	Bilateral posterior cingulate cortex, medial precuneus	4.1	696	-4	-40	46	11%
Supplementary motor area	Bilateral supplementary motor area, superior frontal gyrus, anterior cingulate gyrus	3.82	402	2	10	52	11%

Table 8 Brain areas of differential rCBF increase in patients with VS compared to controls (main effect of group, with and without stimulus).

Group effects at rest - when comparing VS patients to controls during baseline only (at rest without visual stimulus), an equal number of statistically significant clusters of increased rCBF were found (Figure 5.2a). These areas were largely overlapping with the ones defined from the analysis combining the conditions (both with and without stimulation, Figure 5.1, Table 8) and again corresponded to the bilateral cuneus, precuneus IPL, SPL, SMA, FEFs premotor cortex, AG, posterior cingulate cortex, middle frontal gyrus, post central gyrus, middle and superior occipital lobule and left primary auditory cortex, FG, cerebellum area VI and supramarginal gyrus.

Group effects with stimulation - when patients were compared to controls during stimulation only, the areas of significant rCBF difference (Figure 5.2b) were found again to overlap with the first analysis. Some minor differences related to the absence of two clusters, one involving the PCC and one the left IPL, which did not reach the significance threshold in this analysis.

The clear similarity that emerges when testing for the group effect (i.e. comparing patient vs. controls), either at rest or with the stimulus condition, is illustrated in Figure 5.3.

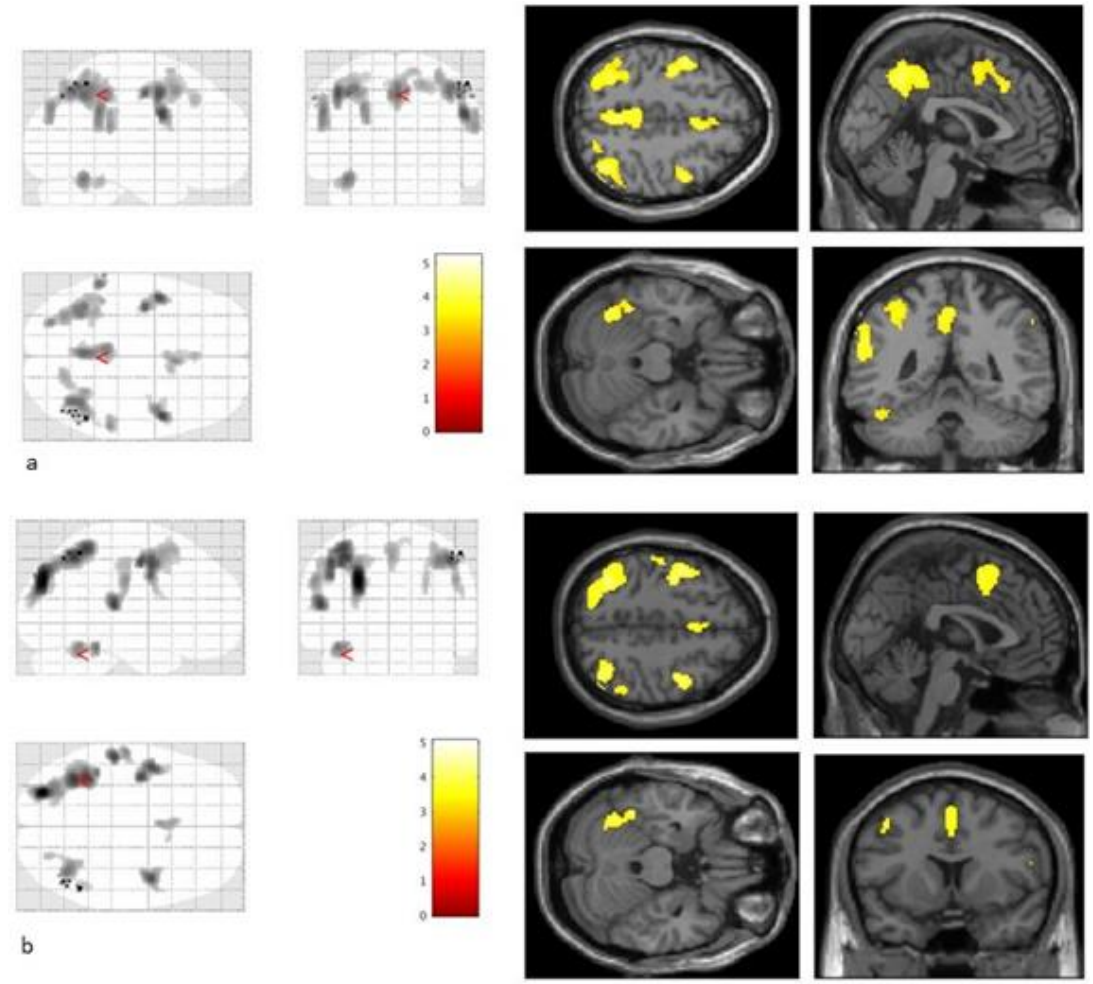

Figure 5.2 Areas of increased CBF in patients with visual snow compared to healthy volunteers when looking at a blank screen (a) and when observing a 'snow-like' visual stimulus (b).

Images are overlaid onto a glass brain on the left side, and a standard anatomical T1 image on the right side.

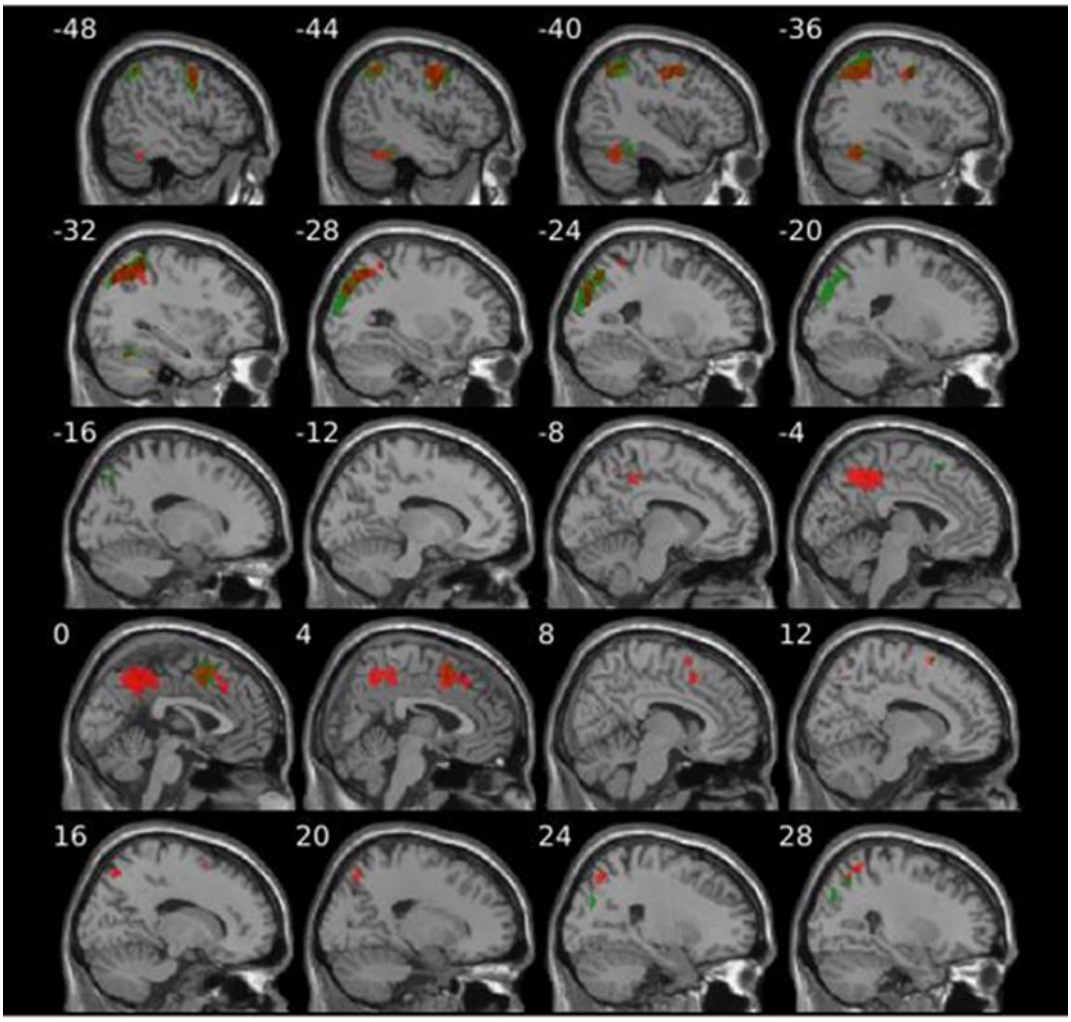

Figure 5.3 Comparative illustration of areas of increased CBF in patients vs. healthy volunteers when looking at a blank screen (red colour areas - as seen in Figure 5.2a) and when observing a 'snow-like' visual stimulus (green colour areas - as seen in Figure 5.2b).

5.2.2 Comparing snow-like simulation to baseline - stimulus effects

When subject to the snow-like stimulus and compared to the baseline resting fixation state, both groups showed an increase in rCBF in a large bilateral cluster involving the primary visual cortex, lingual gyrus and inferior temporal gyrus. In VS patients only, the stimulation also evoked a decrease in rCBF in the mid-cingulate and posterior cingulate cortex (k = 551; MNI coordinates: x = 12 y = -10 z = 46).

Figure 5.4 shows these areas of increased and decreased rCBF in patients and controls, when subject to the snow-like stimulus.

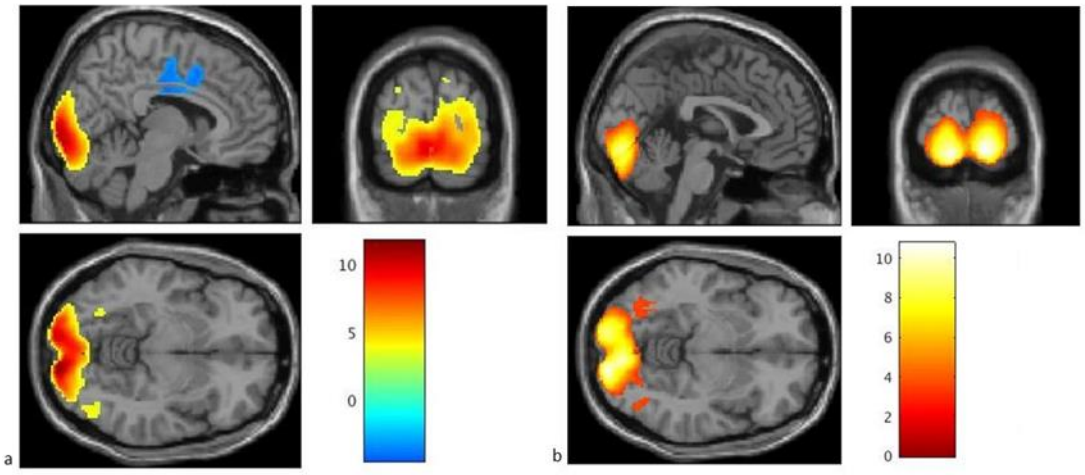

Figure 5.4 Areas of increases (red/yellow) and decreases (blue/green) of rCBF in patients (a) and controls (b) when subject to the snow-like stimulus.

5.2.3 VS patients and stimulation - interaction effects

When considering the interaction between group and stimulus condition (i.e. the difference of the differences), a significant area of increased activation in patients with visual snow compared to volunteers was identified when subject to visual stimulus ('snow-like' vs resting fixation). This cluster of size k = 98 was located in the right insula and was significant for p = 0.01 after SVC by applying a mask over the anatomical area. Figure 5.5 shows the area (MNI coordinates: x = 44 y = 20 z = 2) with bar representing *T*-values and plots for effects of interest contrast, showing values for, respectively: VS patients at rest, VS patients during stimulus, HCs at rest, HCs during stimulus. The plotting allows to observe that, where VS subjects have an increase in rCBF between the baseline and 'activated' condition, the healthy controls have a decreased perfusion in response to the same stimulus.

This result indicates that there is a greater task-related rCBF change in the right anterior insula in the VS group, when they are subject to the visual snow simulation, compared to healthy volunteers.

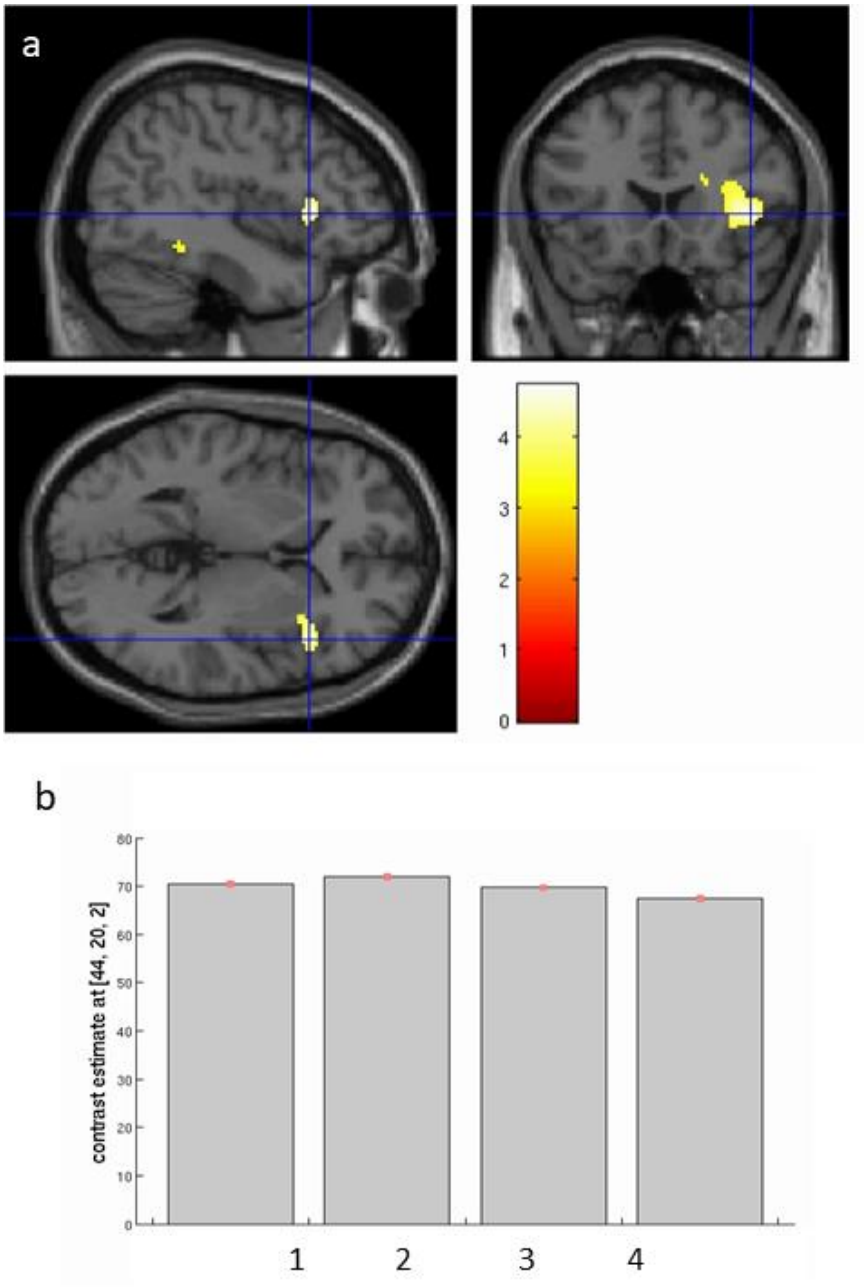

Figure 5.5 Right insula activation in patients with visual snow when testing for group and stimulation interaction (a) and effects of interest contrasts (b) for: VS patients at rest (1), VS patients during visual stimulation (2), HCs at rest (3), HCs during visual stimulation (4).

5.3 Discussion of pCASL analysis

The arterial spin labelling results described in the previous sections show that patients with visual snow exhibit a specific pattern of increased regional cerebral blood flow with respect to controls in several brain areas, which are mostly involved in complex sensory processing. These areas were: the bilateral cuneus, precuneus, IPL, SPL, SMA, premotor cortex, PCC, middle frontal gyrus, AG, post central gyrus, middle and superior occipital lobule, and left primary auditory cortex, FG, cerebellar area VI and SMG (Table 8). The fact that these alterations of cerebral blood flow were found in visual snow both in the resting condition and when the brain was involved in a specific visual task (Figure 5.3), suggests that these regions form an intrinsic pattern of altered neuronal function, which could represent a specific pathophysiological fingerprint of the condition. Further, most of these regions were independent of concomitant migraine presence (Appendix C - pCASL *post-hoc* analysis), and thus likely represent a true alteration pertaining to visual snow biology.

5.3.1 Posterior parietal cortex and the default mode network

With regards to the between-group whole-brain ASL analysis, the clusters showing highest *T* scores of increased perfusion in VS patients involved large areas of the posterior and lateral parietal cortex, in particular the precuneus and parts of the cuneus as well as the superior and inferior parietal lobules of both hemispheres (Figure 5.2, Table 8).

The fundamental role of the parietal cortex in the integration of different sensory stimuli, as well as its involvement in several complex neurological and psychiatric

disorders (Teixeira et al., 2014), is well known. In particular, the majority of the areas showing altered rCBF in the study are part of the dorsal visual stream, which emerged from the morphological analysis as well (see 4.3). This pathway, in which visual information is delivered from the primary visual cortex to the posterior parietal lobe and onwards, represents a critical element in the integration of the occipito-parietal projection system. It is involved in the visual location of objects and is also essential in determining action-oriented behaviours dependent on the perception of space (Goodale et al., 1992; Mishkin et al., 1983). A parietal area showing particularly heightened regional blood flow was the superior parietal cortex, part of Brodmann area 7, which represents a point of convergence between vision and proprioception, and allows to determine where objects are in relation to parts of the body (Scheperjans et al., 2008a; Scheperjans et al., 2008b).

A large part of the parietal cortex however, is not directly involved in the processing of external stimuli; rather, it represents an intrinsic functional system of the brain, which deals with complex internal mental processing (Golland et al., 2006). This system, as defined by several neuroimaging studies, has been termed the default mode network (DMN), and represents an organized mode of brain function active when the brain is at rest and suspended during specific goal-directed behaviours (Raichle et al., 2001; Shulman et al., 1997). The DMN allots a large amount of the brain's energy to create a 'self-centred predictive model of the world' (Raichle, 2010) and has an essential role in monitoring the internal mental landscape through the functions of autobiographical cognitive activity, self-monitoring and spontaneous cognition (Greicius et al., 2003; Qin et al., 2011). It has also been proposed as a

marker of an individual's degree of consciousness (Crone et al., 2015; Vanhaudenhuyse et al., 2010).

The DMN consists of three subdivisions: the ventral medial prefrontal cortex, the dorsal medial prefrontal cortex and the posterior cingulate cortex with the adjacent precuneus. The precuneus, together with the PCC, constitute the posterior elements of the default mode network, which are strongly linked to the recollection of prior experiences, involving both the external and internal world (Raichle, 2015). Recent neuroimaging studies further emphasize the core role of the precuneus as a specialized hub within the DMN, and more broadly as a key processing region in various brain states (Utevsky et al., 2014). The fact that the precuneus showed increased blood flow bilaterally could potentially signify an increased function within the default mode network in VS patients.

5.3.2 Posterior cingulate and midcingulate cortex deactivations

The PCC was also highly relevant in this ASL analysis. Not only did this area show increased rCBF with respect to controls in the whole-brain analysis; it conversely showed a decreased rCBF in its most anterior region (anatomically verging on the posterior midcingulate cortex) when visual snow patients were subject to visual stimulation. This decreased activation did not appear in controls, unlike the widespread and bilateral increase activation over the primary and secondary visual cortices, following the stimulation, that was common to all subjects (Figure 5.4).

The posterior midcingulate cortex is anatomically and functionally connected to the parietal cortex, modulating multisensory action and allowing the orientation of the body in space in response to sensory stimuli (Vogt, 2016). Several neuroimaging

studies have further linked this area to ‘catastrophizing’, which is a cognitive strategy often encountered in subjects that cope with chronic conditions. The deactivation of these areas in visual snow patients only, when subject to a ‘simulated snow’, could further implicate a global dysfunction of sensory integration networks common to the condition.

5.3.3 Attention, executive and salience networks

The more medial aspects of the precuneus - along with the middle cingulate cortex, dorsolateral prefrontal cortex, inferior parietal lobule, dorsal frontal cortex and intraparietal sulcus - are also an element of an intrinsic functional connectivity network known either as the fronto-parietal (FP) network or central executive network (CEN) (Fair et al., 2007). This brain control system is involved in attentional control, by exerting a continuous adaptation and adjustment of goal-directed behaviour in a top-down fashion (Dosenbach et al., 2007). The CEN is critical for the active maintenance and manipulation of information in working memory, and for judgment and decision making (D'Esposito, 2007; Müller et al., 2006). As opposed to the DMN, the CEN is a ‘task-positive’ attention network that can, however, be identified also during resting state when the brain is not focused on the outside world (Michael D. Fox et al., 2006; M. D. Fox et al., 2005).

The FP network is directly connected in its function with the cingulo-opercular network (CON), more recently termed the salience network (SN) (Seeley et al., 2007). This system includes the bilateral anterior insula, dorsal anterior cingulate cortex, frontal operculum, presupplementary motor area (Dosenbach et al., 2006), anterior

prefrontal cortex and thalamus (Dosenbach et al., 2007). The SN has a specific role in integrating different internal and external sensory inputs to evaluate their 'salience' (Sadaghiani et al., 2014) allowing the selection and integration of relevant information amongst the myriad of stimuli reaching our brain. It is thought that the SN and FP networks work in parallel in order to perform and control different cognitive tasks, such as executive functioning, visuospatial perception, episodic memory and motor control, among others (Dosenbach et al., 2008; Sestieri et al., 2014). In this endogenous top-down control process, visceral, autonomic, and sensory data are integrated to assess their relevance for the purpose of general homeostasis.

5.3.4 Insular activations in response to a visual stimulus

The insular lobe of Reil has a pivotal function in the context that has been described up to here, as it relays different somatosensory inputs to other areas of the limbic system (Shelley et al., 2004). The anterior insula, in particular, is considered an integration hub for dynamic interactions between the default mode and central executive networks (Menon et al., 2010). A current leading hypothesis is that the salience network, specifically through the right anterior insula (Sridharan et al., 2008), constantly modulates a switch between the internally oriented self-related cognition of the DMN and the externally goal-directed attention of the CEN (Menon, 2011; Nekovarova et al., 2014), essentially creating a link between exogenous and endogenous control (Figure 5.6).

The fact that this region would exhibit an increased activation when analysing the interaction between group and task (Figure 5.5) is important. It may have been

expected for a snow-like stimulus to be *less* salient in patients with VS compared to healthy subjects. However, from the perspective of a widespread altered excitability of neuronal and cortical networks, secondarily leading to increased sensitivity of multiple sensory pathways in VS (Ffytche et al., 2010; Lauschke et al., 2016), this finding is perhaps less surprising. Such a mechanism could explain the constant perception of sub-threshold stimuli or even, as has been shown in other fMRI studies (Ffytche et al., 1998), of visual hallucinations.

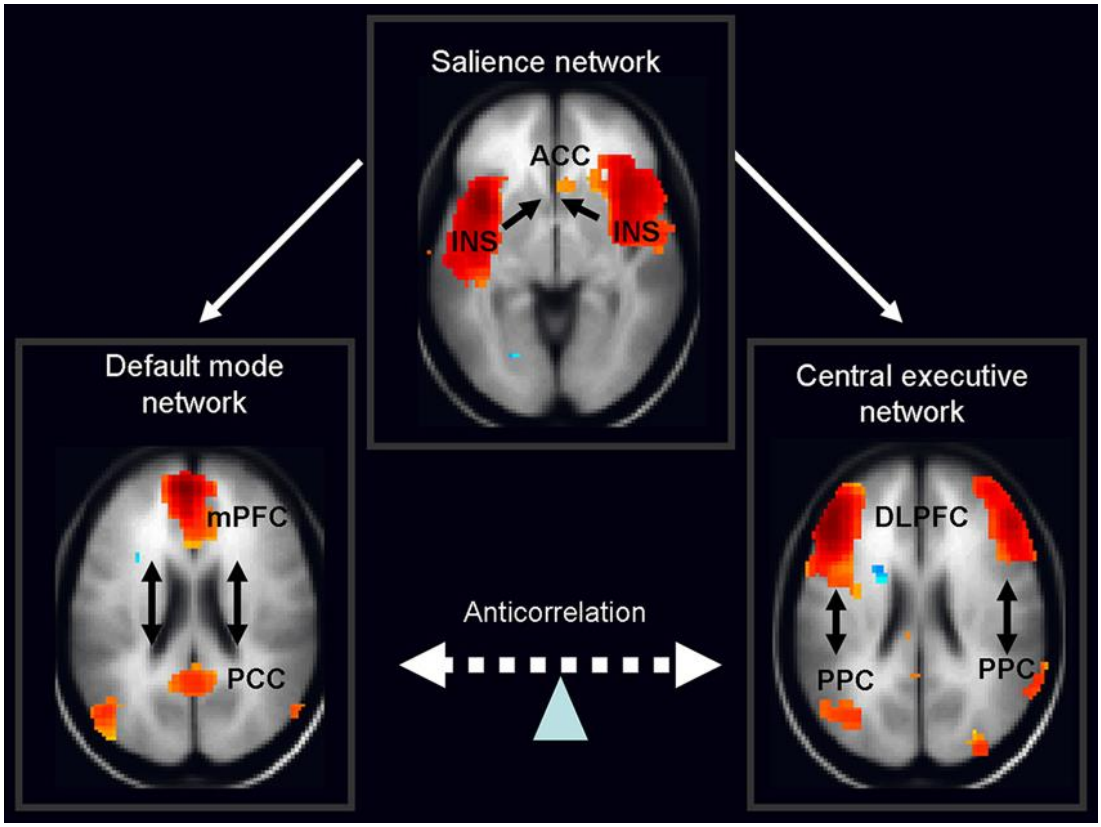

Figure 5.6 Interaction between the default mode network, salience network and central executive network.
Reproduced from (Nekovarova et al., 2014). ACC, anterior cingulate cortex; DPLFC, dorsolateral prefrontal cortex; PPC, posterior parietal cortex; mPFC, medial prefrontal cortex; PPC, posterior cingulate cortex; INS, anterior insula.

5.3.5 Visual motion network involvement

As described above, V5 is the brain area that specializes in processing and computing visual motion (Tootell et al., 1995; Zeki et al., 1991). The fact that the ASL data showed an increased regional cerebral blood flow in V5 - as part of a large parieto-occipital cluster from the whole brain analysis - in visual snow may be relevant.

Another element of the visual motion network that showed activation in this analysis were the frontal eye fields, which have a significant role in visuo-spatial attention (Schall, 2004).

Further, the sensorimotor anterior region of the precuneus has been shown to connect directly to the supplementary motor area (Margulies et al., 2009), another region significantly emerging from this ASL analysis. The important role of the SMA in cognitively demanding tasks (Cabeza et al., 2000) and in the control of movement, in particular when internally generated or visually guided (Brooks et al., 2000; Picard et al., 2003), further suggests that this area might be relevant in VS.

Collectively, the involvement of these areas in visual snow could either represent a compensatory brain mechanism for the continuous perception of moving objects, or rather in itself be responsible for the generation of the moving visual illusion that features the syndrome.

It is relevant to note that the visual stimulus chosen to mimic visual snow here was not designed with the specific purpose of activating the motion pathway. Conflicting literature in fact exists on the topic, with most studies showing that random non-coherent motion results in low activation for the motion pathway but rather of area V1 (Braddick et al., 2001; Snowden et al., 1991), and others showing that an incoherent static stimulus can indeed activate V5 as well (McKeefry et al., 1997). The

choice of this stimulus was based on the idea of mimicking the percept of visual snow. The fact that differential activation of the motion pathway in visual snow patients was found at rest, as well as in response to the task with pCASL, seems to suggest that the findings are independent of the stimulus and are therefore a feature of VSS itself.

5.3.6 The cognitive cerebellum

It is well known that the posterior cerebellum has a relevant role in complex cognitive processing operations in the brain, through associative cerebro-cerebellar networks (Schmahmann, 2004). This pCASL analysis showed an increased regional blood flow in VS patients in a specific region of the posterior cerebellum, involving mostly lobule VI and partly Crus I in the left hemisphere. These areas are a key part of the 'cognitive cerebellum' (Stoodley et al., 2009) and have been shown to activate during attention, language, working memory, executive functions or spatial tasks in several fMRI studies. Interestingly, activation in lobule VI during spatial processing functions is highly left-lateralized, and this is very much in line with our data. Furthermore, activity in lobule VI and Crus I show high correlation with activation of the salience and executive control networks respectively (Habas et al., 2009). It is important to note that the left lobule VI showed an increase in grey matter volume in the VBM analysis (section 4.2.3), in an area partially overlapping with the one found here.

5.3.7 Primary auditory cortex

It cannot be excluded that the increase in blood flow to the primary auditory cortex found here was, at least in part, linked to the high levels of concomitant tinnitus seen in the VS patient cohort (Table 6) (Arnold et al., 1996). The comorbidity between VS and tinnitus is indeed interesting, and was already touched upon in the clinical phenotypical analysis (chapter 2.3). There is increasing literature suggesting that phantom perceptions, present equally and for different sensory modalities in both tinnitus and visual snow, represent a widespread network phenomena (Hullfish et al., 2019), which is not limited to the involvement of the relevant primary sensory cortices (De Ridder et al., 2014; Sedley et al., 2016). The data here strongly supports this 'dysfunctional network' theory, which could also be a key element of visual snow pathophysiology.

5.3.8 Lingual and fusiform gyri

This rCBF analysis found no direct activation in the lingual gyrus, an area that was of interest given the previous PET study in VS (chapter 1.3). It is possible that a difference in imaging techniques played a role in this result. On the other hand, the present data show significant involvement of areas in close anatomical and physiological proximity to the lingual gyrus. In particular, the fusiform gyrus, which is part of the associative visual cortex, showed increased activation in visual snow patients. Importantly, dysfunctional visual processing, as detected through the use of visual evoked potentials, has been attributed to involvement of areas in the extrastriate visual cortex in VS (Eren et al., 2018). The FG, as the primary area

involved in generating the N145 phase of visual evoked potentials, was described as a pivotal structure in the outcome of this particular study that showed increased N145 latency in patients, thus suggesting changes in higher order visual post-processing in visual snow.

5.3.9 Limitations

A potential limitation for this experiment was related to the absence of a fixation requirement during the visual task, as well as eye tracking, which could have caused group differences in eye movement behaviour to explain at least part of the differences in localized rCBF. Free viewing was chosen over fixating on a cross with the specific purpose of avoiding the pattern of brain activations typical of the act of fixation (Anderson et al., 1994). This does however make it difficult to exclude that the two groups may have had different patterns of free viewing eye movements that were not controlled for. However, given that the known network of eye movement regions are different to the areas of altered rCBF found here, particularly with regards to the absence of any involvement of ventrolateral and dorsolateral prefrontal cortices (Ettinger et al., 2007), it is unlikely that they were due to an artefact of eye movements.

6 Functional connectivity in visual snow

This chapter will outline the methods, results and discussion for the functional connectivity part of the MRI project.

6.1 Functional connectivity fMRI methods

ME-EPI images sensitive to BOLD contrast were acquired to measure hemodynamic responses, both at rest and during visual stimulus, with the following parameters: TR = 2500 ms; TE = 12, 28, 44, 60 ms; flip angle = 80°; FOV = 240 mm; matrix = 64x64; slice thickness = 3 mm; 32 axial sections collected with sequential (top down) acquisition and 1-mm interslice gap; in-plane resolution = 3.75 mm. Total acquisition time for each fMRI acquisition was around 10 min.

After resetting of the origins for both T1-weighted and ME-EP images, the 60 ms echo was discarded due to low signal. The remaining three echoes were taken forward to preprocessing as described below. The ME-EPI echoes were separated into distinct time series (corresponding to the three remaining individual echoes), which were then de-spiked using 3dDespike in the Analysis of Functional NeuroImages (AFNI) framework (https://afni.nimh.nih.gov), and slice time corrected. Parameters for motion correction were estimated for the first echo, and subsequently applied to the other echoes; all ME-EP images were then co-registered to the T1 scan. All echoes were spatially normalized to the study-specific template, and from there to MNI space. Finally, the images from all echoes were z-concatenated for further processing, i.e. the space-bytime matrices from each echo were appended to one

another in the z-direction to form a single matrix using the *3dZcat* function in AFNI. TEDANA, a python script that forms part of the Multi Echo Independent Component Analysis (MEICA) package (https://afni.nimh.nih.gov/pub/dist/src/pkundu/meica.py) (P. Kundu et al., 2012; Prantik Kundu et al., 2017) was called to perform TE dependent ICA-based denoising and T2* weighted averaging (optimal combination) of echoes. The denoised, optimally combined images were subsequently regressed out for motion correction, white matter signal and cerebrospinal fluid signal. Band-pass-filtering was applied with AFNI (frequency range 0.08–0.01 Hz).

Eight unilateral seeds were defined based on previous hypotheses (see section 0) and following anatomical areas of interest in the visual network, as well as on results that came from the pCASL analysis, which was completed earlier (section 5.2). These were namely: the right pulvinar (Pv); right primary visual area V1 (V1); right motion area V5 (V5); right lingual gyrus (LG); left cerebellum lobule VI (Cb); posterior midcingulate cortex/posterior cingulate cortex (pMCC/PCC); right parietal lobules/precuneus (PL/PCu) and right insula. The pMCC/PCC, PL/PCu and Cb ROIs were created as binary masks from the positive clusters deriving from the group-level pCASL analysis. Anatomical ROIs for the remaining areas were created with the 'wfu_pickupatlas Anatomical Library' and the 'Juelich Histological Atlas' as detailed in section 4.1. The main seeds for the connectivity analysis are shown in Figure 6.1.

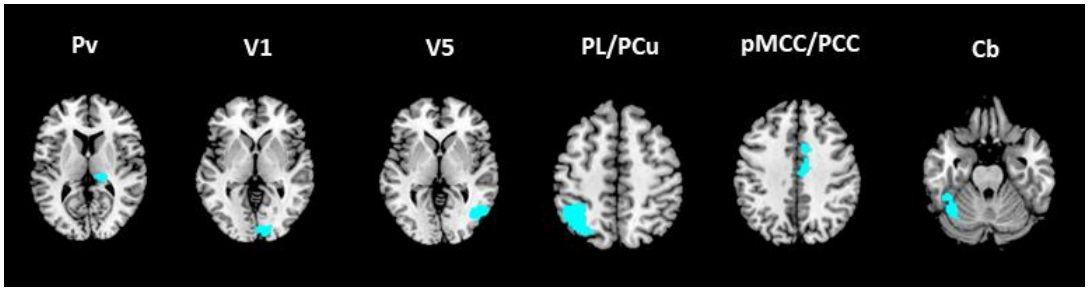

Figure 6.1 Location of main seed regions (in cyan) for the connectivity analysis.

The resting and visual stimulus connectivity data were analysed using a voxel-wise general linear model. A second-level whole brain voxel-wise flexible-factorial design using two-way ANOVA allowed analysis of changes in connectivity related to group and stimulus effect. *Post-hoc* analyses with migraine as a covariate were also run.

Finally, a psychophysiological interaction (PPI) analysis (KJ Friston et al., 1997) was performed, using the visual task (snow simulation) as the psychological condition and the V1 and V5 seeds as regions of interest. BOLD activity for the PPI was quantified from the block-design paradigm described in chapter 0.

6.2 Functional connectivity analysis: results

6.2.1 Group effects

To test the hypothesis that individuals with VS would show altered functional connectivity of the visual network relative to HCs, following Fisher's r-to-Z transformation of connectivity r-maps, whole-brain connectivity for each visual network seed (Pv, V1, V5, LG) between groups was compared, both during the resting state and in the presence of the visual stimulus. This analysis revealed hyper- and hypoconnectivity in VS compared to HCs between key visual areas and the rest of the brain, as outlined below. No difference in connectivity between groups was found in the whole-brain analysis for the LG seed.

As detailed in the methods, given that the pCASL analysis was completed before, clusters in the pMCC/PCC, parietal lobules/precuneus and cerebellar lobule VI (Table 8, Figure 5.2) from the ASL group-level comparison were used as regions of interest for the connectivity analysis. These structures are respectively part of the default mode (PCC/PCu) and the executive (PL/Cb) networks, and are implicated in important sensory and cognitive tasks.

A summary of the increased and decreased connectivity for the main effect of group, both at rest and during the stimulated condition, that was found between these six ROIs (Pv, V1, V5, pMCC/PCC, PL/PCu, Cb) and the rest of the brain is detailed in Table 9.

Figure 6.2 shows the main differences between the two subject groups during the rest condition, whereas Figure 6.4 shows main differences between the two subject

groups during the visual stimulus condition. Figure 6.3 and Figure 6.5 show plots for the mean beta values of the clusters with highest *T* scores from these analyses, respectively at rest and during the visual stimulus.

Pulvinar

Compared to the healthy controls, VS patients in the rest condition showed a greater connectivity between the right pulvinar and the right postcentral gyrus (PoG) and supramarginal gyrus (T = 4.32; k = 382; p = 0.05; x = 50 y = -20 z = 46). When determining the effects of interest and examining the mean beta values of each group, it was ascertained that VS patients had a close to null coupling between these two areas, where controls showed anti-correlation (i.e. negative connectivity values, Table 9). A significantly reduced connectivity between the Pv and the bilateral caudate nuclei (T = 4.68; k = 967; $p < 0.001$; x = -12 y = -6 z = 16; Figure 6.2) was also found, in VS patients with respect to HCs.

When exposed to the task condition, patients with VS showed a significantly positive coupling between the Pv and the right lingual gyrus (T = 4.27; k = 410; p = 0.04; x = 26 y = -54 z = -2; Figure 6.4), which was conversely close to null in controls (Figure 6.5).

V1

In the VS group, compared to HCs, there was evidence of greater connectivity at rest between the right primary visual cortex and the left SMG and postcentral gyrus (T = 4.54; k = 346; p = 0.05; x = -64 y = -20 z = 32; Figure 6.2). When lowering the statistical threshold, this area included the frontal eye fields (FEFs) and was present on the contralateral hemisphere as well.

During the task condition, patients with VS exhibited significantly greater coupling than controls between the right V1 and right V5 areas (T = 5.02; k = 332; p = 0.05; x = 52 y = -64 z = 6; Figure 6.4) and positive or null connectivity rather than anti-correlation in the postcentral and precentral gyri, SMG, premotor cortex, supplementary motor cortex and FEFs of the same hemisphere (Table 9).

V5

At rest, patients with visual snow exhibited significantly reduced connectivity from the right V5 area to the posterior cingulate cortex (T = 4.46; k = 554; p = 0.01; x = -6 y = -52 z = 42; Figure 6.2). Examining the effects of interest showed that, while the connection between these two areas was positive in controls, it was negative in VS patients (Figure 6.3).

In the visually activated state, greater connectivity was found between V5 and several bilateral occipital, parietal and frontal areas, specifically the right cuneus and precuneus, Brodmann visual areas 17, 18 and 19, the FEF, SMG, premotor cortex, SMA, superior parietal lobule and intraparietal sulcus (IPS) (Figure 6.4, Table 9). These areas also showed positive coupling in controls, however, the connection was significantly stronger in VS patients.

During the task, anti-correlation with the PCC was confirmed as in the resting state, and was found as well between V5 and the right temporo-parietal junction (TPJ) (T = 5.12; k = 928; $p < 0.001$; x = 44 y = -56 z = 28).

PL/PCu

At rest, a significantly positive connectivity between the right parietal lobules/ precuneus and the right precentral gyrus/frontal eye fields was found (T = 4.37; k =

337; p = 0.004; x = 48 y = 4 z = 36), as opposed to a negative connectivity between these areas in controls (Figure 6.2).

pMCC/PCC

There was a significantly stronger connectivity in the task state from the pMCC/PCC to the bilateral medial precuneus and PCC itself, in VS patients with respect to controls (Figure 6.4).

Cerebellum

From the cerebellar seed, VS patients in the rest condition showed anti-correlation to the PCC and medial precuneus (Figure 6.2), largely overlapping the area found to have reduced connectivity with the V5 region.

Conversely, during the task, there was greater coupling to the right SPL, lateral precuneus and PoG (Figure 6.4).

Post-hoc analyses covarying for migraine presence generally revealed the same significant clusters for all ROIs with the exception of the cerebellar seed, and occasionally requiring a lower cluster-forming threshold of p = 0.005.

A further *post-hoc* analysis to investigate contralateral connectivity was performed on the main anatomical regions of interest (Pv, V1 and V5) and showed largely overlapping results from the left hemisphere, except for the Pv to PoG increased connectivity, which remained localized to the right side.

ROI	Cond.	Cont.	Brain regions	Mean beta values		k	T, *p*	Peak coordinates		
				VS	HC			x	y	z
Pv	Rest	VS> HC	R SMG, PoG (BA 1,3)	-0.01	-0.18	382	4.32, *	50	-20	46
		VS< HC	Bilateral caudate nuclei	0.09	0.27	967	4.68, ***	-12	-6	16
	Stim	VS> HC	R LG (BA 19)	0.22	0.02	410	4.27, *	26	-54	-2
V1	Rest	VS> HC	L SMG, PoG (BA 1,3)	-0.03	-0.22	346	4.54, *	-64	-20	32
	Stim	VS> HC	R IOG (area V5, BA 18,19)	0.24	0.01	332	5.02, *	52	-64	6
			R SMG, PoG (BA 1,3)	0.00	-0.19	572	4.68, **	58	-24	40
			R PrG (BA 8, 6, FEF)	0.08	-0.13	696	4.53, **	52	10	28
V5	Rest	VS< HC	PCC, L/R medial PCu (BA 7)	-0.13	0.11	554	4.46, **	-6	-52	42
	Stim	VS> HC	Bilateral MOG, SOG, IOG, FG, (BA 17, 18, 19, V1-V3), SMG, cuneus	0.65	0.37	5598	5.71, ***	38	-84	10
			R SPL/IPS (BA 7, BA5)	0.53	0.27	936	5.0, ***	26	-60	60
			R PrG (BA 8, 6, FEF)	0.41	0.16	420	4.25, *	48	2	38
		VS< HC	PCC, bilateral medial PCu	-0.25	0.00	6838	6.16, ***	-4	-52	52
			R TPJ and AG (BA 39, BA 40),	-0.17	0.05	928	5.12, ***	44	-56	28
PCu	Rest	VS> HC	R PrG (BA 8, 6, FEF)	0.38	-0.17	337	4.37, **	48	4	36
PCC	Stim	VS> HC	PCC, bilateral medial PCu	0.28	0.05	1535	4.12, ***	-4	-50	58
Cb	Rest	VS< HC	PCC, bilateral medial PCu	-0.17	0.01	605	4.44, **	-10	-50	38
	Stim	VS> HC	R SPL/lateral PCu, PoG (BA 2, 1,3)	0.05	-0.16	685	4.24, **	36	-40	72

Table 9 Areas of increased and decreased connectivity for main effect of group (VS patients versus HC), at rest and during the visual stimulus (stim), from selected ROIs to the rest of the brain.

** is for 0.01 < p < 0.05; ** for p < 0.01; *** for p < 0.001; Cond. = condition (rest or stimulated); Cont. = contrast used in the model.*

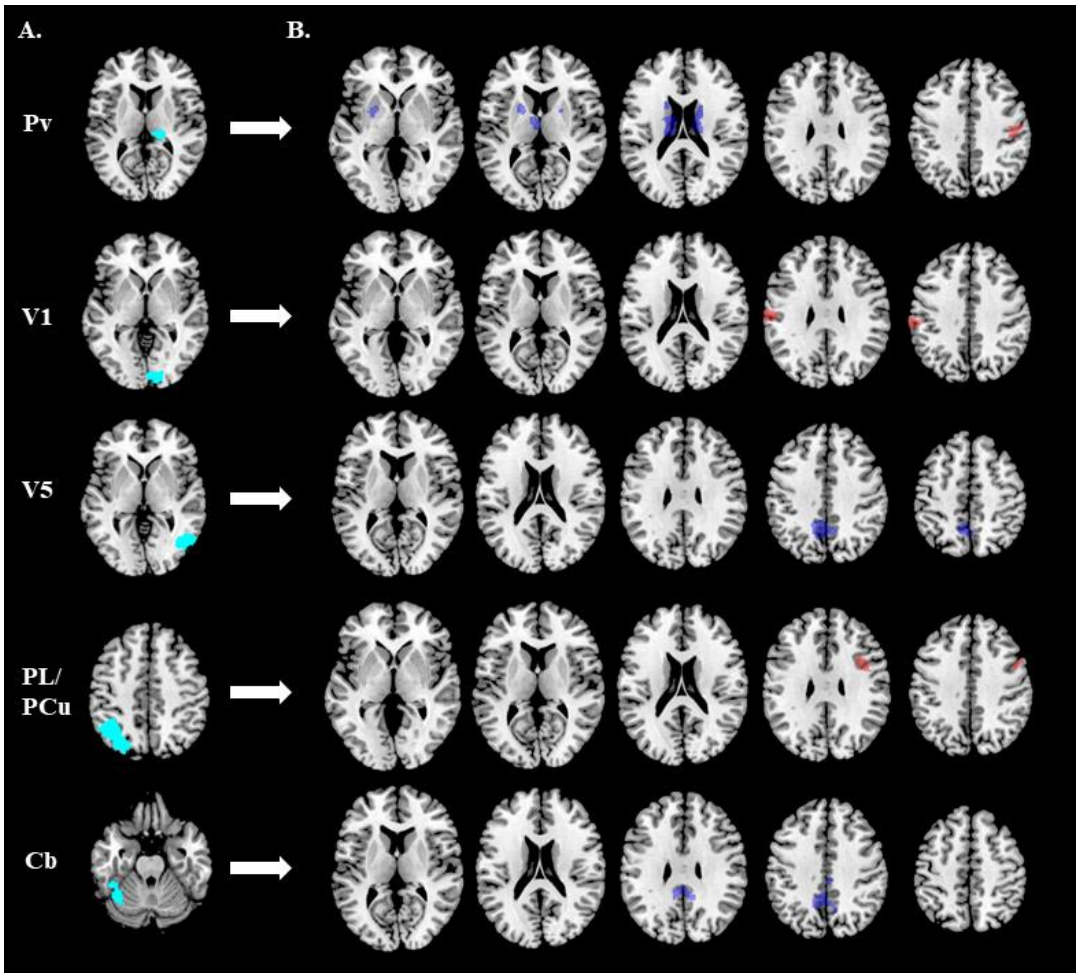

Figure 6.2 Main resting state connectivity differences between visual snow patients and healthy controls.

A) Location of selected seed regions (in cyan).
B) Between-group functional connectivity maps from each seed region to the whole brain in VS patients, at rest. Red refers to increased connectivity and blue to decreased connectivity compared to HCs. Maps are thresholded at $p < 0.001$ and cluster corrected to $p < 0.05$. For T and k values refer to Table 9.
Pv, pulvinar; V1, right primary visual area; V5, right V5 area; PL/PCu, parietal lobules/precuneus; Cb, left cerebellum lobule VI.

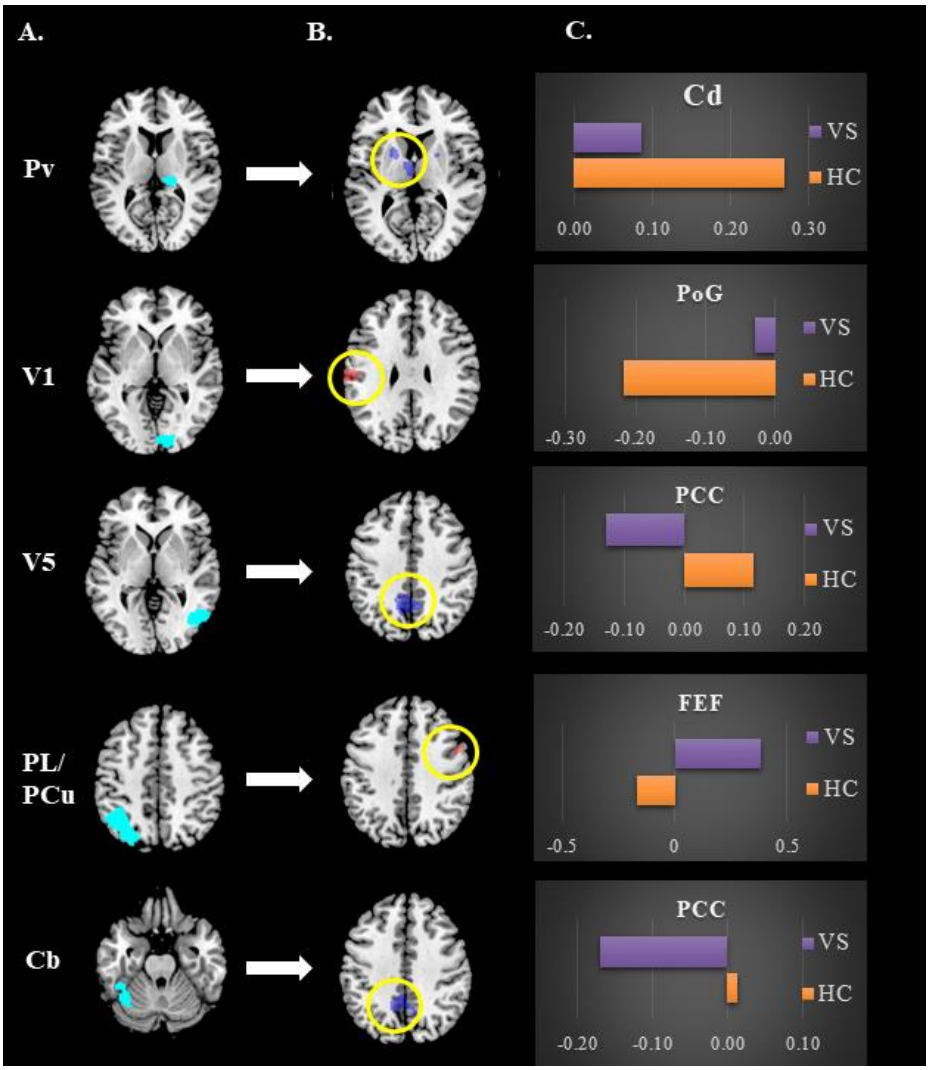

Figure 6.3 Plotting of beta values for clusters of highest altered connectivity at rest in VS patients compared to HCs.

A) Location of selected seed regions (in cyan).
B) Between-group functional connectivity maps in VS patients compared to HCs (as in Figure 6.2*) with clusters with highest T value circled in yellow.*
C) Plots for clusters in B, with respective bar charts of beta values for the two groups (VS in purple, HC in orange).
Pv, pulvinar; V1, right primary visual area; V5, right V5 area; PL/PCu, parietal lobules/precuneus; Cb, left cerebellum lobule VI; Cd, caudate nucleus; PoG, postcentral gyrus; PCC, posterior cingulate cortex; FEF, frontal eye field.

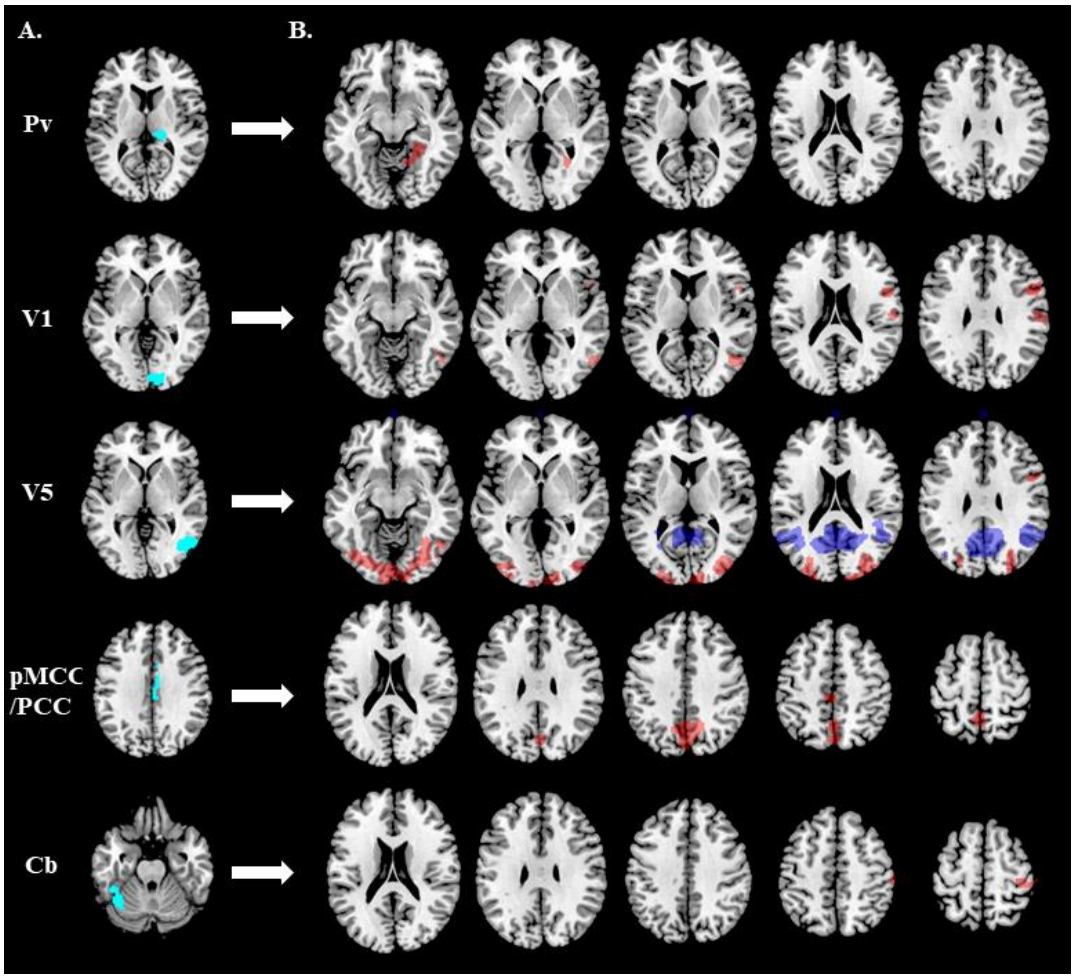

Figure 6.4 Main stimulus-based connectivity differences between visual snow patients and healthy controls.

A) Location of selected seed regions (in cyan);
B) Between-group functional connectivity maps from each seed region to the whole brain in VS patients, during the visual stimulus. Red refers to increased connectivity and blue to decreased connectivity compared to HCs. Maps are thresholded at $p < 0.001$ and cluster corrected to $p < 0.05$. For T and k values refer to Table 9.
Pv, pulvinar; V1, right primary visual area; V5, right V5 area; pMCC/PCC, posterior midcingulate cortex/posterior cingulate cortex; Cb, left cerebellum lobule VI.

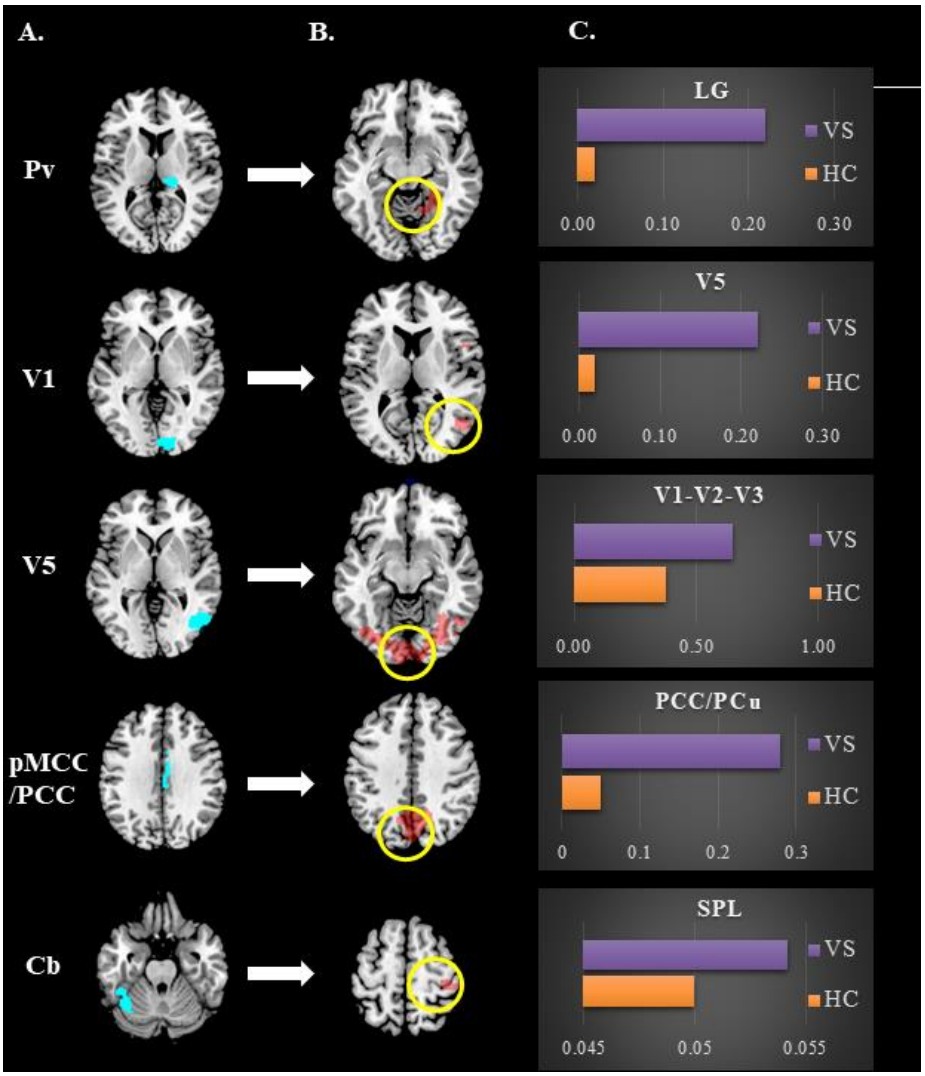

Figure 6.5 Plotting of beta values for clusters of highest altered connectivity during stimulus in VS patients compared to HCs.

A) Location of selected seed regions (in cyan).
B) Between-group functional connectivity maps in VS patients compared to HCs (as in Figure 6.4*) with clusters with highest T value circled in yellow.*
C) Plots for clusters in B, with respective bar charts of beta values for the two groups (VS in purple, HC in orange).
Pv, pulvinar; V1, right primary visual area; V5, right V5 area; pMCC/PCC, posterior midcingulate cortex/posterior cingulate cortex; Cb, left cerebellum lobule VI; LG, lingual gyrus; PCu, precuneus; SPL, superior parietal lobule.

6.2.2 Functional connectivity analysis - interaction effects

When analysing the interaction between group (i.e. VS vs. HCs) and stimulus condition (i.e. rest vs. visual input), a decreased stimulus-related connectivity between the right insula and the anterior-middle cingulate cortex (T = 4.83; k = 505; *p* = 0. 009; x = 2 y = 2 z = 30) and between V5 and the right precuneus (T = 5.29; k = 440; *p* = 0.01; x = 24 y = -54 z = 24) was found in VS patients with respect to controls (Figure 6.6a-d).

Specifically, as can be seen in Figure 6.6e, there was a reduction in the insula to ACC connectivity between the rest and stimulated condition in both groups, however, this was significantly stronger in HCs respect to the patients.

Connectivity from V5 to the right precuneus, on the other hand (Figure 6.6f), showed an opposite behaviour between rest and activation in the two groups. Although both VS and HCs showed anti-correlation between these two areas at rest, during the visual input the VS group showed a stimulus-related strengthening of the anti-correlation, whereas controls switched to an increased connectivity during the stimulated state.

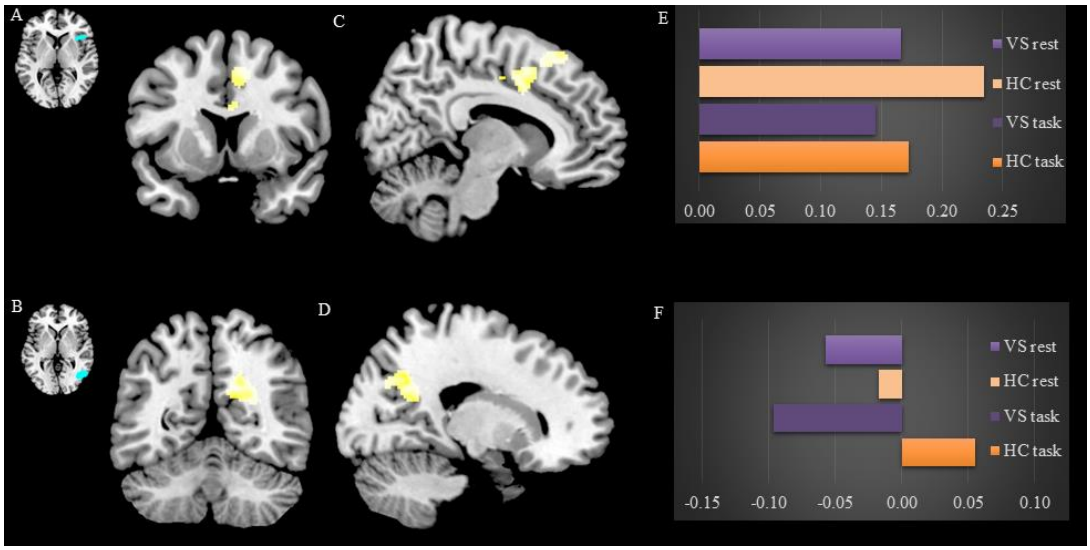

Figure 6.6 Between-group interaction effects of functional connectivity between groups (VS patients and HCs) and conditions (rest vs. stimulation).

The image shows a cluster of decreased task-related connectivity between the right insula seed (A) and the anterior-middle cingulate cortex (C) and between the V5 seed (B) and the right precuneus (D). On the right, plots for the mean beta values of the conditions (E and F, respectively).

6.2.3 Functional connectivity analysis - psychophysiological interactions

Three subjects (two HCs and one VS) were excluded from the final PPI analysis due to the distance of their individual peaks (≥6 mm) from the peak coordinate of the chosen seeds.

For the V1 seed there were no areas of significant coupling changes, in response to the visual stimulation, to any other area of the brain, both within and between the patient and control groups.

From the right V5 seed, on the other hand, while controls showed no areas of increased or decreased coupling to the rest of the brain, patients showed a significant decrease in the visual stimulation-dependent connectivity between V5 and a cluster

involving the cuneus on the left side (T = 5.97; k = 645; *p* = < 0.001; x = -4 y = -92 z = 30), corresponding to Brodmann areas 18 and 19 and particularly involving area V3 and V3A (Figure 6.7).

This result, even though it did not reach significance in the between-group comparison, seems to show that VS patients, unlike HCs, present a reduced modulation of V5 to V3/V3A connectivity, and therefore of within-visual motion network connectivity, in the context of an externally-presented visual input.

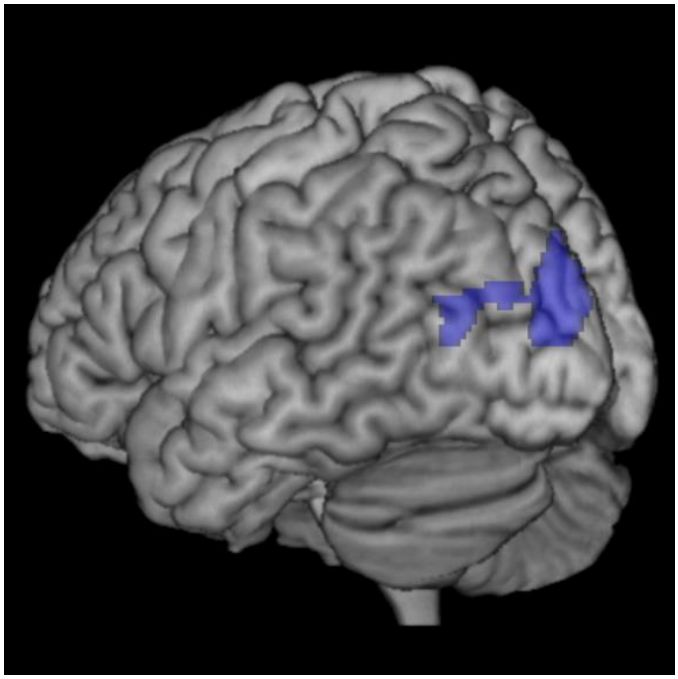

Figure 6.7 Results of psychophysiological interactions in VS patients, showing decreased connectivity from the V5 seed to V3/V3A.

6.3 Discussion of connectivity analysis

The resting state analysis results demonstrate several features that, taken collectively, highlight a pattern of widespread dysfunctional connectivity characterizing the visual snow brain. These results also build on the data coming from ASL (chapter 5.2), and essentially confirm the working hypothesis of a dysfunction in large-scale intrinsic brain connectivity networks taking place in VS, which will be explained in detail further, proceeding from subcortical areas to higher-order processing networks. To summarize, several regions within the visual network showed altered connectivity amongst themselves, as well as with numerous other important areas, such as the basal ganglia, the frontal eye fields and the attention networks. Key elements of the DMN and salience network also presented relevant disruptions of functional coupling. Further, connectivity between certain brain regions exhibited an opposite response to an external visual task in VS, with respect to what was seen in healthy subjects. Finally, the PPI results suggest a reorganization of coupling within the associative visual cortices in visual snow, and in particular of the motion network, in response to a visual task.

6.3.1 Pre-cortical visual pathways

To investigate the hypothesis of thalamo-cortical dysrhythmia, as well as simply to study the role of the thalamus in visual snow, connectivity from the pulvinar to the rest of the brain was studied with a targeted seed. The Pv, part of the 'visual thalamus' is essential in selecting which visual stimuli are relevant for the brain

(Robinson et al., 1992), and was thus part of the areas suspected to have a direct involvement in VS pathophysiology, as explained in chapter 0.

The finding that at rest, the pulvinar in VS has reduced connectivity to the bilateral dorsal aspects of the caudate nuclei is relevant. The tail of the caudate nucleus is part of the visual cortico-striatal loop (VCSL), which is directly implicated in visual learning, due to its recurrent and independent projections to higher order visual cortices (Alexander et al., 1986). The VCSL has the role of categorizing alternative representations of visual information, by selecting and reinforcing relevant peripheral stimuli for further processing and by conversely inhibiting irrelevant 'error' stimulations (Seger, 2013), through a form of feedforward predictive coding that is essential for sensory brain systems (K Friston et al., 2009; Rao et al., 1999). In this context, a bottom-up disruption of the circuitry, such as was found in visual snow subjects, could potentially allow for incorrect ascending noise-like information to reach higher hierarchical levels, thus creating a mismatch between the default prediction of the world and a noise-like perception that would normally be cancelled out by the brain.

The functional connectivity results also showed that, during the visual task, post-thalamic visual pathways from the pulvinar to the lingual gyrus have strengthened connectivity in patients with visual snow. This heightened connection could alone explain the experience of photophobia in VS - present in over 80% of patients (Table 4) - given that the both the Pv (Schwedt et al., 2013) and the lingual gyrus (Denuelle et al., 2011) have shown a significant involvement in the symptom of photophobia, in studies done in migraineurs. However, in the broader picture, it is also possible to speculate that this increased connectivity of the pre-cortical visual pathways in VS

could be one of the underlying phenomena driving a wider cortical network dysfunction, as it is line with a dysfunction of the described gating system, which could ultimately be causing reduced filtering of incoming visual information.

This result further provides a possible explanation of the finding of VS-related increased metabolism in the right lingual gyrus seen with [^{18}F]-FDG PET (Schankin et al., 2014b).

6.3.2 Striate visual cortex involvement

The primary visual cortex in VS patients presented increased coupling to the ipsilateral frontal eye fields, the supramarginal gyrus, the premotor cortex and the supplementary motor area. This heightened connectivity was observed primarily in the presence of the visual stimulus, however, lowering the statistical threshold allowed ascertainment that it was a feature of the resting condition as well. These connections were opposite to what was found in healthy subjects, meaning that the areas showed a blunted coupling where healthy brains exhibited anti-correlation.

Further, VS patients showed a powerful increase in the connectivity between V1 and V5, in the context of the visual stimulus.

An increased connection between dorsal parietal areas and V1 could represent a strengthening of the dorsal visual stream, which (as outlined in chapters 0, 4.3 and 5.3.1) is involved in the integration of vision and proprioception.

The frontal eye fields and SMG direct visual attention and gaze through the generation of active saccades (Schall, 2004) and antisaccades (Ettinger et al., 2007), and are thus essential for the control of visual awareness and visuo-spatial attention (Vernet et al., 2014). An opposite connection between the visual cortex and these

regions, in respect to what is seen in healthy controls, could therefore represent a fundamental alteration of the physiological processes of selecting stimuli that are relevant for the brain and determining how to direct visual attention, in VS subjects. The SMA and premotor cortex, on the other hand, are prerequisite for the control of movement (Rizzolatti et al., 1981). The hyperconnectivity between these areas and the primary visual cortex, antithetic to normal connections and regardless of the underlying brain condition, could potentially suggest a compensatory brain mechanism for the continuous perception of moving objects, as is seen in visual snow. It is also relevant that these areas showed increased blood flow in VS patients in the pCASL analysis (Table 8).

6.3.3 Visual motion network connectivity

In the visually active state, the entire visual motion network showed hyper-integration in VS patients, both within its sub-compartments - in the form of increased coupling from V5 to the striate and extrastriate visual cortices - as well as with other brain areas, mostly pertaining to the dorsal attention network (DAN), such as the SPL and FEF. As has partly been explained (5.3.3) this network enables the selection of stimuli based on endogenous expectations and external cues (Corbetta et al., 2000; Hopfinger et al., 2000), facilitating appropriate cognitive and motor responses that are necessary to orient and allocate attention within the brain, in a top-down fashion (Corbetta et al., 2008).

Anatomically and functionally distinct from the dorsal attention network, is the ventral fronto-parietal attention network, predominantly located in the temporo-parietal junction and the ventral frontal cortex of the right hemisphere (Corbetta et

al., 2002). This group of brain regions responds to the detection of new behaviourally relevant stimuli that are outside of the focus of attention defined by the dorsal attention network, and is responsible for refocusing attention to these unexpected and otherwise unattended external cues (Michael D. Fox et al., 2006).

It is extremely interesting to find that several parts of the ventral attention network, in particular the TPJ, angular gyrus and supramarginal gyrus (see Table 9), are conversely less integrated with the visual motion network in VS patients in the active state. This could potentially mean that in visual snow, the brain is exhibiting a reduced capacity of refocusing visual attention to environmental stimuli - particularly for the detection of motion - to environmental stimuli, while it is allocating increased resources to the integration of internal and pre-existing sensory information, via the dorsal attention network.

Further, in visual snow the main motion network area V5 was less connected to the PCC, regardless of the brain activity state; it also strengthened its anti-correlation to the right precuneus, when exposed to the visual task, as opposed to controls (Figure 6.6f). As already described, both these regions form part of the posterior node of the DMN.

Finally, the PPI analysis performed here showed a decreased connectivity between V5 and V3/V3A areas in visual snow patients, in response to a visual task. This result highlights a reduced modulation of the associative visual cortices in the context of an external stimulus in visual snow, and thus seems to confirm the hypothesis of a reorganization taking place within visual motion network. The fact that this result did not reach significance in the comparison between groups could be due to a power

issue, a common cause of false-negative effects in psychophysiological interaction analysis (O'Reilly et al., 2012).

6.3.4 Default mode and salience network dysfunction

As explained, the DMN represents a group of cortical areas that are specifically active during a non-task state and suspended during goal directed behaviours (Raichle et al., 2001). When placing a seed within the posterior node of the DMN, it was found that patients with visual snow exhibited functional disruptions of its activity, both during the resting and stimulated states. This was represented by an increased connectivity at rest between the precuneus and the frontal eye fields (part of the dorsal attention network), and by a hyper-integration between the dorsal MCC and PCC itself in response to the visual stimulus. It was also confirmed by the anti-correlations found between V5 and the PCC and between the PCC and the cerebellum, again in an area specifically associated with the attention and executive networks (Guell et al., 2018).

Further, results showed that the ACC and the anterior insula had abnormal coupling when the VS brain was requested to process normal external stimuli (Figure 6.6).

In this view, if one takes together the findings of reduced connectivity between lower and higher hierarchical nodes of the visual pathway (as explained in 6.3.1), of altered coupling between the DMN and dorsal attention network, and of aberrant coupling within the salience network itself (IN to ACC), it is possible to hypothesize a disruption within the normal integration of internal stimuli and of the processing of salient stimuli from the outside world, in visual snow. This dysfunctional salience, facilitated

by the hyper-integration of the visual motion network and its reduced connections to the DMN and ventral attention networks, could perhaps be causing the brain to misattribute salience to internal stimuli that would normally be considered as irrelevant, and to not appropriately 'switch' (as shown in Figure 5.6) between internal and external attention, thus causing a constant, moving, 'noise-like' perception. Whether these disruptions are due to aberrant nodes or aberrant architecture within the brain networks, and whether they are in fact *a primum movens* for the genesis of visual snow perception or rather a down-stream effect of the perception itself, will need to be determined by future studies.

6.3.5 Limitations

This part of the imaging study did not specifically investigate all regions of interest bilaterally. This was done initially to avoid errors due to multiple testing. Given the strongly significant results, a *post-hoc* comparison of the main seeds of interest in the contralateral hemisphere was performed. From the evidence of this analysis, it appeared that the connectivity changes reported generalise to both hemispheres, rather than being specific to one or the other.

Analogous limitations related to the absence of eye tracking discussed in chapter 5.3.9 relate to the functional connectivity analysis as well. It is indeed possible that different patterns of free viewing eye movements between the two groups were an explanation for some of the functional connectivity differences found here. However, even if connectivity alterations did involve the frontal eye fields, they did not specifically involve other important areas for the generation of active saccades and antisaccades, such as the ventrolateral and dorsolateral prefrontal cortices.

7 Functional imaging in visual snow: BOLD and MRS

This chapter will outline the methods, results and discussion for the task-based fMRI and MRS parts of the MRI project. The data presented in this chapter are currently in press (Puledda et al., 2020a).

7.1 Task-based fMRI methods

Functional magnetic resonance echo-planar images were acquired with the following parameters: TR = 2000 ms, TE = 28 ms, FA = 75°, 64 x 64 matrix. Each whole-brain image contained 38 3 mm axial slices with a gap of 0.3 mm with 192 time points. As described in section 3.3, the fMRI experiment was characterized by a block-design paradigm of a visual stimulation mimicking the visual snow and rest blocks of 40 seconds each.

Data pre-processing included manual reorientation to the anterior commissure, co-registration and image realignment, spatial normalization via unified segmentation into MNI stereotactic space, and spatial smoothing (FWHM 8mm).

First level voxel-wise analysis was performed using a general linear modelling approach based on subject-specific responses for the visual task. Each participant's head movements were modelled as nuisance regressors. A regressor encoding the blocks of task-stimulus was convolved with the haemodynamic response function, with the blank screen condition left un-coded to serve as an implicit baseline. *T*-statistic maps were calculated for the parameter estimates (beta values) of the main stimulus regressor. The resultant parameter estimates for the conditions of interest

(increases and decreases in BOLD signal) were taken forward to a whole-brain random-effects analysis to test for the effect of task (blank screen vs. visual stimulus) and group (patients vs. controls). The following variables: subject age, gender, handedness, migraine and tinnitus presence were added as covariates in the model. An anatomical ROI was created for the right lingual gyrus using the 'wfu_pickupatlas Anatomical Library' (see chapter 4.1). This area corresponded to the spectroscopy voxel of interest (chapter 3.3, Figure 3.1). Based on the a priori assumption that the lingual gyrus would show activation to the visual stimulus, beta values of BOLD signal were extracted and correlated with MRS metabolite values.

7.2 Magnetic resonance spectroscopy methods

As described in section 3.3, spectroscopy was acquired over a 1.5x3x1.5 cm^3 voxel placed over the right lingual gyrus (Figure 3.1).

T1-weighted images were used for voxel placement and for tissue segmentation. Prior to collection of MRS data, an automated prescan was performed to optimise transmit and receive gains and to optimise linear shimming gradients to improve homogeneity of the magnetic field within the voxel of interest. Acquisition parameters were: TR = 3000 ms, TE = 30 ms, number of averages = 96, bandwidth = 5 kHz, number of points = 4096. Unsuppressed water reference spectra (16 averages) were also acquired. The total acquisition time was six minutes.

MRS data was processed using Linear Combination Model (LCModel), version 6.3-1L (Provencher, 1993, 2001), using an experimentally acquired basis set (acquired at the same field strength and echo time as the *in vivo* data) to calculate water-scaled metabolite concentrations. The structural 3D IR-SPGR was segmented into grey matter, white matter and cerebrospinal fluid fractions using a Matlab script and SPM-12, by creating an image of the MRS voxel in the same coordinate space as the structural image and subsequently calculating the averages of the GM/WM/CSF fractions in the 3D GM/WM/CSF images that lie within the MRS voxel.

Each individual's metabolite concentrations were corrected for partial volume confounds and differing amounts of water in each tissue type with the following formula:

$$Metabolite_{corrected}$$

$$= \frac{Metabolite_{raw} * (43300 * f_{GM} + 35880 * f_{WM} + 55556 * f_{CSF})}{35880 * (1 - f_{CSF})}$$

in which 43300 mM, 35880 mM, and 55556 mM are the water concentrations for GM, WM, and CSF, respectively. $Metabolite_{corrected}$ represents the metabolite concentration from the grey and white matter proportion of the MRS voxel. The numerator corrects for differing tissue water concentrations for the unsuppressed water reference, while the denominator corrects for assumption that CSF is free of metabolites. The additional factor of 35880 in the denominator is applied because the default LC model analysis assumes the voxel is pure white matter. Apart from assuming T_2 = 80 ms for tissue water, no further corrections were applied for metabolite and tissue T1 and T2 relaxation.

The spectra signal-to-noise ratio, line width and Cramér Rao lower bound (CRLB) error estimates (for each metabolite) reported by LC model were used as quality control measures. LC model fitted spectra were visually inspected for artefacts. Spectra with linewidth > 0.067 ppm and SNR < 12 were excluded from further analysis.

7.3 Combined results of BOLD and MRS

7.3.1 BOLD fMRI analysis - Within group comparison (task effects)

A one-sample *t*-test within each group for the effect of the visual task, showed a large cluster of BOLD activation involving the primary and secondary visual cortices bilaterally. These areas were largely overlapping in both patients and controls. In patients, the cluster had the following characteristics: k = 8370 voxels, MNI peak voxel coordinates x = 10, y = -92, z = -6. In controls, the cluster had the following characteristics: k = 7942 voxels, MNI peak voxel coordinates x = 18, y = -96, z = -8. Greater responses at baseline than during visual stimulation (deactivations) were found in five clusters in patients and two clusters in controls, involving the periventricular areas bilaterally, as well as, in patients only, the middle frontal gyrus, superior frontal gyrus, FEFs, supramarginal gyrus, frontal operculum and right insula. A summary of these results can be found in Table 10 and Figure 7.1.

Group, Contrast	Cluster description	k	*p* value	T	Peak coordinates		
					x	y	z
VS, Act	Bilateral primary and secondary visual cortices, lingual and fusiform gyrus, BA 17-18-19	8370	<0.001	13.01	10	-92	-6
VS, Deact	Bilateral periventricular areas, cuneus, precuneus, LG	3862	<0.001	7.73	20	-38	14
	R middle frontal gyrus, R superior frontal gyrus, FEF, BA 8-9-10	1013	<0.001	5.66	34	38	28
	L precentral and L post central gyrus, BA 4-7-31	297	0.024	4.96	-24	-28	36
	R frontal operculum, R inferior frontal gyrus, R insula, BA 13-22	685	<0.001	4.91	50	10	0
	R supramarginal gyrus, R inferior parietal lobule, BA 40-2	288	0.027	4.75	56	-42	44
HC, Act	Bilateral primary and secondary visual cortices, lingual and fusiform gyrus, BA 17-18-19	7942	<0.001	15.87	18	-96	-8
	L precentral gyrus, L inferior frontal gyrus, BA 45-6	304	0.003	5.67	-56	10	40
HC, Deact	Bilateral periventricular areas, cuneus, precuneus, LG	6075	<0.001	12.02	-24	-50	8
	L postcentral gyrus	921	<0.001	4.66	-20	-32	54

Table 10 Brain areas of differential BOLD response to visual stimulus in patients and controls.

Cluster coordinates are shown in MNI space with relative T scores and k values.
VS = visual snow patients; HC = healthy controls
Act = activation; Deact = deactivation

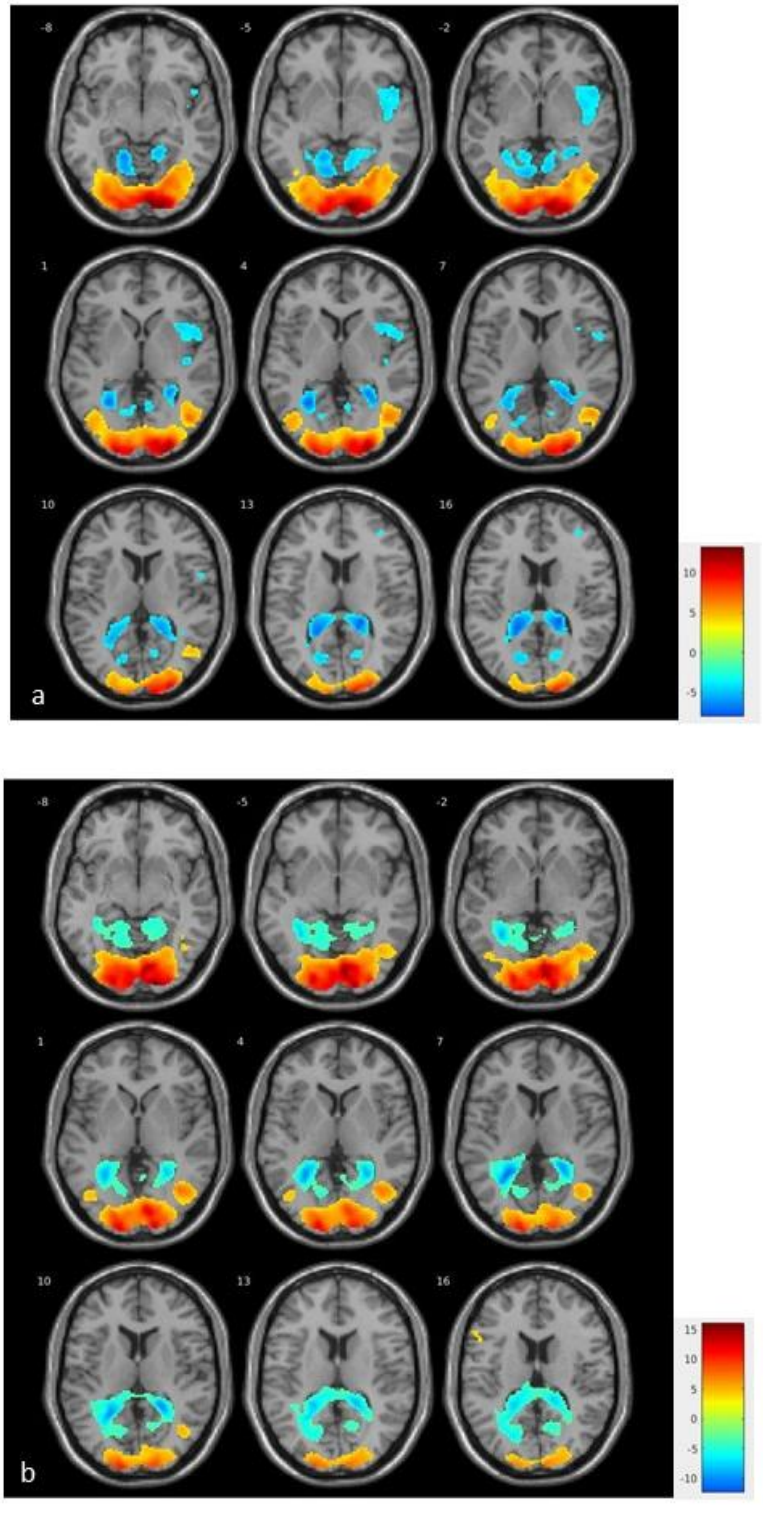

Figure 7.1 Areas of increased (red/yellow) and decreased (blue/green) BOLD signal in patients (a) and controls (b) when subject to visual 'snow-like' stimulus.

7.3.2 BOLD fMRI analysis - Patients vs. controls (group effects)

A whole-brain voxel-wise analysis revealed one significant cluster of difference in the BOLD response of patients with respect to controls, located in the left anterior insula (MNI peak voxel coordinates: x = -34, y = 12, z = -6) of k = 291 voxels. This area is shown in Figure 7.2a. A cluster could also be seen in the contralateral side; this did not reach significance in the whole-brain analysis but did for correction within an anatomically derived insula mask (created in the 'wfu_pickupatlas') (MNI peak voxel coordinates: x = 44, y = 14, z = -2; k = 83) (Figure 7.2b).

When examining the mean beta values and plotting for the effect of group, these bilateral insular clusters were found to reflect a greater deactivation (i.e. greater BOLD activity at baseline than during the visual stimulus) in VS patients compared to controls (Figure 7.2, lower panel).

There were no significant areas of increased BOLD signal between patients and controls.

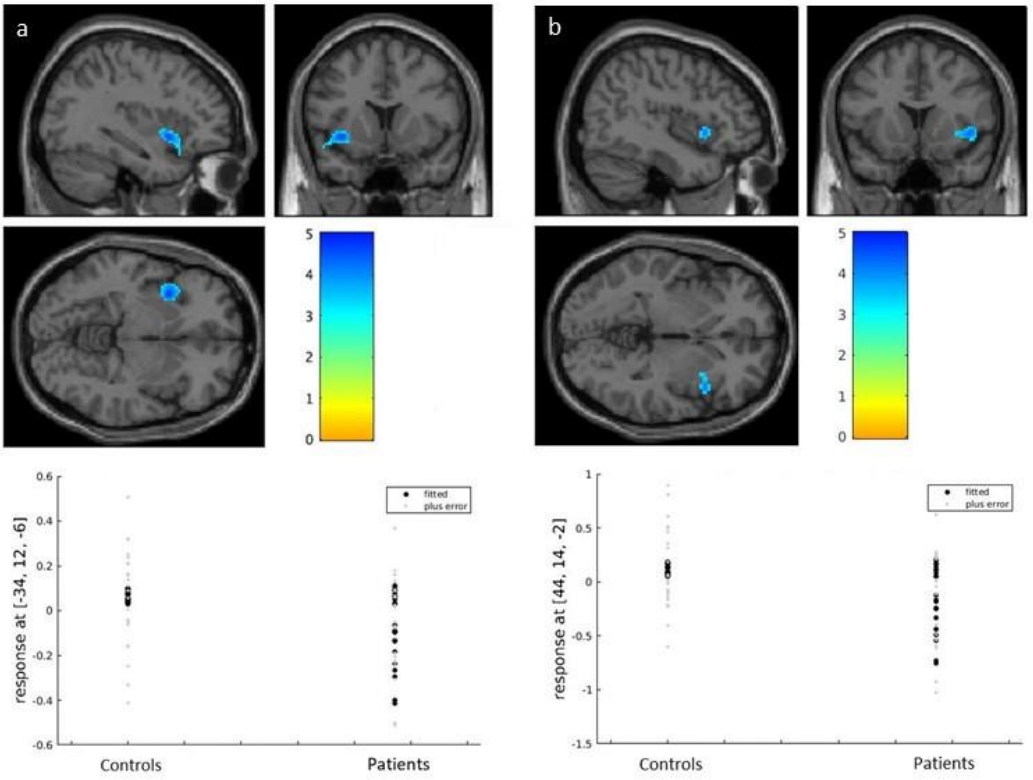

Figure 7.2 Analysis for BOLD group differences in patients vs. controls.

Plots of mean beta values for effects of group for the respective clusters are shown on the bottom part of the image. a) Whole brain analysis showing a reduction of BOLD signal in patients in the left anterior insula (k = 291; p = 0.025; MNI coordinates: x = -34, y = 12, z = -6). b) SVC with anatomical mask over the right anterior insula, showing a significant reduction of BOLD signal in patients (k = 100; p = 0.003 MNI coordinates: x = 44, y = 14, z = -2). Bars represent T-values.

7.3.3 MR spectroscopy

One subject in the control group did not have a spectroscopy scan. Further, one patient had low spectrum signal-to-noise ratio (SNR = 7.0) and was excluded from the analysis.

Figure 7.3 shows an example spectrum for one subject. The average SNR of the remaining forty-six spectra was 22.5 (± 3.4), while average FWHM was 0.05 ± 0.01 ppm (5.77 ± 1.04 Hz).

When comparing the mean metabolite concentrations of NAA, choline (Ch), creatine (Cr), myo-inositol (Myo), glutamate (Glu), glutamate and glutamine (Glx) and lactate, there was a significant increase in lactate levels in the VS patient group with respect to the control group (0.66 ± 0.9 mM vs. 0.07 ± 0.2 mM; $p < 0.001$). There was also a trend of significance for glutamate differences (10.44 ± 2.8 mM vs. 9.18 ± 1.4 mM; $p = 0.06$) (Figure 7.4).

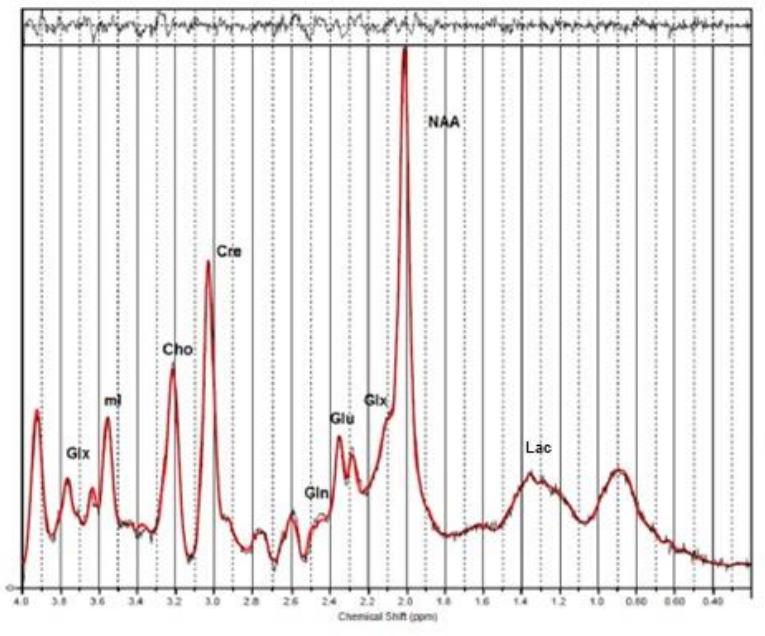

Figure 7.3 Example MRS spectrum in one subject.

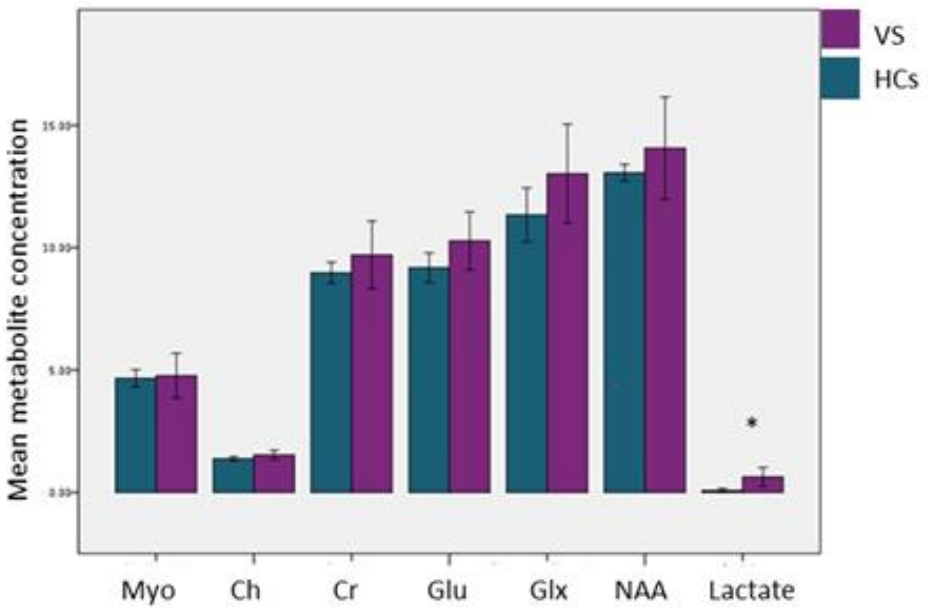

*Figure 7.4 Average metabolite concentrations in visual snow patients vs. controls. * represents significant differences. Error bars represent 95% confidence intervals*

7.3.4 BOLD/MRS correlation analysis

When analysing the beta values for the BOLD response from an anatomical ROI corresponding to the right lingual gyrus, these values were found to be significantly different between the two groups. More specifically, they were found to be reduced in VS patients compared to healthy controls (average values in VS -0.29 vs. HCs 0.03; $p < 0.001$) (Figure 7.5).

With the idea of combining these two techniques, a correlation analysis was performed between the BOLD beta values from the right lingual gyrus ROI and lactate concentration in the MRS voxel across all subjects. This showed that there was a significant negative correlation between the two measures ($p = 0.004$; r = -0.42) (Figure 7.6). A moderated regression to account for group membership further confirmed that lactate concentrations influenced BOLD beta values from the right

lingual gyrus (p = 0.04), and that this relationship was moderated by being in the VS group (OR = -0.221; 95% C.I. = [-0.432 -0.011]).

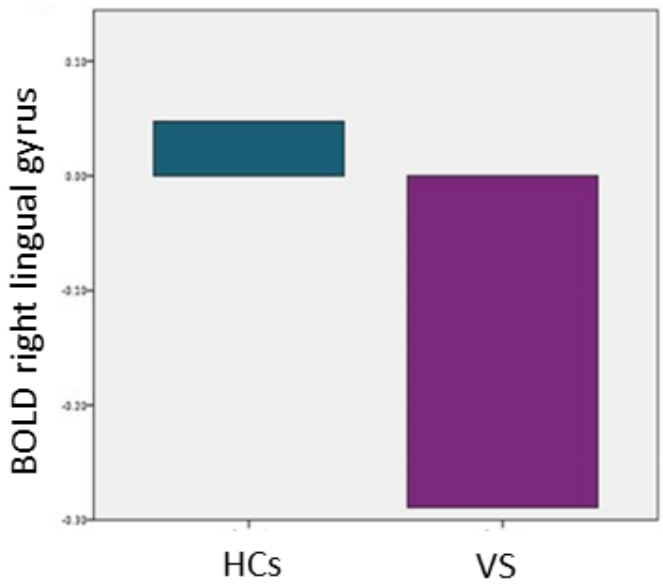

Figure 7.5 Average BOLD responses in the right lingual gyrus, in VS patients vs. controls

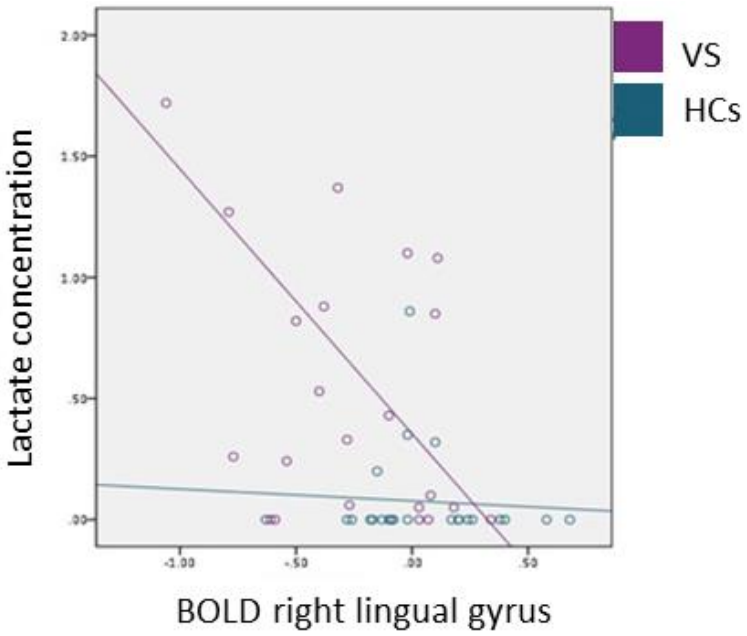

Figure 7.6 Correlation between right lingual gyrus lactate concentrations and average BOLD values in VS patients and controls.

7.4 Discussion of BOLD & MRS analysis

7.4.1 Anterior insula deactivations in VS

The most relevant finding from the task fMRI experiment was that of an abnormal BOLD response to a visual stimulus in the anterior insular cortices of visual snow patients with respect to controls (Figure 7.2). It is an important result, as it reinforces the involvement of this specific area of the salience network in visual snow, found across the other imaging modalities.

The bilateral insular deactivations could be interpreted in two opposite ways. They could in fact represent a reduction of activity when the brain is involved in a visual task, or rather they could be due to an increased activation of the region when the brain is at rest and not involved in the processing of an external stimulus. The latter hypothesis certainly is in line with the described role of the insula within the salience network, and with the arterial spin labelling results (chapter 5.3.4). A dysfunction of the fundamental integration activity of the anterior insula could explain part of the underlying pathophysiology of visual snow, where stimuli that should normally be considered irrelevant are allowed to pass a certain salience threshold in the brain, finally turning into an apparently normal perception. The arterial spin labelling and connectivity analyses in fact confirm this hypothesis, by showing that the anterior insula exhibits task-related change in response to a visual task in VS patients with respect to HCs.

A further possibility is that, unlike healthy subjects in whom the presented visual stimulus captures high levels of attention and behavioural resources, the 'intrinsic' snow is being perceived as more salient by the VS brain than the 'external' snow,

thus causing the apparent deactivation in the insula when patients are exposed to the outside stimulus.

7.4.2 BOLD response to the visual task

The functional MRI paradigm also showed an expected BOLD activation of the bilateral primary and secondary visual cortices, in response to the visual stimulation mimicking VS itself. This response was strong and sustained in both patients and controls (Figure 7.1, Table 10), and confirms that the experimental model of visual snow tested here constitutes an appropriate tool for further investigation of the condition.

Visual cortex activations were accompanied by bilateral deactivations in the occipital horns of the lateral ventricles, which extended to occipital grey matter areas of the cuneus, precuneus and lingual gyrus. In patients only however, there was a decreased BOLD response in several cortical areas, corresponding to the right middle frontal gyrus, superior frontal gyrus, FEFs, supramarginal gyrus, frontal operculum and insula. Aside from the insular region, these deactivations did not survive comparison between groups; nonetheless, they could suggest an abnormal reorganization of attention networks in visual snow in response to an external stimulus. Conversely, periventricular changes in BOLD signal common to both groups could represent noise, the product of a non-stationarity artefact (Eklund et al., 2016), or potentially - given the high *T*-scores and based on previous studies performed in cats (Jin et al., 2010) and humans (Piechnik et al., 2009) - they could be caused by physiological changes in CSF volume in response to rapid changes in visual stimuli.

7.4.3 Spectroscopy of the lingual gyrus

The magnetic resonance spectroscopy results showed increased lactate and a trend for increased glutamate in the right lingual gyrus of visual snow patients (Figure 7.4). Lactate is a product of anaerobic glycolysis; its brain concentrations can rise in response to pathological increases in energy demand, such as in cerebral hypoxia, ischemia or seizures, and more generally in the case of mitochondrial and metabolic dysfunctions (Bertholdo et al., 2013). Transient increases in lactate levels can also be found with (^{1}H) MRS as a physiological response to visual stimulation in healthy subjects (Prichard et al., 1991; Sappey-Marinier et al., 1992); this occurs because of a temporary excess of glycolysis over respiration in the cortex (Belanger et al., 2011). Previous studies have found similar lactate alterations in the visual cortex of migraine with aura patients, when subject to photic stimulation (Sandor et al., 2005; Sarchielli et al., 2005). It is important to note however, that the protocol used here involved spectroscopy acquisitions at rest, thus suggesting that the less efficient metabolism is more permanent in visual snow and not caused by an external demand. This finding, combined with the cited [^{18}F]-FDG PET study, allows one to hypothesize that the pathologically continuous perception of visual symptoms could be in part caused by an abnormal involvement of the lingual gyrus, that is metabolically hyperactivated in VS patients.

The trend for glutamate increase in the lingual gyrus that was found in VS subjects is also of note. As glutamate represents the major excitatory neurotransmitter in the brain, an increase in its concentrations could strengthen the hypothesis of hyperexcitability. Furthermore, lactate concentrations can rise in response to glutamate increase as a protective mechanism against excitotoxicity (Jourdain et al.,

2016), and this could partially explain the association between the increase in these two metabolites in VS subjects. Given the difficulties in distinguishing glutamate from glutamine peaks reliably at lower field strengths however (Gu et al., 2013; Schubert et al., 2004), these results should be considered with caution.

7.4.4 Impaired visual cortex metabolism in visual snow

Finally, by combining the MRS analysis of the lingual gyrus with BOLD responses from the same cortical area, it was possible to study both the function and metabolism of the associative visual cortex in VS. The correlation between decreased BOLD responses and increased lactate levels (Figure 7.6) suggests that the discussed localised disturbance in extrastriate anaerobic metabolism could, in turn, be causing a decreased capacity for the processing of regular visual stimuli, presented in the form of a snow simulation in the experiment. In other words, it is possible that if the associative visual cortex is continuously hyperactivated (as partially confirmed by the ASL and functional connectivity data), in the processing of an irrelevant, but nonetheless continuously perceived visual symptom, this pre-activation could then cause a decrease in the metabolic reserve necessary to respond to a physiological external stimulus. This mechanism could also represent a useful explanation for the presence of photophobia in the visual snow syndrome.

Indeed, a similar dysfunction has been described in migraine, where a decreased habituation, thought to be caused by high pre-activation levels of sensory cortices, causes an anomalous response to sensory stimuli. This pathophysiological mechanism, even if from a different starting point - given that migraineurs typically have increased visual cortex activation, as explained in chapter 8.3.3 - could indeed

represent part of the link between migraine and visual snow, already touched upon in chapter 2.3.

It is however necessary to interpret these results with caution, taking into account the important limitations of this technique, as described in the following section.

7.4.5 Limitations

There are several limitations pertaining to the MRS analysis, which require careful interpretation of the data presented in this chapter. First of all, there are known difficulties with lactate detection at 3 Tesla (Kelley et al., 1999; Lange et al., 2006). However, given that the shortcomings for this field strength are typically characterized by false-negative rather than false-positive results, this aspect seems to represent a minor issue when interpreting the specific finding of increased lactate in the VS population.

Most importantly, even if the shimming and pre-processing techniques were performed with standard practice, the modelling of the spectrum was not optimized for specific detection of lactate. This might have therefore caused sub-optimal acquisition and spectral fitting of the metabolite, which might in turn explain the high number of zero values encountered, particularly in the control group (Figure 7.6).

Unfortunately, no similar studies with control or medication free subjects, of similar age and gender and even considering voxels positioned in different brain regions, were available from the same laboratory, making it impossible to compare these values across studies with a similar methodology and pipeline.

For this reason, future work allowing a better interpretation of lactate levels in visual snow subjects is warranted. This could involve the use of spectral editing optimized

for lactate (Oeltzschner et al., 2019), a longer echo time of 288 ms (at which the doublet at 1.33 ppm will be positive and in-phase) (Lange et al., 2006), larger voxel sizes, and possibly the modulation of the underlying neurochemistry of the system through a glucose challenge. Given the current findings, it would also be interesting to integrate these future studies with a more comprehensive investigation of the underlying neurochemistry, including localised GABA measurements through MEGA-PRESS, and also considering other brain areas, such as the ones showing differences in cerebral blood flow.

8 General discussion, conclusions and future work

8.1 Summary of key findings

8.1.1 Questionnaire study

The findings from the questionnaire part of this PhD thesis, involving a large cohort of patients with visual snow and outlined in chapter 2, have uncovered several aspects of the typical VS presentation and have helped configure it as a well-delineated, clinically recognisable disorder. Visual snow appears to be more prevalent in a young population (albeit with a certain level of selection bias, as discussed in chapter 2.3.1) and affects both genders equally. It most commonly starts in early life in a gradual manner, although a proportion of subjects have a very acute onset. It is most commonly featured by different combinations of static, with black and white and transparent being the most common types. In the complete syndrome, floaters, afterimages and photophobia are almost ubiquitously present.

It has further emerged that VS does not manifest with specific biological subtypes and rather represents a clinical continuum, with patients ranging in different degrees of severity. On the severe end of the spectrum, visual snow is more likely to present with the comorbidities of migraine and tinnitus, which are quite common and possibly share some biology with the syndrome.

A final important finding is that visual snow syndrome is completely independent of the use of hallucinogenic substances. At the same time however, it appears that hallucinogen persisting perception disorder can manifest in the visual snow spectrum, showing a certain degree of overlap between the two conditions.

8.1.2 Neuroimaging study

Taken together, the results from the imaging study have provided important insight into the biology of the visual snow syndrome. The main findings show that visual snow is characterized by morphological and widespread functional changes that involve important brain networks pertaining to attention, salience, sensory processing and cognition.

Specifically, the VBM analysis revealed subtle, yet significant, anatomical brain changes in VS. The morphological grey matter alterations that were found involve relevant neocortical visual areas pertaining to visual processing and motion pathways, as well as to important cognitive and attentional cerebellar areas. Given that these anatomical differences are not associated with clinical parameters, such as the total number of disease years and the number of associated symptoms, it is quite possible that they represent an inherent trait of visual snow, rather than a consequence of the condition. The abnormalities can also partially explain the functional changes found through the other neuroimaging techniques, and potentially justify some of its clinical elements as well.

The pCASL analysis showed that patients with visual snow present increased activation in a wide network of intrinsic brain connectivity areas that are key in the processing of complex sensory and cognitive states. The fact that this rCBF increase was independent of the presence of an external visual stimulus, suggests that a state of dysfunction in connectivity networks, such as the salience and default mode networks, could be a causal factor of the disorder.

The functional connectivity results highlight that visual snow, like other neurological and psychiatric disorders, is characterized by a complex disturbance in the interaction of multiple brain systems. This dysfunction particularly involves the pre-cortical and cortical visual pathways, the visual motion network as a whole, the attention networks and finally the salience network; further, it does not depend on the activity state of the brain. These observations suggest that there is a disruption in the filtering and integration of incoming sensory visual stimuli, versus the modulation of internally generated visual information, in visual snow.

The task-based fMRI experiment showed that visual snow is characterized by a difference in bilateral insular responses to a visual stimulus mimicking the snow itself, as well as by a similar reduction of BOLD activity in the right lingual gyrus. The latter functional abnormality was further correlated with an increased lactate level in the same region, as shown by MRS. This finding suggests a localised disturbance in extrastriate anaerobic metabolism, which in turn seems to cause a decreased metabolic reserve for the regular processing of visual stimuli. Importantly, however, due to the MRS limitations outlined in chapter 7.4.5, this result should be interpreted with caution and even considered preliminary until confirmed by further data.

8.2 Towards a new visual snow model

At the start of this thesis some pathophysiological hypotheses presumed to underlie visual snow were outlined, with the intent of explaining the mechanisms involved in this syndrome (chapter 0, Figure 1.5). The research conducted here has in part corroborated these ideas, ultimately allowing the proposal of a new neurobiological model for visual snow, building on the initial hypotheses. This framework, along with a discussion of the main findings of this thesis, is described within this chapter and summarized in Figure 8.1.

First, it is important to note that the finding of multiple morphological and functional changes characterizing the VS brain compared to that of healthy subjects, ultimately confirms visual snow as a neurological syndrome. Therefore, even if at the present stage it is not possible to exclude a potential role played by ophthalmological disturbances, which could possibly serve as a trigger for disease onset in certain cases, it is clear that the primary dysfunction responsible for visual snow is located within the central nervous system.

By examining these brain dysfunctions collectively, it emerges that, as expected, the visual system is of particular importance. The posterior visual pathways, from the thalamus onwards, show a disrupted activity, both in the form of a disconnection within the inhibitory cortico-striatal circuitry that acts as a filter, and of a strengthened connection to the extrastriate visual cortex itself. Both these changes could collectively be causing a 'flooding in' of irrelevant bottom-up sensory

information, predisposing the brain to the perception of a visual noise that would normally be tuned-out directly at these lower hierarchical levels.

As for the thalamo-cortical dysrhythmia hypothesis, this can be neither confirmed nor dismissed with the methodology that was used here, and will need to be investigated with more focused experimental approaches in the future.

The functional imaging data, taken together, point out several important neurobiological disturbances pertaining to cortical activity. Possibly the most relevant finding is that, consistently, the main functional alterations are not to do with primary sensory cortices, but rather with mechanisms of higher order visual processing and integration between wide-spread cortical brain networks.

Several areas in particular showed dysfunctional activity in visual snow, across different MRI modalities. These were: the anterior insula, the PCC and precuneus, the SMA, the lateral/posterior cerebellum and of course the extrastriate visual cortex - chiefly the fusiform and lingual gyri and area V5.

The associative visual cortex is most likely hyperactivated in visual snow. This is confirmed by multiple findings: increased bilateral cerebral perfusion in the cuneus and precuneus, increased metabolic activity in the lingual gyrus, hyper-integration of key elements of the dorsal visual network, and particularly of V5, with multiple other brain areas. Spectroscopy data has also confirmed lingual gyrus hyperactivity, as had been found with [^{18}F]-FDG PET (Schankin et al., 2014b). If one combines this finding with the functional connectivity data of increased connectivity between pulvinar and

LG, it is even possible to hypothesize that the lingual hyperactivity is being driven by a strengthening of sub-cortical visual pathways.

Hyperactivity of the extrastriate visual cortex alone does not explain the entire symptomatology of the syndrome. However, if this pre-activation were in turn responsible for abnormal processing of external stimuli, this would certainly clarify several clinical elements pertaining to VSS. Hypothesizing that the associative visual cortex presents increased cortical pre-activation levels, due to a reduced 'bottom-up' filtering of incoming sensory information (see above), this could then be causing a reduced functional reserve necessary for the processing of physiological external stimuli, such as light or moving objects. A confirmation of this hypothesis comes from the link between BOLD activity in the lingual gyrus and lactate elevation in this area. Intuitively, this theory can also be inferred by observing certain clinical elements of the syndrome, such as the high prevalence of photophobia, which is in itself a highly suggestive neurological symptom of sensory processing dysfunction.

The dorsal visual stream and motion network are undoubtedly connected to visual snow pathophysiology. Indirect signs of increased neuronal function of V5, as observed through its increased regional perfusion and heightened connectivity to several brain regions, fit well with the finding of an increased cortical volume in this area. The same stands for the postero-lateral cerebellar cortex, which, as has been described, is part of important networks involved in cognitive and sensory integration processes, and has a fundamental role within the central attention system.

On the other hand, it is more difficult to understand the increase of grey matter volume in V1. This finding was unmatched by a parallel increase of blood flow in the region - as was seen for the other two areas with altered brain morphology - but rather was associated with increased coupling to the dorsal visual stream. The higher connectivity between V1 and the visual attention network and V5 however, can partly explain this finding. These areas are in fact more activated in visual snow, as can be seen from the pCASL findings, possibly because of an abnormal processing of visual stimuli. Morphological changes in V1, therefore, could be an effect of the strengthened connections with these hyperactived regions.

Ultimately, visual snow should be considered as a complex brain network dysfunction; there are several elements within the neuroimaging results provided here to support this thesis.

Both in a normal baseline as well as in an activated state, the default mode network was found to be more functionally active in VS: its nodes show a clear increase in brain perfusion, and are more integrated with frontal attention regions and occipital hubs important for higher-order visual processing. On the other hand, the DMN is less coupled with the motion network, which is in turn increasingly connected to the dorsal attention network and less connected to the ventral attention network. These findings of altered functioning between the attention networks and the DMN, could be resulting in the VS brain allocating more resources to interiorized and pre-existing visual motion information (such as the 'internal' snow), rather than on refocusing attention to new and relevant environmental stimuli (such as the 'external' snow presented during the scanning).

Further, the salience network in visual snow showed aberrant functioning in its main region, the insula, as highlighted by pCASL and BOLD imaging, as well as disrupted activity within its two principal nodes, shown by an altered functional coupling compared to controls between the insula and the ACC.

The perfusion and BOLD fMRI analyses gave opposing results with regards to anterior insular activity, even if both responses were significantly different from those of controls. In fact, with one technique there was increased perfusion, whereas with the latter there was a decreased neuronal coupling in the same region. The explanation for this peculiar difference most likely lies in the different time frames of presentation of the visual stimulus - even if the stimulus itself was identical in its other features - between the two investigations, and thus of the physiological responses that were being measured. With ASL, the acquisition lasted several minutes and participants were shown an on-going video of the visual task, thus allowing to detect a more prolonged and sustained change in brain activity. With the BOLD experiment, on the contrary, the change between the visual task and the blank screen was taking place continuously over half a minute, therefore only rapid neuronal responses could be measured.

It is thus possible to interpret the rapid decrease in insular activity in response to the external stimulus as an immediate change from a baseline of increased cortical activation, with insular activity subsequently reverting to the original state with a more prolonged observation. This hypothesis is somewhat confirmed by the functional connectivity findings, that showed an increased baseline coupling of the insula with the ACC, which failed to decrease as much as in healthy controls, in response to the visual stimulus.

Knowing of the fundamental role of the salience network for sensory integration, and most importantly of the insula in switching between an internally oriented state and externally directed attention (section 5.3.4, Figure 5.6), this could confirm that a disrupted modulation between the perception of visual information and its internalization is taking place in visual snow.

This disruption, facilitated by a lack of filtering in lower pre-cortical nodes of the visual pathway, and in the context of a hyper-activation of the visual motion network - that is more connected to the dorsal attention network and less connected to the default mode and ventral attention networks - could be causing irrelevant, 'noise-like' visual information to pass through the brain salience threshold, thus becoming a normal perception (Figure 8.1).

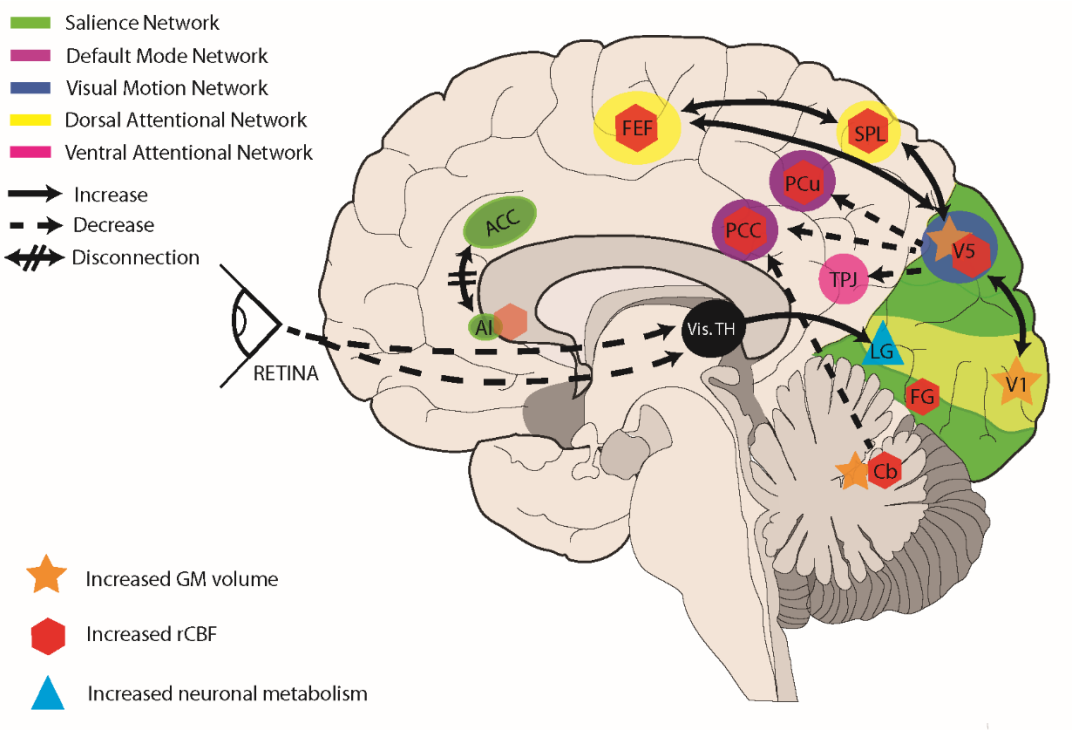

Figure 8.1 A new model for visual snow

Building on the main findings of this thesis, it is possible to hypothesize that a form of bottom-up facilitation, explained by the heightened connections between the visual thalamus (Vis.TH) and the lingual gyrus (LG), is driving an increased pre-activation of the associative visual cortex, highlighted by raised lactate levels in the LG. This increased excitation could justify the perception of sub-threshold 'noise-like' stimuli, and also cause abnormal processing of physiological visual information.
In parallel, the visual motion network, localized mostly in the cuneus and precuneus (PCu) and with its key region in motion area V5, is increased in volume, hyperactivated, more integrated with the dorsal attention network (SPL) and less with the ventral attention network (TPJ), possibly causing an increased allocation of attention to the abnormal visual noise.
Important areas of the primary (V1) and associative visual cortices (fusiform gyrus = FG) as well as the cerebellum (Lobule VI/Crus I = Cb), are also increased in volume and/or hyperfunctional in visual snow.
Finally, activity within the posterior elements of the default mode network (PCC = posterior cingulate cortex; precuneus) is increased, although these areas are less connected to the visual motion network. The two key nodes of the salience network (AI = anterior insula; ACC = anterior cingulate cortex), show disrupted coupling, while the anterior insula presents increased activity following exposure to a prolonged external stimulus (shadowed red hexagon).
Ultimately, these dysfunctions could result in a strengthening of the misattribution of salience to irrelevant internalized sensory information.

Finally, by examining possible links between the clinical data and the imaging findings, we can see that the spectrum type presentation of visual snow syndrome, as well as its relative stability through time, fit well with its description as a network issue. If VS were caused by a simple gain or loss of function within a specific brain region, one would have expected a clinical presentation characterized, as in neurodegenerative diseases, by different clinical subtypes and clear-cut differences between them, as well as a more or less gradual worsening of symptoms. This was not found however, when observing clinical characteristics in a large number of patients, although these observations were not longitudinal.

Another important message pertaining to the clinical findings is that the comorbidities associated with the clinical presentation of VS will most likely represent a key element for understanding more about the disorder in the future. Both migraine and tinnitus have shown to worsen the phenotype of visual snow independently, and HPPD presents clear clinical similarities with VS. What still needs to be understood, however, is how much neurobiology is effectively shared across these conditions.

8.3 Methodological considerations

8.3.1 Study strengths

The investigational approaches used in this thesis present some important strengths. The questionnaire study was the first to involve such a large sample of visual snow patients, with origins from all parts of the world, making it quite representative of the real population. This allows inferences of several uncovered aspects of the condition that are likely generalizable to most patients presenting with visual snow, which will in turn hopefully facilitate future research on the subject. Further, this study was the first to investigate functional subtypes in visual snow, helping to uncover something hitherto not recognised, specifically that VS clinically manifests on a spectrum of severity and therefore might be easily ignored if not presenting in its most severe form.

The neuroimaging study represents the first ever magnetic resonance imaging investigation of visual snow syndrome. Its multi-modal design allowed examination of several different aspects of VS pathophysiology, and provided a unique opportunity to characterise fully the whole-brain structural and functional alterations that are typical of affected individuals.

8.3.2 Study limitations

The main limitation for the questionnaire study is centred around selection bias. The patients that were recruited had autonomously contacted the study group in order to be involved in research. It is possible that this resulted in selecting subjects at a more severe end of the clinical spectrum. Nonetheless, most subjects were not

seeking medical help when they contacted the group, stating that their primary reason for contact was simple curiosity regarding their disorder.

Further, access to the study was solely through the internet, and this might have also biased towards a younger population, as specified in chapter 2.3.1.

The absence of an objective measure of clinical severity is another limitation; unfortunately, a suitable instrument is simply not available for visual snow as yet.

Finally, the design and methodology were based on subjects completing questionnaires remotely, and as such it relied heavily on patient participation. In some cases, it is possible that the absence of a structured interview conducted by a physician might have hindered the clinical description. The main reasoning behind this methodology was that using a web-based survey allowed reaching a broader geographical population, and this would not have been feasible through in-person approaches. Moreover, the web-based approach guaranteed the largest possible participation to the study, which again would have been very challenging if all subjects were to have had telephone interviews.

With regards to the MRI study, the main limitation is to do with not having been able to study the interactions between morphological or functional changes and clinical features of VS. This is caused, as in the questionnaire study, by the absence of an objective and reliable instrument to measure the severity of the condition. However, knowing from the questionnaire study that visual snow is a relatively homogenous condition, and having selected a patient population with similar clinical features, it is possible to generalize the changes found in this study to a larger number of patients.

A further relevant weakness of the study is to do with the lack of eye movement monitoring, which might have caused some of the changes in functional connectivity and pCASL to be caused by differences in eye movement behaviours between the two groups, as discussed in 5.3.9 and 6.3.5.

Individual limitations pertaining to each technique have been discussed in the relevant chapters.

8.3.3 Migraine comorbidity

The high association between visual snow and migraine, confirmed by both the clinical study results (Table 3) and the population that took part in the neuroimaging study (Table 6), could have potentially influenced some of the MRI findings that were presented here. Unfortunately, this comorbidity confounds the investigation of visual snow syndrome, limiting generalizability of results away from patients who do not have co-existent migraine. On the other hand, specifically selecting visual snow patients without migraine would result in a selection bias, creating a patient group not representative of the full condition. Therefore, other measures have been used in this thesis to help reduce the 'migraine confounder' and to aid the interpretation of the neuroimaging results, either by comparing the findings with existing migraine literature or by performing specific *post-hoc* analyses for the available data.

With regards to the morphological analysis, an important consideration to be made is that studies in the literature have shown opposite morphological grey matter changes in the visual areas and cerebellum of migraineurs, with respect to what was found in the visual snow group here. One VBM study in particular showed a grey

matter volume decrease in V5 in migraineurs with respect to controls, and this was correlated to disease activity (Palm-Meinders et al., 2017). Another study found decreased GM volume in the left V1/V2 area and cerebellum in chronic migraineurs without aura (Coppola et al., 2017). These literature findings, together with the sub-analysis in which migraine presence was included as a covariate leaving results unvaried (section 4.2.2), seem to suggest that the described GM volume increases in VS patients are due to the visual snow condition and not to migraine.

For the arterial spin labelling data, a separate analysis was run exclusively in VS patients without concomitant migraine, the results of which are outlined in Appendix C - pCASL *post-hoc* analysis. Overall, even if significance was lower due to power issues - the total number of VS subjects without migraine was only nine - it appears that the most relevant findings pertaining to the VS condition survived this analysis. Unfortunately, no similar pCASL study has been performed to date in a migraine population to allow for comparison with the current literature.

For functional connectivity, a *post-hoc* analysis with migraine as a covariate was also run, and showed largely overlapping results to the initial seed-based analysis. Further, functional connectivity studies in the literature that have focused on the visual system of migraineurs have shown results that are opposite to the current findings for VS. One study for example, found decreased connectivity between the sensorimotor network and the visual cortex, while conversely, increased connectivity was found between the DMN and the visual cortices bilaterally (Amin et al., 2016).

Another study found reduced connectivity between the DMN and the visuo-spatial system in migraineurs respect to healthy controls (Coppola et al., 2016).

With regards to the BOLD task, a reduced activation was found in the extrastriate visual cortex in VS patients, while most studies in the literature have repeatedly found migraine with and without aura to be associated with increased BOLD response in the primary and associative visual cortex and higher-order visual areas, both during the interictal or premonitory period (Antal et al., 2011; Schulte et al., 2016; Vincent et al., 2003) and during visually triggered attacks (Cao et al., 2002). Unfortunately, no specific study performed in migraineurs to date has focused on metabolism of the lingual gyrus directly.

Finally, it must be again specified that none of the VS patients were in the ictal migraine phase (i.e. 48 hours before or after an attack) when they were being scanned for this study.

8.4 Directions for future research

Several questions remain open with regards to visual snow pathophysiology, which will require future studies for clarification. To begin with, it is not certain that the altered network dysfunction theory highlighted here represents the main pathophysiological fingerprint underlying the condition, and is indeed a *primum movens* for the genesis of the snow illusion itself. It is certainly possible that other mechanisms, not measurable through neuroimaging, are at play in VS; these could be either simultaneous to the alterations that were found with fMRI, or could even represent their underlying cause.

Further, the fact that visual snow starts in early life could potentially hint to a congenital brain dysfunction, or even to a genetic predisposition. Only studies with targeted genetic testing will help to elucidate this aspect.

Finally, the lack of effective treatment strategies is indeed a complex issue in visual snow. No systematic clinical trials have been performed in this condition before, and all available data on treatment come from single patients or case reports. The current evidence seems to show that commonly used medications such as migraine preventives, antidepressants, or pain medication do not consistently improve or worsen visual snow (Puledda et al., 2017). There has been some positive experience with lamotrigine (Unal-Cevik et al., 2015), particularly in five subjects of a fifty-eight case series involving VS patients (van Dongen et al., 2019); however, this medication is still far from useful in most subjects. Some improvement on the other hand has

been obtained with non-pharmacological interventions such as tinted lenses, particularly with filters in the yellow-blue colour spectrum (Lauschke et al., 2016), showing that other avenues of therapy need to be explored as well in visual snow.

In the future, more work and in depth approaches will be needed in the fields of Neurology, Neuroscience and Neuro-ophthalmology in order to uncover all aspects of this complex condition, ultimately with the objective of offering better care for affected patients.

8.5 Conclusion

In the data presented in this thesis, I have shown evidence that allows recognition of visual snow as a unique neurological disorder, that is well defined by the current diagnostic criteria, and which presents with a spectrum of severity and several important comorbidities.

Further, visual snow syndrome seems to be characterized by the rupture of a delicate equilibrium across and within intrinsic brain networks. Its main feature is likely a global dysfunction in the physiological mechanism of attention, where salience is being misattributed to internal stimuli that should normally be considered irrelevant, and, possibly as a consequence, with abnormal sensory integration and reduced attention to elements of the outside world.

9 Appendices

9.1 Appendix A - Latent class analysis

Latent class analysis for the questionnaire study (chapter 2) performed on VSS patients only (1, 2; *n* = 1060) and on patients with VSS and VS (3; *n* = 1104).

1) Model fit criteria of latent class analysis on VSS patients suggested that a two class solution (in bold) provided the most parsimonious explanation of the data. The classes obtained separated patients into groups based solely on frequency of additional visual symptoms.

	1	2	3	4	5	6
n	1060	1060	1060	1060	1060	1060
AIC	9496.78	9073.196	9035.735	9018.37	9013.908	9003.152
BIC	9536.516	**9157.634**	9164.876	9192.214	9227.488	9266.401

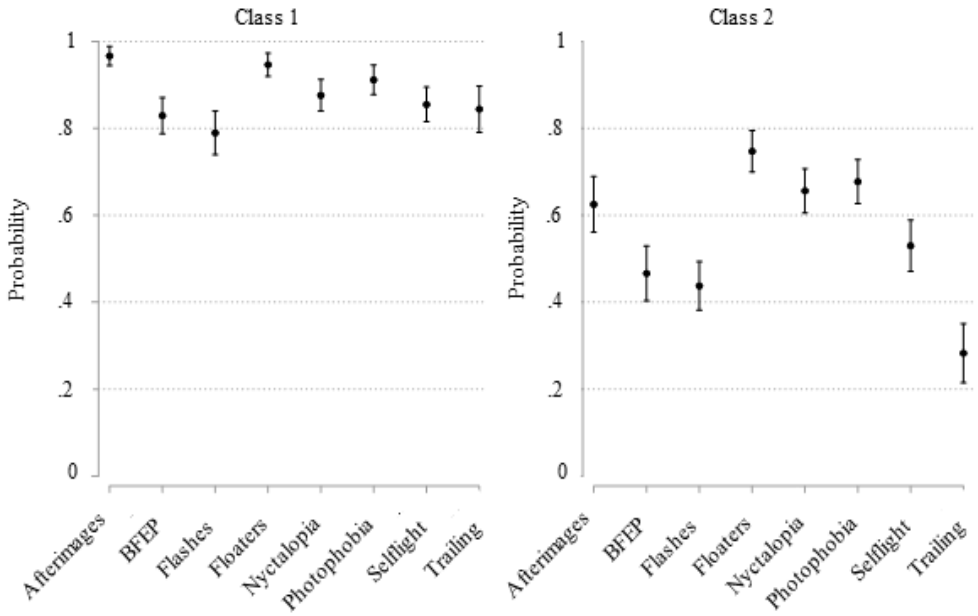

2) Logistic regression of the latent class analysis for VSS patients. The same variables were used as in the ordinal logistic regression in Table 5, reinforcing the relationship between frequency of additional visual symptoms and latent class membership. Number of observations *n* = 753; LR chi2 = 50.84; Prob > chi2 = 0.0000; pseudo R2 = 0.0491; Log likelihood = -492.78.

	OR	SE	z	C.I.
Age	0.99	0.009	-0.85	[0.97 - 1.01]
Gender	1.3	0.202	1.7	[0.96 - 1.77]
Disease years	0.99	0.010	-0.34	[0.98 - 1.02]
Migraine	2.36	0.390	5.18	[1.7 - 3.23]
Tinnitus	1.9	0.330	3.7	[1.35 - 2.67]
Onset type				
1	1.1	0.288	0.31	[0.64 - 1.83]
2	0.9	0.284	-0.4	[0.466 - 1.65]

3) Latent class analysis with VSS and VS patients (*n* = 1104). Model fit criteria of latent class analysis suggested that a three class solution (in bold) provided the most parsimonious explanation of the data. An extra class is recovered in the analysis with respect to the table in 1), however, the model still separated patients into groups based solely on frequency of additional visual symptoms.

	1	2	3	4	5	6
n	1104	1104	1104	1104	1104	1104
AIC	10283.85	9636.164	9585.471	9569.977	9561.652	9558.281
BIC	10323.9	9721.278	**9715.645**	9745.212	9781.947	9823.636

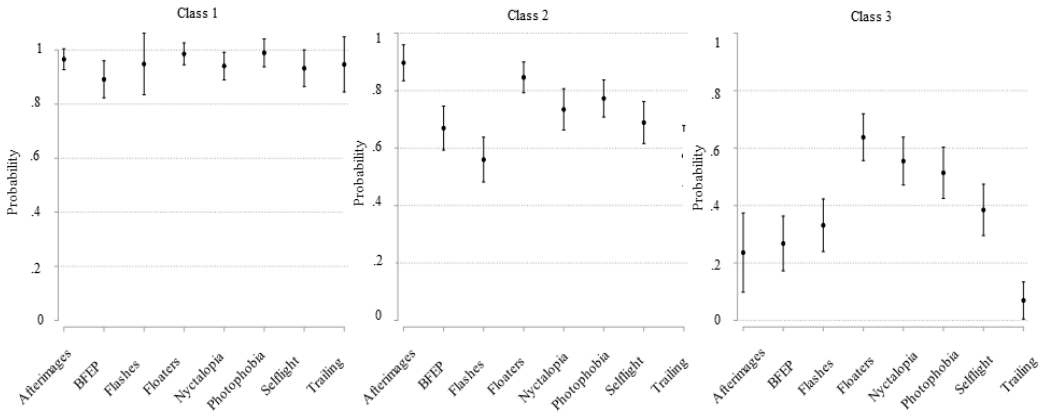

9.2 Appendix B - Evaluation of visual snow MRI simulation

Summary of 'similarity' evaluations between visual snow simulation used for the MRI task and patients' personal visual snow experience. Scores for density, speed and size of their own snow could be given by patients as either equal (=) increased (>) or reduced (<) respect to the simulation. Patient could also describe their visual snow as more black and white (BW), transparent (T), flashing (F) or coloured (C) than the simulation.

Patient number	Static Density	Static Speed	Colour	Size
1	<	<	C	<
2	=	>	=	=
3	=	=	=	=
4	=	=	F	<
5	=	=	=	=
6	=	=	=	=
7	=	=	=	=
8	=	=	=	=
9	=	=	T	=
10	>	=	=	<
11	>	=	T	=
12	>	=	=	<
13	=	=	T	<
14	=	=	=	<
15	=	<	=	=
16	=	=	T	=
17	=	=	=	=
18	=	=	C	<
19	=	=	=	<
20	=	=	=	=
21	>	=	=	=
22	>	=	T	<
23	=	=	=	=
24	=	=	T	=

9.3 Appendix C - pCASL *post-hoc* analysis

A *post-hoc* analysis for the pCASL methodology was performed in subjects without concomitant migraine (n = 9) compared to healthy volunteers (n = 24). Due to low power, the cluster-forming threshold was lowered to p <0.01 and cluster corrected to p < 0.05. A total of four clusters of significantly increased rCBF were found in patients, largely overlapping the areas from the complete whole brain analysis.

In the figure below, the clusters are imposed over a glass brain (a) and standard T1 image (b). Clusters are located in left superior temporal gyrus (x = -52 y = -28 z = 12; T = 4.19; k = 624), right SPL, cuneus and precuneus (x = 28 y = -44 z = 44; T = 3.79; k =767), left posterior cingulate gyrus (x = -8 y = -42 z = 40; T = 3.71; k =631) and left SPL, cuneus and precuneus (x = -32 y = -58 z = 48; T = 3.36; k = 930). A comparative image (c) with the whole brain analysis between VS patients and healthy controls shows that the clusters overlap significant areas from the original results, as presented in chapter 5.2.1.

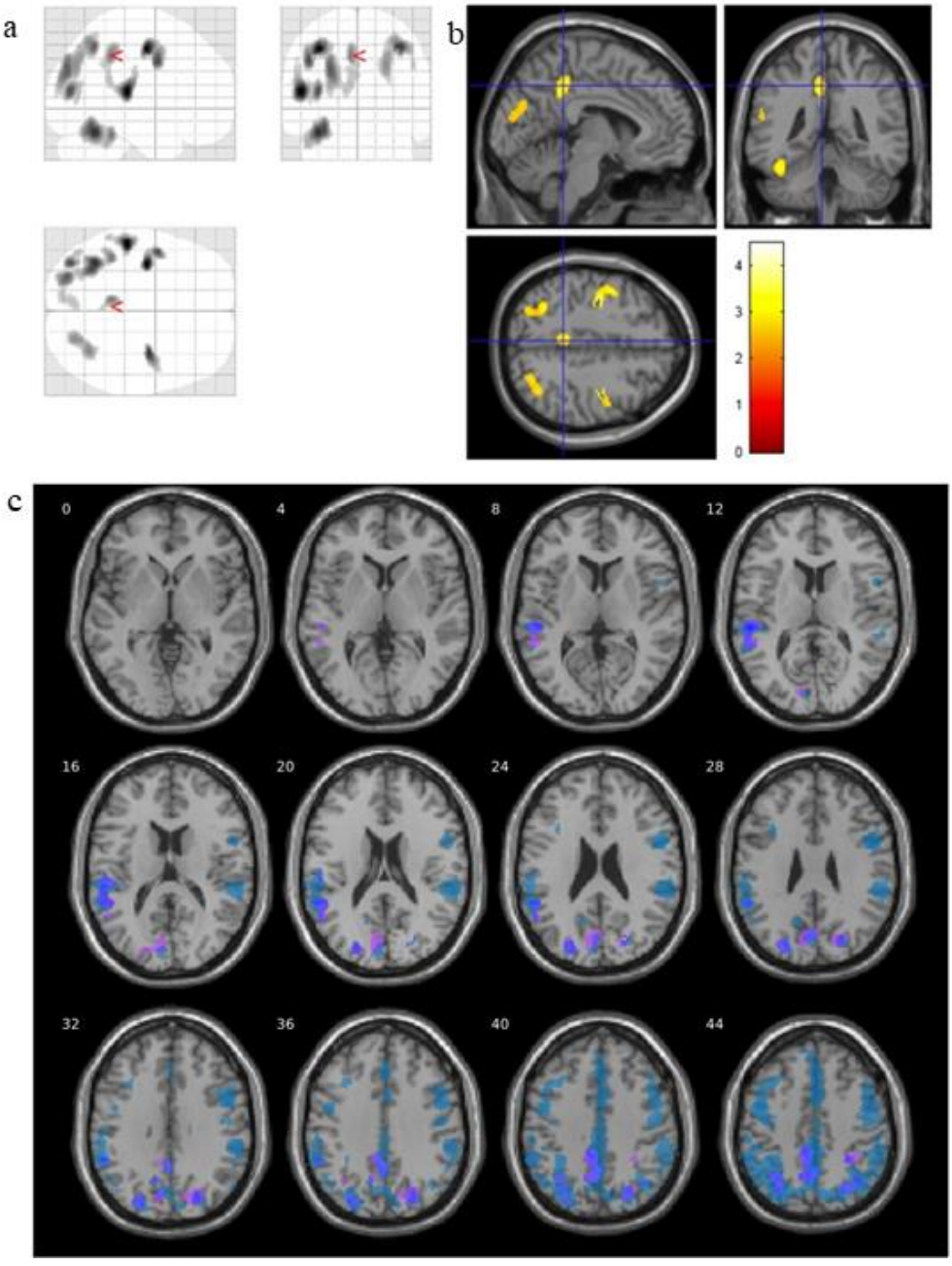
a
b
4
3
2
1
0
c
0
4
8
12
16
20
24
28
32
36
40
44

10 References

Abraham, H. D. (1983). Visual phenomenology of the LSD flashback. *Arch Gen Psychiatry, 40*(8), 884-889.

Abraham, H. D., Mc Cann, U. D., & Ricaurte, G. A. (2002). Psychedelic Drugs. In K. L. Davis, D. Charney, C. J.T., & C. Nemeroff (Eds.), *Neuropsychopharmacology: The Fifth Generation of Progress*. Philadelphia, Pennsylvania: Lippincott, Williams, & Wilkins.

Alexander, G. E., DeLong, M. R., & Strick, P. L. (1986). Parallel organization of functionally segregated circuits linking basal ganglia and cortex. *Annu Rev Neurosci, 9*, 357-381. doi:10.1146/annurev.ne.09.030186.002041

Alsop, D. C., Detre, J. A., Golay, X., Gunther, M., Hendrikse, J., Hernandez-Garcia, L., et al. (2015). Recommended implementation of arterial spin-labeled perfusion MRI for clinical applications: A consensus of the ISMRM perfusion study group and the European consortium for ASL in dementia. *Magn Reson Med, 73*(1), 102-116. doi:10.1002/mrm.25197

Amin, F. M., Hougaard, A., Magon, S., Asghar, M. S., Ahmad, N. N., Rostrup, E., et al. (2016). Change in brain network connectivity during PACAP38-induced migraine attacks: A resting-state functional MRI study. *Neurology, 86*(2), 180-187. doi:10.1212/wnl.0000000000002261

Anderson, T. J., Jenkins, I. H., Brooks, D. J., Hawken, M. B., Frackowiak, R. S. J., & Kennard, C. (1994). Cortical control of saccades and fixation in man A PET study. *Brain, 117*(5), 1073-1084. doi:10.1093/brain/117.5.1073

Antal, A., Polania, R., Saller, K., Morawetz, C., Schmidt-Samoa, C., Baudewig, J., et al. (2011). Differential activation of the middle-temporal complex to visual stimulation in migraineurs. *Cephalalgia, 31*(3), 338-345. doi:10.1177/0333102410379889

Arnold, W., Bartenstein, P., Oestreicher, E., Romer, W., & Schwaiger, M. (1996). Focal metabolic activation in the predominant left auditory cortex in patients suffering from tinnitus: a PET study with [18F]deoxyglucose. *ORL J Otorhinolaryngol Relat Spec, 58*(4), 195-199.

Ashburner, J. (2007). A fast diffeomorphic image registration algorithm. *Neuroimage, 38*(1), 95-113. doi:10.1016/j.neuroimage.2007.07.007

Ashburner, J., & Friston, K. J. (2000). Voxel-based morphometry--the methods. *Neuroimage, 11*(6 Pt 1), 805-821. doi:10.1006/nimg.2000.0582

Bandettini, P. A., Wong, E. C., Hinks, R. S., Tikofsky, R. S., & Hyde, J. S. (1992). Time course EPI of human brain function during task activation. *Magn Reson Med, 25*(2), 390-397. doi:10.1002/mrm.1910250220

Belanger, M., Allaman, I., & Magistretti, P. J. (2011). Brain energy metabolism: focus on astrocyte-neuron metabolic cooperation. *Cell Metab, 14*(6), 724-738. doi:10.1016/j.cmet.2011.08.016

Bernasconi, N., Duchesne, S., Janke, A., Lerch, J., Collins, D. L., & Bernasconi, A. (2004). Whole-brain voxel-based statistical analysis of gray matter and white matter in temporal lobe epilepsy. *Neuroimage, 23*(2), 717-723. doi:10.1016/j.neuroimage.2004.06.015

Bertholdo, D., Watcharakorn, A., & Castillo, M. (2013). Brain proton magnetic resonance spectroscopy: introduction and overview. *Neuroimaging Clin N Am, 23*(3), 359-380. doi:10.1016/j.nic.2012.10.002

Beschoner, P., Richter, S., Lo, H., Sim, E. J., Baron, K., Osterfeld, N., et al. (2008). Baseline brain perfusion and working memory capacity: a neuroimaging study. *Neuroreport, 19*(18), 1803-1807. doi:10.1097/WNR.0b013e32831997f1

Bessero, A. C., & Plant, G. T. (2014). Should 'visual snow' and persistence of after-images be recognised as a new visual syndrome? *J Neurol Neurosurg Psychiatry, 85*(9), 1057-1058. doi:10.1136/jnnp-2013-306827

Biswal, B., Yetkin, F. Z., Haughton, V. M., & Hyde, J. S. (1995). Functional connectivity in the motor cortex of resting human brain using echo-planar MRI. *Magn Reson Med, 34*(4), 537-541. doi:10.1002/mrm.1910340409

Born, R. T., & Bradley, D. C. (2005). Structure and Function of Visual Area MT. *Annu Rev Neurosci, 28*(1), 157-189. doi:10.1146/annurev.neuro.26.041002.131052

Braddick, O. J., O'Brien, J. M., Wattam-Bell, J., Atkinson, J., Hartley, T., & Turner, R. (2001). Brain areas sensitive to coherent visual motion. *Perception, 30*(1), 61-72. doi:10.1068/p3048

Brooks, D. J., Jenkins, I. H., Jahanshahi, M., Jueptner, M., & Passingham, R. E. (2000). Self-initiated versus externally triggered movements: II. The effect of movement predictability on regional cerebral blood flow. *Brain, 123*(6), 1216-1228. doi:10.1093/brain/123.6.1216 %J Brain

Brown, G. C., Brown, M. M., & Fischer, D. H. (2015). Photopsias: A Key to Diagnosis. *Ophthalmology, 122*(10), 2084-2094. doi:10.1016/j.ophtha.2015.06.025

Buxton, R. B., Wong, E. C., & Frank, L. R. (1998). Dynamics of blood flow and oxygenation changes during brain activation: The balloon model. *Magn Reson Med, 39*(6), 855-864. doi:10.1002/mrm.1910390602

Cabeza, R., & Nyberg, L. (2000). Imaging Cognition II: An Empirical Review of 275 PET and fMRI Studies. *J Cogn Neurosci, 12*(1), 1-47. doi:10.1162/08989290051137585

Cao, Y., Aurora, S. K., Nagesh, V., Patel, S. C., & Welch, K. M. (2002). Functional MRI-BOLD of brainstem structures during visually triggered migraine. *Neurology, 59*(1), 72-78. doi:10.1212/wnl.59.1.72

Chappell, M., Macintosh, B., & Okell, T. (2017). *Introduction to perfusion quantification using Arterial Spin labelling*. 198 Madison Avenue, New York, NY 10016, United Stated of America: Oxford University Press.

Chen, B. S., Lance, S., Lallu, B., & Anderson, N. E. (2019). Visual snow: Not so benign. *J Clin Neurosci, 64*, 37-39. doi:10.1016/j.jocn.2019.03.023

Chen, W. T., Lin, Y. Y., Fuh, J. L., Hamalainen, M. S., Ko, Y. C., & Wang, S. J. (2011). Sustained visual cortex hyperexcitability in migraine with persistent visual aura. *Brain, 134*(Pt 8), 2387-2395. doi:10.1093/brain/awr157

Collerton, D., Perry, E., & McKeith, I. (2005). Why people see things that are not there: a novel Perception and Attention Deficit model for recurrent complex visual hallucinations. *Behav Brain Sci, 28*(6), 737-757; discussion 757-794. doi:10.1017/s0140525x05000130

Coppola, G., Ambrosini, A., Di Clemente, L., Magis, D., Fumal, A., Gerard, P., et al. (2007). Interictal abnormalities of gamma band activity in visual evoked

responses in migraine: an indication of thalamocortical dysrhythmia? *Cephalalgia, 27*(12), 1360-1367. doi:10.1111/j.1468-2982.2007.01466.x

Coppola, G., Di Renzo, A., Tinelli, E., Lepre, C., Di Lorenzo, C., Di Lorenzo, G., et al. (2016). Thalamo-cortical network activity between migraine attacks: Insights from MRI-based microstructural and functional resting-state network correlation analysis. *J Headache Pain, 17*(1), 100. doi:10.1186/s10194-016-0693-y

Coppola, G., Petolicchio, B., Di Renzo, A., Tinelli, E., Di Lorenzo, C., Parisi, V., et al. (2017). Cerebral gray matter volume in patients with chronic migraine: correlations with clinical features. *J Headache Pain, 18*(1), 115. doi:10.1186/s10194-017-0825-z

Corbetta, M., Kincade, J. M., Ollinger, J. M., McAvoy, M. P., & Shulman, G. L. (2000). Voluntary orienting is dissociated from target detection in human posterior parietal cortex. *Nat Neurosci, 3*(3), 292-297. doi:10.1038/73009

Corbetta, M., Patel, G., & Shulman, G. L. (2008). The reorienting system of the human brain: from environment to theory of mind. *Neuron, 58*(3), 306-324. doi:10.1016/j.neuron.2008.04.017

Corbetta, M., & Shulman, G. L. (2002). Control of goal-directed and stimulus-driven attention in the brain. *Nat Rev Neurosci, 3*(3), 201-215. doi:10.1038/nrn755

Critchley, M. (1951). Types of visual perseveration: "paliopsia" and "illusory visual spread". *Brain, 74*(3), 267-299.

Crone, J. S., Schurz, M., Holler, Y., Bergmann, J., Monti, M., Schmid, E., et al. (2015). Impaired consciousness is linked to changes in effective connectivity of the

posterior cingulate cortex within the default mode network. *Neuroimage, 110*, 101-109. doi:10.1016/j.neuroimage.2015.01.037

D'Esposito, M. (2007). From cognitive to neural models of working memory. *Philos Trans R Soc Lond B Biol Sci, 362*(1481), 761-772. doi:10.1098/rstb.2007.2086

Dai, W., Garcia, D., de Bazelaire, C., & Alsop, D. C. (2008). Continuous flow-driven inversion for arterial spin labeling using pulsed radio frequency and gradient fields. *Magn Reson Med, 60*(6), 1488-1497. doi:10.1002/mrm.21790

De Ridder, D., Vanneste, S., Langguth, B., & Llinas, R. (2015). Thalamocortical Dysrhythmia: A Theoretical Update in Tinnitus. *Front Neurol, 6*, 124. doi:10.3389/fneur.2015.00124

De Ridder, D., Vanneste, S., Weisz, N., Londero, A., Schlee, W., Elgoyhen, A. B., et al. (2014). An integrative model of auditory phantom perception: tinnitus as a unified percept of interacting separable subnetworks. *Neurosci Biobehav Rev, 44*, 16-32. doi:10.1016/j.neubiorev.2013.03.021

Denuelle, M., Boulloche, N., Payoux, P., Fabre, N., Trotter, Y., & Geraud, G. (2011). A PET study of photophobia during spontaneous migraine attacks. *Neurology, 76*(3), 213-218. doi:10.1212/WNL.0b013e3182074a57

Detre, J. A., Leigh, J. S., Williams, D. S., & Koretsky, A. P. (1992). Perfusion imaging. *Magn Reson Med, 23*(1), 37-45. doi:10.1002/mrm.1910230106

Detre, J. A., Wang, J., Wang, Z., & Rao, H. (2009). Arterial spin-labeled perfusion MRI in basic and clinical neuroscience. *Curr Opin Neurol, 22*(4), 348-355. doi:10.1097/WCO.0b013e32832d9505

Diedrichsen, J. (2006). A spatially unbiased atlas template of the human cerebellum. *Neuroimage, 33*(1), 127-138. doi:10.1016/j.neuroimage.2006.05.056

Diedrichsen, J., Balsters, J. H., Flavell, J., Cussans, E., & Ramnani, N. (2009). A probabilistic MR atlas of the human cerebellum. *Neuroimage, 46*(1), 39-46. doi:10.1016/j.neuroimage.2009.01.045

Dosenbach, N. U., Fair, D. A., Cohen, A. L., Schlaggar, B. L., & Petersen, S. E. (2008). A dual-networks architecture of top-down control. *Trends Cogn Sci, 12*(3), 99-105. doi:10.1016/j.tics.2008.01.001

Dosenbach, N. U., Fair, D. A., Miezin, F. M., Cohen, A. L., Wenger, K. K., Dosenbach, R. A., et al. (2007). Distinct brain networks for adaptive and stable task control in humans. *Proc Natl Acad Sci U S A, 104*(26), 11073-11078. doi:10.1073/pnas.0704320104

Dosenbach, N. U., Visscher, K. M., Palmer, E. D., Miezin, F. M., Wenger, K. K., Kang, H. C., et al. (2006). A core system for the implementation of task sets. *Neuron, 50*(5), 799-812. doi:10.1016/j.neuron.2006.04.031

Dresel, C., Castrop, F., Haslinger, B., Wohlschlaeger, A. M., Hennenlotter, A., & Ceballos-Baumann, A. O. (2005). The functional neuroanatomy of coordinated orofacial movements: sparse sampling fMRI of whistling. *Neuroimage, 28*(3), 588-597. doi:10.1016/j.neuroimage.2005.06.021

Edelman, R. R., Siewert, B., Darby, D. G., Thangaraj, V., Nobre, A. C., Mesulam, M. M., et al. (1994). Qualitative mapping of cerebral blood flow and functional localization with echo-planar MR imaging and signal targeting with alternating radio frequency. *Radiology, 192*(2), 513-520. doi:10.1148/radiology.192.2.8029425

Eklund, A., Nichols, T. E., & Knutsson, H. (2016). Cluster failure: Why fMRI inferences for spatial extent have inflated false-positive rates. *Proceedings of the National Academy of Sciences, 113*(28), 7900-7905. doi:10.1073/pnas.1602413113

Eren, O., Rauschel, V., Ruscheweyh, R., Straube, A., & Schankin, C. J. (2018). Evidence of dysfunction in the visual association cortex in visual snow syndrome. *Ann Neurol, 84*(6), 946-949. doi:10.1002/ana.25372

Ettinger, U., ffytche, D. H., Kumari, V., Kathmann, N., Reuter, B., Zelaya, F., et al. (2007). Decomposing the Neural Correlates of Antisaccade Eye Movements Using Event-Related fMRI. *Cerebral Cortex, 18*(5), 1148-1159. doi:10.1093/cercor/bhm147

Fair, D. A., Dosenbach, N. U., Church, J. A., Cohen, A. L., Brahmbhatt, S., Miezin, F. M., et al. (2007). Development of distinct control networks through segregation and integration. *Proc Natl Acad Sci U S A, 104*(33), 13507-13512. doi:10.1073/pnas.0705843104

Ffytche, D. H. (2008). The hodology of hallucinations. *Cortex, 44*(8), 1067-1083. doi:10.1016/j.cortex.2008.04.005

Ffytche, D. H., Blom, J. D., & Catani, M. (2010). Disorders of visual perception. *J Neurol Neurosurg Psychiatry, 81*(11), 1280-1287. doi:10.1136/jnnp.2008.171348

Ffytche, D. H., Howard, R. J., Brammer, M. J., David, A., Woodruff, P., & Williams, S. (1998). The anatomy of conscious vision: an fMRI study of visual hallucinations. *Nat Neurosci, 1*(8), 738-742. doi:10.1038/3738

Fox, M. D., Corbetta, M., Snyder, A. Z., Vincent, J. L., & Raichle, M. E. (2006). Spontaneous neuronal activity distinguishes human dorsal and ventral

attention systems. *Proceedings of the National Academy of Sciences, 103*(26), 10046-10051. doi:10.1073/pnas.0604187103

Fox, M. D., & Raichle, M. E. (2007). Spontaneous fluctuations in brain activity observed with functional magnetic resonance imaging. *Nat Rev Neurosci, 8*(9), 700-711. doi:10.1038/nrn2201

Fox, M. D., Snyder, A. Z., Vincent, J. L., Corbetta, M., Van Essen, D. C., & Raichle, M. E. (2005). The human brain is intrinsically organized into dynamic, anticorrelated functional networks. *Proc Natl Acad Sci U S A, 102*(27), 9673-9678. doi:10.1073/pnas.0504136102

Fraser, C. L., & White, O. B. (2018). There's something in the air. *Surv Ophthalmol, 64*(5), 729-733. doi:10.1016/j.survophthal.2018.08.004

Friston, K., & Kiebel, S. (2009). Predictive coding under the free-energy principle. *Philos Trans R Soc Lond B Biol Sci, 364*(1521), 1211-1221. doi:10.1098/rstb.2008.0300

Friston, K. J., Buechel, C., Fink, G. R., Morris, J., Rolls, E., & Dolan, R. J. (1997). Psychophysiological and modulatory interactions in neuroimaging. *Neuroimage, 6*(3), 218-229. doi:10.1006/nimg.1997.0291

Friston, K. J., Holmes, A. P., Poline, J. B., Grasby, P. J., Williams, S. C. R., Frackowiak, R. S. J., et al. (1995). Analysis of fMRI Time-Series Revisited. *Neuroimage, 2*(1), 45-53. doi:https://doi.org/10.1006/nimg.1995.1007

Gilbert, C. D., & Li, W. (2013). Top-down influences on visual processing. *Nat Rev Neurosci, 14*(5), 350-363. doi:10.1038/nrn3476

Golland, Y., Bentin, S., Gelbard, H., Benjamini, Y., Heller, R., Nir, Y., et al. (2006). Extrinsic and Intrinsic Systems in the Posterior Cortex of the Human Brain

Revealed during Natural Sensory Stimulation. *Cerebral Cortex, 17*(4), 766-777. doi:10.1093/cercor/bhk030

Goodale, M. A., & Milner, A. D. (1992). Separate visual pathways for perception and action. *Trends Neurosci, 15*(1), 20-25.

Greicius, M. D., Krasnow, B., Reiss, A. L., & Menon, V. (2003). Functional connectivity in the resting brain: a network analysis of the default mode hypothesis. *Proc Natl Acad Sci U S A, 100*(1), 253-258. doi:10.1073/pnas.0135058100

Gu, M., Zahr, N. M., Spielman, D. M., Sullivan, E. V., Pfefferbaum, A., & Mayer, D. (2013). Quantification of glutamate and glutamine using constant-time point-resolved spectroscopy at 3 T. *NMR Biomed, 26*(2), 164-172. doi:10.1002/nbm.2831

Guell, X., Schmahmann, J. D., Gabrieli, J. D. E., & Ghosh, S. S. (2018). Functional gradients of the cerebellum. *eLife, 7*, e36652. doi:10.7554/eLife.36652

Gujar, S. K., Maheshwari, S., Bjorkman-Burtscher, I., & Sundgren, P. C. (2005). Magnetic resonance spectroscopy. *J Neuroophthalmol, 25*(3), 217-226.

Haase, A., Frahm, J., Hanicke, W., & Matthaei, D. (1985). 1H NMR chemical shift selective (CHESS) imaging. *Physics in Medicine and Biology, 30*(4), 341-344. doi:10.1088/0031-9155/30/4/008

Habas, C., Kamdar, N., Nguyen, D., Prater, K., Beckmann, C. F., Menon, V., et al. (2009). Distinct cerebellar contributions to intrinsic connectivity networks. *J Neurosci, 29*(26), 8586-8594. doi:10.1523/jneurosci.1868-09.2009

Headache Classification Committee of the International Headache Society (IHS). (2018). The International Classification of Headache Disorders, 3rd edition. *Cephalalgia, 38*(1), 1-211. doi:10.1177/0333102417738202

Heeger, D. J., & Ress, D. (2002). What does fMRI tell us about neuronal activity? *Nat Rev Neurosci, 3*(2), 142-151. doi:10.1038/nrn730

Hermes, M., Hagemann, D., Britz, P., Lieser, S., Bertsch, K., Naumann, E., et al. (2009). Latent state-trait structure of cerebral blood flow in a resting state. *Biol Psychol, 80*(2), 196-202. doi:10.1016/j.biopsycho.2008.09.003

Hodkinson, D. J., Krause, K., Khawaja, N., Renton, T. F., Huggins, J. P., Vennart, W., et al. (2013). Quantifying the test-retest reliability of cerebral blood flow measurements in a clinical model of on-going post-surgical pain: A study using pseudo-continuous arterial spin labelling. *Neuroimage Clin, 3*, 301-310. doi:10.1016/j.nicl.2013.09.004

Hodkinson, D. J., O'Daly, O., Zunszain, P. A., Pariante, C. M., Lazurenko, V., Zelaya, F. O., et al. (2014). Circadian and homeostatic modulation of functional connectivity and regional cerebral blood flow in humans under normal entrained conditions. *J Cereb Blood Flow Metab, 34*(9), 1493-1499. doi:10.1038/jcbfm.2014.109

Honea, R., Crow, T. J., Passingham, D., & Mackay, C. E. (2005). Regional deficits in brain volume in schizophrenia: a meta-analysis of voxel-based morphometry studies. *Am J Psychiatry, 162*(12), 2233-2245. doi:10.1176/appi.ajp.162.12.2233

Hopfinger, J. B., Buonocore, M. H., & Mangun, G. R. (2000). The neural mechanisms of top-down attentional control. *Nat Neurosci, 3*(3), 284-291. doi:10.1038/72999

Howard, M. A., Krause, K., Khawaja, N., Massat, N., Zelaya, F., Schumann, G., et al. (2011). Beyond patient reported pain: perfusion magnetic resonance imaging

demonstrates reproducible cerebral representation of ongoing post-surgical pain. *PLoS One, 6*(2), e17096. doi:10.1371/journal.pone.0017096

Howard, M. A., Sanders, D., Krause, K., O'Muircheartaigh, J., Fotopoulou, A., Zelaya, F., et al. (2012). Alterations in resting-state regional cerebral blood flow demonstrate ongoing pain in osteoarthritis: An arterial spin-labeled magnetic resonance imaging study. *Arthritis Rheum, 64*(12), 3936-3946. doi:10.1002/art.37685

Hullfish, J., Abenes, I., Yoo, H. B., De Ridder, D., & Vanneste, S. (2019). Frontostriatal network dysfunction as a domain-general mechanism underlying phantom perception. *Hum Brain Mapp, 40*(7), 2241-2251. doi:10.1002/hbm.24521

Jack, C. R., Jr., Bernstein, M. A., Borowski, B. J., Gunter, J. L., Fox, N. C., Thompson, P. M., et al. (2010). Update on the magnetic resonance imaging core of the Alzheimer's disease neuroimaging initiative. *Alzheimers Dement, 6*(3), 212-220. doi:10.1016/j.jalz.2010.03.004

Jager, H. R., Giffin, N. J., & Goadsby, P. J. (2005). Diffusion- and perfusion-weighted MR imaging in persistent migrainous visual disturbances. *Cephalalgia, 25*(5), 323-332. doi:10.1111/j.1468-2982.2004.00858.x

Jaramillo, J., Mejias, J. F., & Wang, X.-J. (2019). Engagement of Pulvino-cortical Feedforward and Feedback Pathways in Cognitive Computations. *Neuron, 101*(2), 321-336.e329. doi:https://doi.org/10.1016/j.neuron.2018.11.023

Jin, T., & Kim, S. G. (2010). Change of the cerebrospinal fluid volume during brain activation investigated by T(1rho)-weighted fMRI. *Neuroimage, 51*(4), 1378-1383. doi:10.1016/j.neuroimage.2010.03.047

Jourdain, P., Allaman, I., Rothenfusser, K., Fiumelli, H., Marquet, P., & Magistretti, P. J. (2016). L-Lactate protects neurons against excitotoxicity: implication of an ATP-mediated signaling cascade. *Scientific Reports, 6*, 21250. doi:10.1038/srep21250

Karsan, N., Bose, P., Zelaya, F., & Goadsby, P. J. (2018). Alterations in cerebral blood flow associated with the premonitory phase of migraine. *Cephalalgia, 38*(1_suppl), 36. doi:10.1177/0333102418789865

Keller, S. S., Wieshmann, U. C., Mackay, C. E., Denby, C. E., Webb, J., & Roberts, N. (2002). Voxel based morphometry of grey matter abnormalities in patients with medically intractable temporal lobe epilepsy: effects of side of seizure onset and epilepsy duration. *J Neurol Neurosurg Psychiatry, 73*(6), 648-655. doi:10.1136/jnnp.73.6.648

Kelley, D. A. C., Wald, L. L., & Star-Lack, J. M. (1999). Lactate detection at 3T: Compensating J coupling effects with BASING. *Journal of Magnetic Resonance Imaging, 9*(5), 732-737. doi:10.1002/(sici)1522-2586(199905)9:5<732::Aid-jmri17>3.0.Co;2-q

Keszthelyi, D., Aziz, Q., Ruffle, J. K., O'Daly, O., Sanders, D., Krause, K., et al. (2018). Delineation between different components of chronic pain using dimension reduction - an ASL fMRI study in hand osteoarthritis. *Eur J Pain, 22*(7), 1245-1254. doi:10.1002/ejp.1212

Khaleeli, Z., Tucker, W. R., del Porto, L., Virgo, J. D., & Plant, G. T. (2018). Remember the retina: retinal disorders presenting to neurologists. *Pract Neurol, 18*(2), 84-96. doi:10.1136/practneurol-2016-001534

Kim, H. J., Lee, H. J., An, S. Y., Sim, S., Park, B., Kim, S. W., et al. (2015). Analysis of the prevalence and associated risk factors of tinnitus in adults. *PLoS One, 10*(5), e0127578. doi:10.1371/journal.pone.0127578

King, M., Hernandez-Castillo, C. R., Poldrack, R. A., Ivry, R. B., & Diedrichsen, J. (2019). Functional boundaries in the human cerebellum revealed by a multi-domain task battery. *Nat Neurosci, 22*(8), 1371-1378. doi:10.1038/s41593-019-0436-x

Kinsbourne, M., & Warrington, E. K. (1963). A study of visual perseveration. *J Neurol Neurosurg Psychiatry, 26*, 468-475.

Kondziella, D., Olsen, M. H., & Dreier, J. P. (2020). Prevalence of visual snow syndrome in the UK. *Eur J Neurol*. doi:10.1111/ene.14150

Kriegeskorte, N., Simmons, W. K., Bellgowan, P. S., & Baker, C. I. (2009). Circular analysis in systems neuroscience: the dangers of double dipping. *Nat Neurosci, 12*(5), 535-540. doi:10.1038/nn.2303

Kundu, P., Inati, S. J., Evans, J. W., Luh, W. M., & Bandettini, P. A. (2012). Differentiating BOLD and non-BOLD signals in fMRI time series using multi-echo EPI. *Neuroimage, 60*(3), 1759-1770. doi:10.1016/j.neuroimage.2011.12.028

Kundu, P., Voon, V., Balchandani, P., Lombardo, M. V., Poser, B. A., & Bandettini, P. A. (2017). Multi-echo fMRI: A review of applications in fMRI denoising and analysis of BOLD signals. *Neuroimage, 154*, 59-80. doi:https://doi.org/10.1016/j.neuroimage.2017.03.033

Kwong, K. K., Belliveau, J. W., Chesler, D. A., Goldberg, I. E., Weisskoff, R. M., Poncelet, B. P., et al. (1992). Dynamic magnetic resonance imaging of human brain activity during primary sensory stimulation. *Proc Natl Acad Sci U S A, 89*(12), 5675-5679. doi:10.1073/pnas.89.12.5675

Lakatos, P., O'Connell, Monica N., & Barczak, A. (2016). Pondering the Pulvinar. *Neuron, 89*(1), 5-7. doi:https://doi.org/10.1016/j.neuron.2015.12.022

Lange, T., Dydak, U., Roberts, T. P., Rowley, H. A., Bjeljac, M., & Boesiger, P. (2006). Pitfalls in lactate measurements at 3T. *AJNR Am J Neuroradiol, 27*(4), 895-901.

Lauschke, J. L., Plant, G. T., & Fraser, C. L. (2016). Visual snow: A thalamocortical dysrhythmia of the visual pathway? *J Clin Neurosci, 28*, 123-127. doi:10.1016/j.jocn.2015.12.001

Liu, G. T., Schatz, N. J., Galetta, S. L., Volpe, N. J., Skobieranda, F., & Kosmorsky, G. S. (1995). Persistent positive visual phenomena in migraine. *Neurology, 45*(4), 664-668.

Llinas, R. R., Ribary, U., Jeanmonod, D., Kronberg, E., & Mitra, P. P. (1999). Thalamocortical dysrhythmia: A neurological and neuropsychiatric syndrome characterized by magnetoencephalography. *Proc Natl Acad Sci U S A, 96*(26), 15222-15227.

Luna, S., Lai, D., & Harris, A. (2018). Antagonistic Relationship Between VEP Potentiation and Gamma Power in Visual Snow Syndrome. *Headache, 58*(1), 138-144. doi:10.1111/head.13231

Mai, J., Paxinos, G., & Voss, T. (2008). *Atlas of the Human Brain* (Elsevier Ed. third ed.): Elsevier.

Maleki, N., Becerra, L., Upadhyay, J., Burstein, R., & Borsook, D. (2012). Direct optic nerve pulvinar connections defined by diffusion MR tractography in humans: implications for photophobia. *Hum Brain Mapp, 33*(1), 75-88. doi:10.1002/hbm.21194

Maniyar, F. H., Sprenger, T., Schankin, C., & Goadsby, P. J. (2014). Photic hypersensitivity in the premonitory phase of migraine--a positron emission tomography study. *Eur J Neurol, 21*(9), 1178-1183. doi:10.1111/ene.12451

Margulies, D. S., Vincent, J. L., Kelly, C., Lohmann, G., Uddin, L. Q., Biswal, B. B., et al. (2009). Precuneus shares intrinsic functional architecture in humans and monkeys. *Proc Natl Acad Sci U S A, 106*(47), 20069-20074. doi:10.1073/pnas.0905314106

Mato Abad, V., Garcia-Polo, P., O'Daly, O., Hernandez-Tamames, J. A., & Zelaya, F. (2016). ASAP (Automatic Software for ASL Processing): A toolbox for processing Arterial Spin Labeling images. *Magn Reson Imaging, 34*(3), 334-344. doi:10.1016/j.mri.2015.11.002

Matsuda, H. (2016). MRI morphometry in Alzheimer's disease. *Ageing Res Rev, 30*, 17-24. doi:10.1016/j.arr.2016.01.003

May, A., Ashburner, J., Buchel, C., McGonigle, D. J., Friston, K. J., Frackowiak, R. S., et al. (1999). Correlation between structural and functional changes in brain in an idiopathic headache syndrome. *Nat Med, 5*(7), 836-838. doi:10.1038/10561

McKeefry, D. J., Watson, J. D., Frackowiak, R. S., Fong, K., & Zeki, S. (1997). The activity in human areas V1/V2, V3, and V5 during the perception of coherent and incoherent motion. *Neuroimage, 5*(1), 1-12. doi:10.1006/nimg.1996.0246

McKendrick, A. M., Chan, Y. M., Tien, M., Millist, L., Clough, M., Mack, H., et al. (2017). Behavioral measures of cortical hyperexcitability assessed in people who experience visual snow. *Neurology, 88*, 1243-1249. doi:10.1212/wnl.0000000000003784

Menon, V. (2011). Large-scale brain networks and psychopathology: a unifying triple network model. *Trends Cogn Sci, 15*(10), 483-506. doi:https://doi.org/10.1016/j.tics.2011.08.003

Menon, V., & Uddin, L. Q. (2010). Saliency, switching, attention and control: a network model of insula function. *Brain Struct Funct, 214*(5-6), 655-667. doi:10.1007/s00429-010-0262-0

Middleton, F. A., & Strick, P. L. (1998). Cerebellar output: motor and cognitive channels. *Trends Cogn Sci, 2*(9), 348-354.

Mishkin, M., Ungerleider, L. G., & Macko, K. A. (1983). Object vision and spatial vision: two cortical pathways. *Trends in Neurosciences, 6*, 414-417. doi:https://doi.org/10.1016/0166-2236(83)90190-X

Modinos, G., Egerton, A., McMullen, K., McLaughlin, A., Kumari, V., Barker, G. J., et al. (2018). Increased resting perfusion of the hippocampus in high positive schizotypy: A pseudocontinuous arterial spin labeling study. *Hum Brain Mapp, 39*(10), 4055-4064. doi:10.1002/hbm.24231

Müller, N. G., & Knight, R. T. (2006). The functional neuroanatomy of working memory: Contributions of human brain lesion studies. *Neuroscience, 139*(1), 51-58. doi:https://doi.org/10.1016/j.neuroscience.2005.09.018

Murphy, K., Harris, A. D., Diukova, A., Evans, C. J., Lythgoe, D. J., Zelaya, F., et al. (2011). Pulsed arterial spin labeling perfusion imaging at 3 T: estimating the number of subjects required in common designs of clinical trials. *Magn Reson Imaging, 29*(10), 1382-1389. doi:10.1016/j.mri.2011.02.030

Nekovarova, T., Fajnerova, I., Horacek, J., & Spaniel, F. (2014). Bridging disparate symptoms of schizophrenia: a triple network dysfunction theory. *Frontiers in Behavioral Neuroscience, 8*(171). doi:10.3389/fnbeh.2014.00171

Novotny, E. J., Jr., Fulbright, R. K., Pearl, P. L., Gibson, K. M., & Rothman, D. L. (2003). Magnetic resonance spectroscopy of neurotransmitters in human brain. *Ann Neurol, 54 Suppl 6*, S25-31. doi:10.1002/ana.10697

O'Reilly, J. X., Woolrich, M. W., Behrens, T. E. J., Smith, S. M., & Johansen-Berg, H. (2012). Tools of the trade: psychophysiological interactions and functional connectivity. *Social Cognitive and Affective Neuroscience, 7*(5), 604-609. doi:10.1093/scan/nss055

Oeltzschner, G., Saleh, M. G., Rimbault, D., Mikkelsen, M., Chan, K. L., Puts, N. A. J., et al. (2019). Advanced Hadamard-encoded editing of seven low-concentration brain metabolites: Principles of HERCULES. *Neuroimage, 185*, 181-190. doi:https://doi.org/10.1016/j.neuroimage.2018.10.002

Ogawa, S., Lee, T. M., Kay, A. R., & Tank, D. W. (1990). Brain magnetic resonance imaging with contrast dependent on blood oxygenation. *Proceedings of the National Academy of Sciences, 87*(24), 9868-9872. doi:10.1073/pnas.87.24.9868

Ogawa, S., Tank, D. W., Menon, R., Ellermann, J. M., Kim, S. G., Merkle, H., et al. (1992). Intrinsic signal changes accompanying sensory stimulation: functional brain mapping with magnetic resonance imaging. *Proc Natl Acad Sci U S A, 89*(13), 5951-5955. doi:10.1073/pnas.89.13.5951

Palm-Meinders, I. H., Arkink, E. B., Koppen, H., Amlal, S., Terwindt, G. M., Launer, L. J., et al. (2017). Volumetric brain changes in migraineurs from the general

population. *Neurology, 89*(20), 2066-2074. doi:10.1212/wnl.0000000000004640

Picard, N., & Strick, P. L. (2003). Activation of the Supplementary Motor Area (SMA) during Performance of Visually Guided Movements. *Cerebral Cortex, 13*(9), 977-986. doi:10.1093/cercor/13.9.977 %J Cerebral Cortex

Piechnik, S. K., Evans, J., Bary, L. H., Wise, R. G., & Jezzard, P. (2009). Functional changes in CSF volume estimated using measurement of water T2 relaxation. *Magn Reson Med, 61*(3), 579-586. doi:10.1002/mrm.21897

Pollock, J. M., Tan, H., Kraft, R. A., Whitlow, C. T., Burdette, J. H., & Maldjian, J. A. (2009). Arterial spin-labeled MR perfusion imaging: clinical applications. *Magn Reson Imaging Clin N Am, 17*(2), 315-338. doi:10.1016/j.mric.2009.01.008

Prichard, J., Rothman, D., Novotny, E., Petroff, O., Kuwabara, T., Avison, M., et al. (1991). Lactate rise detected by 1H NMR in human visual cortex during physiologic stimulation. *Proc Natl Acad Sci U S A, 88*(13), 5829-5831. doi:10.1073/pnas.88.13.5829

Provencher, S. W. (1993). Estimation of metabolite concentrations from localized in vivo proton NMR spectra. *Magn Reson Med, 30*(6), 672-679. doi:10.1002/mrm.1910300604

Provencher, S. W. (2001). Automatic quantitation of localized in vivo 1H spectra with LCModel. *NMR in Biomedicine, 14*(4), 260-264. doi:10.1002/nbm.698

Puledda, F., Ffytche, D. H., Lythgoe, D. J., O'Daly, O., Schankin, C., Williams, S. C., et al. (2020a). Insular and occipital changes in visual snow syndrome: a BOLD fMRI and MRS study. *Annals of Clinical and Translational Neurology. In press*.

Puledda, F., Ffytche, D. H., O'Daly, O., & Goadsby, P. J. (2019). Imaging the Visual Network in the Migraine Spectrum. *Front Neurol, 10*(1325). doi:10.3389/fneur.2019.01325

Puledda, F., Lau, T., Schankin, C., & Goadsby, P. J. (2017). Treatment effect in visual snow. *Cephalalgia, 37*(1_suppl), 231-232.

Puledda, F., Schankin, C., Digre, K., & Goadsby, P. J. (2018). Visual snow syndrome: what we know so far. *Curr Opin Neurol, 31*(1), 52-58. doi:10.1097/wco.0000000000000523

Puledda, F., Schankin, C., & Goadsby, P. J. (2020b). Visual snow syndrome. A clinical and phenotypical description of 1,100 cases. *Neurology, 94*(6), e564-e574. doi:10.1212/wnl.0000000000008909

Qin, P., & Northoff, G. (2011). How is our self related to midline regions and the default-mode network? *Neuroimage, 57*(3), 1221-1233. doi:10.1016/j.neuroimage.2011.05.028

Raichle, M. E. (2010). Two views of brain function. *Trends Cogn Sci, 14*(4), 180-190. doi:10.1016/j.tics.2010.01.008

Raichle, M. E. (2015). The Brain's Default Mode Network. *Annu. Rev. Neurosci, 38*(1), 433-447. doi:10.1146/annurev-neuro-071013-014030

Raichle, M. E., MacLeod, A. M., Snyder, A. Z., Powers, W. J., Gusnard, D. A., & Shulman, G. L. (2001). A default mode of brain function. *Proc Natl Acad Sci U S A, 98*(2), 676-682. doi:10.1073/pnas.98.2.676

Rao, R. P. N., & Ballard, D. H. (1999). Predictive coding in the visual cortex: A functional interpretation of some extra-classical receptive-field effects. *Nat Neurosci, 2*(1), 79-87. doi:10.1038/4580

Rastogi, R. G., VanderPluym, J., & Lewis, K. S. (2016). Migrainous Aura, Visual Snow, and "Alice in Wonderland" Syndrome in Childhood. *Semin Pediatr Neurol, 23*(1), 14-17. doi:10.1016/j.spen.2016.01.006

Rizzolatti, G., Scandolara, C., Matelli, M., & Gentilucci, M. (1981). Afferent properties of periarcuate neurons in macaque monkeys. II. Visual responses. *Behavioural Brain Research, 2*(2), 147-163. doi:https://doi.org/10.1016/0166-4328(81)90053-X

Robinson, D. L., & Petersen, S. E. (1992). The pulvinar and visual salience. *Trends Neurosci, 15*(4), 127-132.

Ross, A. J., & Sachdev, P. S. (2004). Magnetic resonance spectroscopy in cognitive research. *Brain Res Brain Res Rev, 44*(2-3), 83-102. doi:10.1016/j.brainresrev.2003.11.001

Sadaghiani, S., & D'Esposito, M. (2014). Functional Characterization of the Cingulo-Opercular Network in the Maintenance of Tonic Alertness. *Cerebral Cortex, 25*(9), 2763-2773. doi:10.1093/cercor/bhu072 %J Cerebral Cortex

Sandor, P. S., Dydak, U., Schoenen, J., Kollias, S. S., Hess, K., Boesiger, P., et al. (2005). MR-spectroscopic imaging during visual stimulation in subgroups of migraine with aura. *Cephalalgia, 25*(7), 507-518. doi:10.1111/j.1468-2982.2005.00900.x

Santhouse, A. M., Howard, R. J., & ffytche, D. H. (2000). Visual hallucinatory syndromes and the anatomy of the visual brain. *Brain, 123 (Pt 10)*, 2055-2064.

Sappey-Marinier, D., Calabrese, G., Fein, G., Hugg, J. W., Biggins, C., & Weiner, M. W. (1992). Effect of photic stimulation on human visual cortex lactate and phosphates using 1H and 31P magnetic resonance spectroscopy. *J Cereb Blood Flow Metab, 12*(4), 584-592. doi:10.1038/jcbfm.1992.82

Sarchielli, P., Tarducci, R., Presciutti, O., Gobbi, G., Pelliccioli, G. P., Stipa, G., et al. (2005). Functional 1H-MRS findings in migraine patients with and without aura assessed interictally. *Neuroimage, 24*(4), 1025-1031. doi:10.1016/j.neuroimage.2004.11.005

Schall, J. D. (2004). On the role of frontal eye field in guiding attention and saccades. *Vision Res, 44*(12), 1453-1467. doi:https://doi.org/10.1016/j.visres.2003.10.025

Schankin, C. J., Maniyar, F. H., Digre, K. B., & Goadsby, P. J. (2014a). 'Visual snow' - a disorder distinct from persistent migraine aura. *Brain, 137*(Pt 5), 1419-1428. doi:10.1093/brain/awu050

Schankin, C. J., Maniyar, F. H., Sprenger, T., Chou, D. E., Eller, M., & Goadsby, P. J. (2014b). The relation between migraine, typical migraine aura and "visual snow". *Headache, 54*(6), 957-966. doi:10.1111/head.12378

Schankin, C. J., Viana, M., & Goadsby, P. J. (2017). Persistent and Repetitive Visual Disturbances in Migraine: A Review. *Headache, 57*, 1-16. doi:10.1111/head.12946

Scheperjans, F., Eickhoff, S. B., Homke, L., Mohlberg, H., Hermann, K., Amunts, K., et al. (2008a). Probabilistic maps, morphometry, and variability of cytoarchitectonic areas in the human superior parietal cortex. *Cereb Cortex, 18*(9), 2141-2157. doi:10.1093/cercor/bhm241

Scheperjans, F., Hermann, K., Eickhoff, S. B., Amunts, K., Schleicher, A., & Zilles, K. (2008b). Observer-independent cytoarchitectonic mapping of the human superior parietal cortex. *Cereb Cortex, 18*(4), 846-867. doi:10.1093/cercor/bhm116

Schmahmann, J. D. (2004). Disorders of the cerebellum: ataxia, dysmetria of thought, and the cerebellar cognitive affective syndrome. *J Neuropsychiatry Clin Neurosci, 16*(3), 367-378. doi:10.1176/jnp.16.3.367

Schoenen, J., Wang, W., Albert, A., & Delwaide, P. J. (1995). Potentiation instead of habituation characterizes visual evoked potentials in migraine patients between attacks. *Eur J Neurol, 2*(2), 115-122. doi:10.1111/j.1468-1331.1995.tb00103.x

Schubert, F., Gallinat, J., Seifert, F., & Rinneberg, H. (2004). Glutamate concentrations in human brain using single voxel proton magnetic resonance spectroscopy at 3 Tesla. *Neuroimage, 21*(4), 1762-1771. doi:10.1016/j.neuroimage.2003.11.014

Schulte, L. H., & May, A. (2016). The migraine generator revisited: continuous scanning of the migraine cycle over 30 days and three spontaneous attacks. *Brain, 139*(Pt 7), 1987-1993. doi:10.1093/brain/aww097

Schwedt, T. J., Schlaggar, B. L., Mar, S., Nolan, T., Coalson, R. S., Nardos, B., et al. (2013). Atypical resting-state functional connectivity of affective pain regions in chronic migraine. *Headache, 53*(5), 737-751. doi:10.1111/head.12081

Sedley, W., Friston, K. J., Gander, P. E., Kumar, S., & Griffiths, T. D. (2016). An Integrative Tinnitus Model Based on Sensory Precision. *Trends Neurosci, 39*(12), 799-812. doi:10.1016/j.tins.2016.10.004

Seeley, W. W., Menon, V., Schatzberg, A. F., Keller, J., Glover, G. H., Kenna, H., et al. (2007). Dissociable intrinsic connectivity networks for salience processing and executive control. *J Neurosci, 27*(9), 2349-2356. doi:10.1523/jneurosci.5587-06.2007

Seger, C. A. (2013). The visual corticostriatal loop through the tail of the caudate: circuitry and function. *Front Syst Neurosci, 7*, 104. doi:10.3389/fnsys.2013.00104

Sestieri, C., Corbetta, M., Spadone, S., Romani, G. L., & Shulman, G. L. (2014). Domain-general signals in the cingulo-opercular network for visuospatial attention and episodic memory. *J Cogn Neurosci, 26*(3), 551-568. doi:10.1162/jocn_a_00504

Shargorodsky, J., Curhan, G. C., & Farwell, W. R. (2010). Prevalence and characteristics of tinnitus among US adults. *Am J Med, 123*(8), 711-718. doi:10.1016/j.amjmed.2010.02.015

Shelley, B. P., & Trimble, M. R. (2004). The insular lobe of Reil--its anatamico-functional, behavioural and neuropsychiatric attributes in humans--a review. *World J Biol Psychiatry, 5*(4), 176-200.

Shine, J. M., Halliday, G. M., Gilat, M., Matar, E., Bolitho, S. J., Carlos, M., et al. (2014). The role of dysfunctional attentional control networks in visual misperceptions in Parkinson's disease. *Hum Brain Mapp, 35*(5), 2206-2219. doi:10.1002/hbm.22321

Shine, J. M., Halliday, G. M., Naismith, S. L., & Lewis, S. J. (2011). Visual misperceptions and hallucinations in Parkinson's disease: dysfunction of attentional control networks? *Mov Disord, 26*(12), 2154-2159. doi:10.1002/mds.23896

Shulman, G. L., Fiez, J. A., Corbetta, M., Buckner, R. L., Miezin, F. M., Raichle, M. E., et al. (1997). Common Blood Flow Changes across Visual Tasks: II. Decreases in Cerebral Cortex. *J Cogn Neurosci, 9*(5), 648-663. doi:10.1162/jocn.1997.9.5.648

Simpson, J. C., Goadsby, P. J., & Prabhakar, P. (2013). Positive persistent visual symptoms (visual snow) presenting as a migraine variant in a 12-year-old girl. *Pediatr Neurol, 49*(5), 361-363. doi:10.1016/j.pediatrneurol.2013.07.005

Sinclair, S. H., Azar-Cavanagh, M., Soper, K. A., Tuma, R. F., & Mayrovitz, H. N. (1989). Investigation of the source of the blue field entoptic phenomenon. *Invest Ophthalmol Vis Sci, 30*(4), 668-673.

Snowden, R. J., Treue, S., Erickson, R. G., & Andersen, R. A. (1991). The response of area MT and V1 neurons to transparent motion. *J Neurosci, 11*(9), 2768-2785. doi:10.1523/jneurosci.11-09-02768.1991

Sporns, O., Chialvo, D. R., Kaiser, M., & Hilgetag, C. C. (2004). Organization, development and function of complex brain networks. *Trends Cogn Sci, 8*(9), 418-425. doi:10.1016/j.tics.2004.07.008

Sridharan, D., Levitin, D. J., & Menon, V. (2008). A critical role for the right fronto-insular cortex in switching between central-executive and default-mode networks. *Proc Natl Acad Sci U S A, 105*(34), 12569-12574. doi:10.1073/pnas.0800005105

Stoodley, C. J., & Schmahmann, J. D. (2009). Functional topography in the human cerebellum: a meta-analysis of neuroimaging studies. *Neuroimage, 44*(2), 489-501. doi:10.1016/j.neuroimage.2008.08.039

Stoodley, C. J., & Schmahmann, J. D. (2010). Evidence for topographic organization in the cerebellum of motor control versus cognitive and affective processing. *Cortex, 46*(7), 831-844. doi:10.1016/j.cortex.2009.11.008

Teixeira, S., Machado, S., Velasques, B., Sanfim, A., Minc, D., Peressutti, C., et al. (2014). Integrative parietal cortex processes: neurological and psychiatric aspects. *J Neurol Sci, 338*(1-2), 12-22. doi:10.1016/j.jns.2013.12.025

Thirion, B., Pinel, P., Meriaux, S., Roche, A., Dehaene, S., & Poline, J. B. (2007). Analysis of a large fMRI cohort: Statistical and methodological issues for group analyses. *Neuroimage, 35*(1), 105-120. doi:10.1016/j.neuroimage.2006.11.054

Tootell, R. B., Reppas, J. B., Kwong, K. K., Malach, R., Born, R. T., Brady, T. J., et al. (1995). Functional analysis of human MT and related visual cortical areas using magnetic resonance imaging. *J Neurosci, 15*(4), 3215-3230.

Tyler, C. W. (1978). Some new entoptic phenomena. *Vision Res, 18*(12), 1633-1639.

Unal-Cevik, I., & Yildiz, F. G. (2015). Visual Snow in Migraine With Aura: Further Characterization by Brain Imaging, Electrophysiology, and Treatment - Case Report. *Headache, 55*(10), 1436-1441. doi:10.1111/head.12628

Utevsky, A. V., Smith, D. V., & Huettel, S. A. (2014). Precuneus Is a Functional Core of the Default-Mode Network. *34*(3), 932-940. doi:10.1523/JNEUROSCI.4227-13.2014 %J The Journal of Neuroscience

van den Berge, M. J. C., Free, R. H., Arnold, R., de Kleine, E., Hofman, R., van Dijk, J. M. C., et al. (2017). Cluster Analysis to Identify Possible Subgroups in Tinnitus Patients. *Front Neurol, 8*, 115. doi:10.3389/fneur.2017.00115

van Dongen, R. M., Waaijer, L. C., Onderwater, G. L. J., Ferrari, M. D., & Terwindt, G. M. (2019). Treatment effects and comorbid diseases in 58 patients with visual snow. *Neurology, 93*(4), e398-e403. doi:10.1212/wnl.0000000000007825

Vanhaudenhuyse, A., Noirhomme, Q., Tshibanda, L. J., Bruno, M. A., Boveroux, P., Schnakers, C., et al. (2010). Default network connectivity reflects the level of

consciousness in non-communicative brain-damaged patients. *Brain, 133*(Pt 1), 161-171. doi:10.1093/brain/awp313

Vernet, M., Quentin, R., Chanes, L., Mitsumasu, A., & Valero-Cabré, A. (2014). Frontal eye field, where art thou? Anatomy, function, and non-invasive manipulation of frontal regions involved in eye movements and associated cognitive operations. *Front Integr Neurosci, 8*, 66. doi:10.3389/fnint.2014.00066

Vincent, M., Pedra, E., Mourão-Miranda, J., Bramati, I., Henrique, A., & Moll, J. (2003). Enhanced Interictal Responsiveness of the Migraineous Visual Cortex to Incongruent Bar Stimulation: A Functional MRI Visual Activation Study. *23*(9), 860-868. doi:10.1046/j.1468-2982.2003.00609.x

Vogt, B. A. (2016). Midcingulate cortex: Structure, connections, homologies, functions and diseases. *J Chem Neuroanat, 74*, 28-46. doi:10.1016/j.jchemneu.2016.01.010

Wang, Y. F., Fuh, J. L., Chen, W. T., & Wang, S. J. (2008). The visual aura rating scale as an outcome predictor for persistent visual aura without infarction. *Cephalalgia, 28*(12), 1298-1304. doi:10.1111/j.1468-2982.2008.01679.x

Watson, J. D., Myers, R., Frackowiak, R. S., Hajnal, J. V., Woods, R. P., Mazziotta, J. C., et al. (1993). Area V5 of the human brain: evidence from a combined study using positron emission tomography and magnetic resonance imaging. *Cereb Cortex, 3*(2), 79-94.

Williams, D. S., Detre, J. A., Leigh, J. S., & Koretsky, A. P. (1992). Magnetic resonance imaging of perfusion using spin inversion of arterial water. *Proc Natl Acad Sci U S A, 89*(1), 212-216.

Wolf, R. L., & Detre, J. A. (2007). Clinical neuroimaging using arterial spin-labeled perfusion magnetic resonance imaging. *Neurotherapeutics, 4*(3), 346-359. doi:10.1016/j.nurt.2007.04.005

Wolke, S. A., Mehta, M. A., O'Daly, O., Zelaya, F., Zahreddine, N., Keren, H., et al. (2019). Modulation of anterior cingulate cortex reward and penalty signalling in medication-naive young-adult subjects with depressive symptoms following acute dose lurasidone. *Psychol Med, 49*(8), 1365-1377. doi:10.1017/s0033291718003306

Wong, E. C. (2014). An introduction to ASL labeling techniques. *J Magn Reson Imaging, 40*(1), 1-10. doi:10.1002/jmri.24565

Worsley, K. J., & Friston, K. J. (1995). Analysis of fMRI time-series revisited--again. *Neuroimage, 2*(3), 173-181. doi:10.1006/nimg.1995.1023

Wright, I. C., McGuire, P. K., Poline, J. B., Travere, J. M., Murray, R. M., Frith, C. D., et al. (1995). A voxel-based method for the statistical analysis of gray and white matter density applied to schizophrenia. *Neuroimage, 2*(4), 244-252. doi:10.1006/nimg.1995.1032

Wu, B. P., Searchfield, G., Exeter, D. J., & Lee, A. (2015). Tinnitus prevalence in New Zealand. *N Z Med J, 128*(1423), 24-34.

Yildiz, F. G., Turkyilmaz, U., & Unal-Cevik, I. (2019). The Clinical Characteristics and Neurophysiological Assessments of the Occipital Cortex in Visual Snow Syndrome With or Without Migraine. *Headache, 59*(4), 484-494. doi:10.1111/head.13494

Zeki, S., Watson, J. D., Lueck, C. J., Friston, K. J., Kennard, C., & Frackowiak, R. S. (1991). A direct demonstration of functional specialization in human visual cortex. *J Neurosci, 11*(3), 641-649.